

SCREENING OF p53-MDM2 INTERACTION INHIBITORS THROUGH GENOME  
EDITING, HIGH-CONTENT SCREENING, AND SURFACE PLASMON  
RESONANCE

by

HAKAN TAŞKIRAN

Submitted to the Graduate School of Engineering and Natural Sciences

in partial fulfillment of

the requirements for the degree of

Master of Science

Sabancı University

July 2018

SCREENING OF p53-MDM2 INTERACTION INHIBITORS THROUGH  
GENOME EDITING, HIGH-CONTENT SCREENING, AND SURFACE  
PLASMON RESONANCE

APPROVED BY:

Prof. Dr. Batu Erman  
(Thesis Supervisor)



Prof. Dr. Selim Çetiner



Asst. Prof. Dr. Tuğba Bağcı Önder



DATE OF APPROVAL: 23/07/2018

© Hakan Taşkıran

All Rights Reversed

*To my family...*

*Canım aileme...*

*#ŞÜKÜR*

## ABSTRACT

### SCREENING OF p53-MDM2 INTERACTION INHIBITORS THROUGH GENOME EDITING, HIGH-CONTENT SCREENING, AND SURFACE PLASMON RESONANCE

HAKAN TAŞKIRAN

Molecular Biology, Genetics and Bioengineering, MSc Thesis, July 2018

Thesis supervisor: Prof. Batu Erman

Keywords: p53-MDM2 interaction, drug screening, CRISPR/Cas9, genome engineering, fluorescent two-hybrid assay, surface plasmon resonance

The tumor suppressor p53 is the central mediator of cell-cycle arrest, senescence, and apoptosis. p53 protein levels increase upon various cellular stresses to prevent the improper proliferation of cells harboring DNA damage. Under normal conditions, cells keep p53 protein levels suppressed due to its main antagonist, MDM2. This oncogenic protein acts on p53 as an E3 ubiquitin ligase for the polyubiquitination of p53 and its subsequent proteasomal degradation. Activating the p53 pathway is one of the prime targets for novel cancer therapeutics because almost all human cancers have inactivated p53 either by a mutation or by a defect in its regulators, such as the overexpression of MDM2. In this study, we aimed to construct three methods for the screening of novel compounds generated by *in silico* design and organic synthesis and attempted to inhibit the protein-protein interaction between p53 and MDM2. We generated HCT116 p53<sup>-/-</sup>MDM2<sup>-/-</sup> cell lines as a novel assay system through CRISPR/Cas9 genome editing for studying the activity of candidate small molecule compounds targeting the p53-MDM2 interaction. We also constructed a Fluorescent Two-Hybrid (F2H) assay system for high-content screening of these compounds in real time in living cells and finally a surface plasmon resonance assay for high-throughput screening of these compounds *in vitro*.

## ÖZET

### p53-MDM2 ETKİLEŞİM İNHİBİTÖRLERİNİN GENOM MÜHENDİSLİĞİ, FLORESAN İKİLİ HİBRİT VE YÜZEY PLAZMON REZONANS TEKNİKLERİ İLE TARANMASI

HAKAN TAŞKIRAN

Moleküler Biyoloji, Genetik ve Biyomühendislik, Yüksek Lisans Tezi, Temmuz 2018

Tez danışmanı: Prof. Batu Erman

Anahtar kelimeler: p53-MDM2 etkileşimi, ilaç taranması, CRISPR/Cas9, genom mühendisliği, floresan ikili hibrit tekniği, yüzey plazmon rezonans

Tümör baskılayıcı protein p53 hücre bölünmesinin durdurulmasında, senesensde ve apoptozda görev almaktadır. Hücrede p53 seviyesi çeşitli stresler nedeni ile artmaktadır ve DNA hasarı olan hücrelerin bölünmesine engel olmaktadır. Normal hücrelerde p53 protein seviyeleri antagonisti olan MDM2 tarafından düşük tutulmaktadır. Bu onkogenik protein E3 ligaz aktivitesi ile p53'ün ubiquitinlenmesine ve daha sonra proteazomda yıkılmasını sağlar. p53 yolağının aktifleştirilmesi kanser ilacı geliştirmelerinin odak noktasıdır çünkü kanserlerde p53 ya mutasyon ya da regülatörlerindeki bozukluklar nedeniyle etkisiz durumdadır. Bu çalışmada, bilgisayar ortamında p53 ve MDM2 etkileşimine karşı tasarlanmış, ve organik sentezlenmiş moleküllerin taranması için üç yöntem kurduk. CRISPR/Cas9 genom mühendisliği ile geliştirilmiş HCT116 p53-/- MDM2-/- hücre hattında moleküllerin aktivitelerini test ettik. Floresan ikili hibrit tekniğini moleküllerin canlı içinde gerçek zamanlı yüksek içerikli aktivite taranması için ve yüzey plazmon rezonans tekniğini moleküllerin canlı dışında yüksek hızda aktivite taraması için kurduk.

## ACKNOWLEDGEMENTS

First of all, I would like to express my deep sense of gratitude to my thesis advisor Prof. Dr. Batu Erman for his continuous help and support of my M.Sc study, for his patience, motivation and huge knowledge. I truly enjoyed working in a research environment that boosts my scientific background and skeptical thinking, which he created. I am forever grateful for having the chance to become a member of his research laboratory. I would also like to thank the rest of my thesis jury, Prof. Selim Çetiner, and Asst. Prof. Tuğba Bağcı Önder for their interest and insightful feedbacks about my thesis project. I also want to express my sincere appreciation to Dr. Tolga Sütü for his valuable scientific comments.

I thank all my fellow past and present labmates of Ermanlab and Sutlulab, who made this journey full of memories: Ronay Çetin, Nazife Tolay, Sinem Usluer, Melike Gezen, Dr. Canan Sayitoğlu, Sofia Piepoli, Sarah Barakat, Liyne Nogay, Sanem Sarıyar, Cevriye Pamukçu, Mertkaya Aras, Alp Ertunga Eyüpoğlu, Aydan Saraç, Didem Özkazanç, Ayhan Parlar, Lolai Ikromzoda, Pegah Zahadimaram and Elif Çelik. Especially, among these great people, I would like to express my great appreciation to Nazife Tolay, Ronay Çetin and Sofia Piepoli for imparting all their knowledge, support and guidance. Without them, it would not be possible to conduct this thesis study. I am also thankful to my undergraduate students Fulya, Ezgi, and Oğuz for their great energy and close friendships and to all the students of Başağa Lab, Atılgan Lab and Gözaçık Lab for their support.

Last but not least I would like to thank my family and my friends, whose love and support have been with me during this journey. My hard-working parents provided me with everything they have with unconditional love and without them, I would not have made it this far. My sister has been encouraging me in all of my pursuits. My friends are too many to list here, but they know who they are. I want to thank all of them for their support throughout my life and especially, to Berfin, Oğuz and Uyaniker Sisters for standing by my side from the beginning.

This study was supported by TUBITAK 1003 grant ‘ Özgün 2-indolinon bileşiklerinin anti-interlökin-1 ve kemoterapötik ilaçlar olarak geliştirilmesi’ Grant Number: T.A.CF-16-01568 (215S615)

## TABLE OF CONTENTS

<b>ABSTRACT.....</b>	<b>i</b>
<b>ÖZET .....</b>	<b>ii</b>
<b>ACKNOWLEDGEMENTS .....</b>	<b>iii</b>
<b>LIST OF FIGURES .....</b>	<b>ix</b>
<b>LIST OF TABLES .....</b>	<b>xii</b>
<b>LIST OF ABBREVIATIONS .....</b>	<b>xiii</b>
<b>1. INTRODUCTION .....</b>	<b>1</b>
<b>1.1. p53-MDM2 Interaction in Tumor Development.....</b>	<b>1</b>
1.1.1. The significance of p53-MDM2 Interaction in Human Tumors.....	1
1.1.2. p53 Biology.....	3
1.1.2.1. Gene Structure and Protein Motifs of p53 .....	3
1.1.2.2. Tumor-suppressor pathways downstream of p53 .....	5
1.1.2.3. Modes of p53 regulation .....	7
1.1.3. MDM2 Biology.....	8
1.1.3.1. Gene Structure and Protein Motifs of MDM2 .....	8
1.1.3.2. MDM2-p53 Regulation.....	9
1.1.4. Strategies targeting the p53-MDM2 pathway for cancer therapy.....	12
1.1.4.1. Targeting mutant-p53 .....	12
1.1.4.2. Targeting Cancer with Wild-type p53 .....	14

<b>1.2. Genome Editing by Cluster Regularly Interspaced Short Palindromic Repeats (CRISPR)</b> .....	<b>15</b>
<b>2. AIM OF THE STUDY</b> .....	<b>18</b>
<b>3. MATERIALS &amp; METHODS</b> .....	<b>19</b>
<b>3.1. Materials</b> .....	<b>19</b>
3.1.1. Chemicals.....	19
3.1.2. Equipment.....	19
3.1.3. Solutions and Buffers.....	19
3.1.4. Growth Media .....	21
3.1.5. Molecular Biology Kits .....	22
3.1.6. Enzymes.....	22
3.1.7. Antibodies.....	22
3.1.8. Bacterial Strains .....	22
3.1.9. Mammalian Cell Lines.....	22
3.1.10. Plasmid and Oligonucleotides .....	22
3.1.11. DNA and Protein Molecular Weight Markers .....	24
3.1.12. DNA Sequencing .....	24
3.1.13. Software, Computer-based Programs, and Websites.....	24
<b>3.2. Methods</b> .....	<b>26</b>
3.2.1. Bacterial Cell Culture .....	26
3.2.1.1. The growth of Bacterial Culture .....	26

3.2.1.2.	Preparation of competent bacteria .....	26
3.2.1.3.	Transformation of competent bacteria .....	27
3.2.1.4.	Plasmid DNA isolation .....	27
3.2.2.	Mammalian Cell Culture .....	27
3.2.2.1.	Maintenance of cell lines .....	27
3.2.2.2.	Cryopreservation of the cells .....	27
3.2.2.3.	Thawing of frozen mammalian cells .....	28
3.2.2.4.	Transient Transfection of Mammalian Cell Lines using Polyethyleneimine (PEI).....	28
3.2.2.5.	Genomic DNA isolation .....	29
3.2.2.6.	Cell Lysis, SDS Gel, Transfer, and Western-Blot .....	29
3.2.3.	Vector Construction .....	29
3.2.4.	CRISPR/Cas9 Genome Editing .....	30
3.2.4.1.	sgRNA design and off-target analysis .....	30
3.2.4.2.	Phosphorylation and annealing of top and bottom oligonucleotide pairs .....	31
3.2.4.3.	pSpCas9(BB)-2A-Puro plasmid digestion and ligation.....	31
3.2.4.4.	Transformation of pSpCas9(BB)-2A-Puro.....	32
3.2.4.5.	Transfection with Cas9 expressing plasmids.....	33
3.2.4.6.	Flow Cytometry .....	33
3.2.4.7.	Preparation of clonal cell lines.....	33

3.2.4.8.	Determination Genome Targeting Efficiency.....	33
3.2.4.9.	Determination of Cell Viability by MTT assay .....	34
3.2.4.10.	Real-Time Cell Growth .....	34
3.2.5.	Fluorescent two-hybrid (F2H) assay.....	34
3.2.5.1.	pcDNA3.1/myc-His(-)B-GBP-LacI Vector Construction .....	34
3.2.5.2.	PEI transfection of F2H-assay plasmids and Compound Treatment..	36
3.2.5.3.	Live Cell Imaging .....	36
3.2.6.	Protein purification .....	36
3.2.6.1.	Vector Construction .....	36
3.2.6.2.	His-tagged protein expression .....	38
3.2.6.3.	Affinity chromatography of His-tagged proteins.....	39
3.2.6.4.	SDS-PAGE gel and Coomassie Blue Staining .....	40
3.2.6.5.	Concentrating Protein .....	40
3.2.6.6.	Size-exclusion chromatography.....	41
3.2.6.7.	Dialysis .....	41
3.2.6.8.	3C Protease Digestion and GST pull-down.....	42
3.2.6.9.	His pull-down .....	42
3.2.7.	Surface Plasmon Resonance .....	43
<b>4.</b>	<b>RESULTS .....</b>	<b>44</b>
<b>4.1.</b>	<b>Generation of the p53<sup>-/-</sup> MDM2<sup>-/-</sup> Cell Line for Testing the Activity of Compounds.....</b>	<b>44</b>

4.1.1.	CRISPR/Cas9 targeting the Human MDM2 gene .....	44
4.1.2.	Analysis of Compounds by using HCT116 p53 <sup>-/-</sup> MDM2 <sup>-/-</sup> cell line... 51	
4.1.3.	Effect of MDM2 in Cellular Growth Rate Independently of p53.....	52
<b>4.2.</b>	<b>Fluorescent two-hybrid (F2H) assay for screening the compounds.....</b>	<b>54</b>
<b>4.3.</b>	<b>Protein purification of TagGFP-p53 and MDM2 proteins and screening compounds <i>in vitro</i> by surface plasmon resonance (SPR).....</b>	<b>62</b>
4.3.1.	Protein purification of TagGFP-p53 and MDM2 proteins .....	62
4.3.2.	Surface Plasmon Resonance Assay .....	70
<b>5.</b>	<b>DISCUSSION.....</b>	<b>75</b>
<b>6.</b>	<b>REFERENCES.....</b>	<b>79</b>
<b>7.</b>	<b>APPENDICES.....</b>	<b>89</b>
<b>7.1.</b>	<b>APPENDIX A- Chemicals.....</b>	<b>89</b>
<b>7.2.</b>	<b>APPENDIX B – Equipment.....</b>	<b>91</b>
<b>7.3.</b>	<b>APPENDIX C- Molecular Biology Kits.....</b>	<b>93</b>
<b>7.4.</b>	<b>APPENDIX D- Antibodies.....</b>	<b>93</b>
<b>7.5.</b>	<b>APPENDIX E – DNA and Protein Molecular Weight Marker.....</b>	<b>94</b>
<b>7.6.</b>	<b>APPENDIX F- Plasmid Maps.....</b>	<b>95</b>

## LIST OF FIGURES

Figure 1.1. Gene structure and Protein Motifs of p53..	4
Figure 1.2. Tumor suppressor pathways of p53. ....	6
Figure 1.3. Gene Structure and Protein Motifs of MDM2.....	9
Figure 1.4. Regulation of the p53-MDM2 pathway. ....	11
Figure 1.5. CRISPR/Cas9 system and DSB Repair.....	17
Figure 3.1. Bacterial expression and induction of His-tagged proteins.....	38
Figure 3.2. Affinity chromatography steps of His-tagged proteins. ....	40
Figure 4.1. MDM2-sgRNA design..	44
Figure 4.2. Experimental design of CRISPR/Cas9 system targeting <i>MDM2</i> gene using pSpCas9(BB)-2A-Puro..	45
Figure 4.3. Mutation analysis of MDM2-sgRNA mediated mutations. ....	46
Figure 4.4. Detection of CRISPR/Cas9 induced mutations in single cell clones.....	47
Figure 4.5. Sequencing Analysis of MDM2-sgRNA targeted genome of single cell clones..	48
Figure 4.6. Early stop codon formation due to CRISPR-Cas9 mediated mutations.....	49
Figure 4.7. Analysis of MDM2 protein expression in single cell clones by western blotting.....	50
Figure 4.8. Cell viability analysis of a compound. ....	52
Figure 4.9. Growth rate analysis of double knockout HCT116 cells. ....	53
Figure 4.10. Experimental design of fluorescent 2 hybrid (F2H) assay. ....	55

Figure 4.11. Verification of F2H assay.....	56
Figure 4.12. The disappearance of red foci in F2H assay using our positive control, Nutlin-3a. ....	57
Figure 4.13. Screening of 1 $\mu$ M compounds in F2H assay.. ....	58
Figure 4.14. Screening of 10 $\mu$ M compounds in F2H assay.. ....	61
Figure 4.15. Vector construction design of bacterial expression plasmids.. ....	63
Figure 4.16. Bacterial expression and affinity purification of His-tagged TagGFP-p53 fusion protein.. ....	64
Figure 4.17. Size exclusion chromatography of His-tagged TagGFP-p53 fusion protein.. ....	65
Figure 4.18. Affinity and Size-exclusion chromatography of His-tagged TagRFP-MDM2 fusion protein.. ....	67
Figure 4.19. Affinity purification of His-tagged MDM2 protein.. ....	68
Figure 4.20. 3C 'Prescission' protease digestion of His-tagged MDM2 proteins.....	69
Figure 4.21. Purification of MDM2 protein after 3C protease digestion.. ....	70
Figure 4.22. Immobilization of His-tagged TagGFP-p53 onto NTA chip at different concentrations. ....	72
Figure 4.23. The binding ability of MDM2 protein without the His-tag to the NTA chip. ....	73
Figure 4.24. Binding assay of MDM2 protein.....	74
Figure 7.1. GeneRuler DNA Ladder Mix & Figure 7.2. Color Prestained Protein ....	94
Figure 7.3. The plasmid map of pUC19 .....	95
Figure 7.4. The plasmid map of pcDNA3-GFP .....	95

Figure 7.5. The plasmid map of pSpCas9(BB)-2A-Puro.....	96
Figure 7.6. The Plasmid map of pcDNA3-Flag-p53 .....	96
Figure 7.7. The plasmid map of pcDNA3.1/Myc His (-) B.....	97
Figure 7.8. The plasmid map of pET-47b(+ ).....	97

## LIST OF TABLES

Table 3.1. List of oligonucleotides .....	23
Table 3.2. List of plasmids.....	24
Table 3.3. List of software and computer-based programs and websites. ....	25
Table 3.4. List of PEI transfection conditions depending on the plate type. ....	28

## LIST OF ABBREVIATIONS

$\alpha$	Alpha
$\beta$	Beta
$\lambda$	Lambda
$\mu$	Micro
A	Ampere
Apaf1	Apoptotic protease activating factor 1
ARF	Alternative reading frame protein
ATM	Ataxia telangiectasia mutated
ATR	Ataxia telangiectasia and Rad3 related
Bad	Bcl-2-associated death promoter
Bak	Bcl-2 homologous antagonist/killer
Bax	Bcl-2-associated X protein
Bcl-2	B-cell lymphoma 2
Bcr	Breakpoint cluster region protein
bGH	Bovine growth hormone
BHK	Baby Hamster kidney
Bid	BH3 interacting domain death agonist
bp	Base pair
Cas9	CRISPR-associated protein 9
CBP	CREB-binding protein
ARF	ADP ribosylation factor
Cas9	CRISPR-associated protein 9
CBh	Chicken beta hybrid
CBP	CREB-binding protein
Cdk	Cyclin-dependent kinase
Chl	Chloramphenicol
CIP/CIAP	Calf intestinal alkaline phosphatase
CRISPR	Clustered regularly interspaced short palindromic repeats
crRNA	CRISPR ribonucleic acid
DBD	DNA binding domain
DMEM	Dulbecco's Modified Eagle Medium
DMSO	Dimethyl sulfoxide
DNA	Deoxyribonucleic acid
dNTPs	Deoxynucleotide triphosphates
Dr5	Death receptor 5
DSB	Double-stranded break
<i>E. coli</i>	<i>Escherichia coli</i>
EDTA	Ethylenediaminetetraacetic acid
F2H	Fluorescent 2 hybrid
FACS	Fluorescence-activated cell sorting
FBS	Fetal bovine serum
GADD45	Growth Arrest and DNA-damage-inducible 45

GFP	Green Fluorescent Protein
GBP	GFP-binding protein
HDR	Homology-directed repair
IMAC	Immobilized Metal Affinity Chromatography
Kan	Kanamycin
kDa	Kilo Dalton
LB	Luria Broth
MDM2	Murine double minute 2
mRNA	Messenger ribonucleic acid
mTOR	Mammalian target of rapamycin
NCBI	National Center for Biotechnology
NES	Nuclear export signal
NF- $\kappa$ B	Nuclear factor- kappa light chain enhancer of activated B cells
NHEJ	Non-homologous end joining
NLS	Nuclear localization signal
NR	Non-retained
nts	nucleotides
o/n	overnight
PAM	Protospacer-adjacent motif
PBS	Phosphate-buffered saline
PCR	Polymerase chain reaction
PEI	Polyethyleneimine
PI3K	Phosphoinositide 3-kinase
Puma	p53 upregulated modulator of apoptosis
Puro	Puromycin
RB	Retinoblastoma tumor suppressor
RFLP	Restriction fragment length
RING	Really Interesting New Gene
Rpm	Revolution per minute
RU	Response Unit
SDS-PAGE	Sodium Dodecyl Sulfate-Polyacrylamide Gel Electrophoresis
sgRNA	Single guide ribonucleic acid
SPR	Surface Plasmon Resonance
TAD	Trans-activation domain
TB	Terrific Broth
TBE	Tris-Borate-EDTA
TCEP	Tris (2-carboxyethyl) phosphine hydrochloride
TF	Transcription factor
tracrRNA	Trans-activating crRNA
V	Volt
WT	Wild-type
ZFN	Zinc-finger nuclease

# 1. INTRODUCTION

## 1.1. p53-MDM2 Interaction in Tumor Development

### 1.1.1. The significance of p53-MDM2 Interaction in Human Tumors

Human cancers are caused by a series of genetic and epigenetic changes, which give rise to alterations in gene expression, and in turn, tumorigenesis<sup>1,2</sup>. Although these malignant changes usually take place in somatic cells, heritable cancers can also occur due to germline-mutations<sup>1</sup>. A single gene mutation is rarely adequate for the entire transformation process, thereby genetic changes, which include chromosomal translocations, point mutations, deletions, and insertions, happen as a multistep process affecting many oncogenes, tumor-suppressor genes or microRNAs<sup>1,3,4</sup>. This multistep nature of tumor development requires eight biological processes: Sustained proliferative potential, escape from growth suppressors, cell-death resistance, replicative immortality, induced angiogenesis, active invasion and metastasis, immune-system evasion, and reprogrammed cellular energetics<sup>5</sup>. These eight hallmarks of cancer are a result of genome instability, which changes cell signaling, gene expression, and cell cycle progression<sup>5,6</sup>.

The molecular mechanisms responsible for cancer development consist of oncogenes, tumor suppressor genes, and the factors associated with growth, angiogenesis, signal transduction and cell adhesion<sup>2</sup>. The identification of genes playing important roles in tumor initiation and development is important for biomarker discovery. Further screening of therapeutic agents, such as small molecules, peptides, and antibodies have been generating novel drug discoveries<sup>2</sup>. Among the many cancer-related molecular mechanisms, especially oncogene activation and tumor suppressor inactivation are the most well-studied. Most oncogenes and tumor suppressor genes encode cell cycle- and apoptosis-related proteins<sup>2,7</sup>. Oncogene activation takes place in tumor tissues through gain-of-function mutations, gene fusion or amplification or the association with enhancers. On the other hand, tumor suppressor genes, which prevent malignant transformation by activating anti-proliferative or pro-apoptotic pathways, are silenced

through deletions, nonsense mutations, frame-shift mutations, insertions or missense mutations<sup>6,8</sup>. Oncogenes are preferred as a therapeutic target because inhibiting an excessive activity is easier than restoring a lost activity<sup>2,7</sup>. Small molecules, peptides, antibodies or antisense oligos have been identified and validated as oncogene-based therapeutics through high-throughput screening and combinatorial chemistry<sup>2,9</sup>.

Tumor suppressor genes have also been targeted with gene therapy to restore mutated or deleted genes, which lead to the re-establishment of cell-cycle control and of apoptosis mechanisms<sup>10</sup>. Tumor suppressor gene therapy includes the transfer of genetic material into a host by using viral or non-viral vectors<sup>11</sup>. Although cancer gene therapy is promising and there were many possible tumor suppressor candidates for gene therapy, such as *TP53*, *pRb*, and *PTEN*, it is also highly challenging because it should include an efficient gene delivery system, suitable target gene and tumor type, and determination of appropriate traditional strategies for combinational gene therapy<sup>10,11</sup>. In gene therapy clinical trials, encouraging results were obtained in patients with chronic lymphocytic leukemia, acute lymphocytic leukemia, and brain tumors<sup>11</sup>.

p53 is arguably the most important and the most widely studied tumor suppressor. This transcription factor plays a central part in the cell cycle and apoptosis<sup>12</sup>. Upon diverse stresses, such as DNA damage or oncogene activation, p53 becomes activated and gives rise to the induction of cell-cycle arrest, DNA repair, senescence or apoptosis to control the formation of transformed cells with genomic instabilities<sup>6,12</sup>. Under normal conditions, cellular p53 protein levels remain low due to its negative regulators; MDM2 and MDMX<sup>12</sup>. Moreover, there is an autoregulatory negative feedback loop between p53 and MDM2 because p53 induces transcription of MDM2, which, in turn, acts on p53 as an E3 ubiquitin ligase and results in its proteasomal degradation<sup>12,13</sup>. Although MDMX has no intrinsic E3 ligase activity, it also inhibits p53 by forming a heterodimer with MDM2 and modulating its E3 ligase activity and also by directly binding to p53's transactivation domain<sup>12,14</sup>.

In around 50% of human cancer types, p53 tumor suppressor activity is lost by a mutation or deletion of the *TP53* gene. The prevalence of these mutations significantly changes depending on the tumor type and the developmental stage of the tumor, ranging from 5% in cervical cancers to 90% in ovarian cancers<sup>12,15</sup>. Although the remaining 50% of human cancer types have wild-type p53 status, its activity is greatly suppressed by various mechanisms, such as overexpression of MDM2 through gene amplification, enhanced

transcription or translation<sup>15,16</sup>. In about 7% of all human tumors, *MDM2* gene amplification is observed. The highest frequency is reported in soft tissue tumors, osteosarcomas, and esophageal carcinomas<sup>15,16</sup>. The mutations in p53 and overexpression of MDM2 lead to tumor survival, poor prognosis, and treatment failure, thereby discovering novel strategies that aim to restore functional p53 in tumor cells has been a central goal of both academic and industrial cancer research<sup>6,15</sup>.

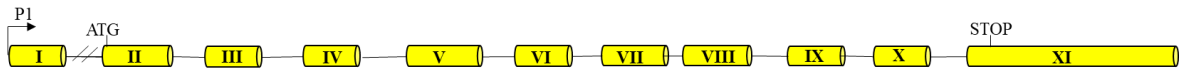
### **1.1.2. p53 Biology**

The tumor suppressor protein p53 was first discovered in 1979, and since then it has been identified as a transcription factor playing a central role in a complex signaling pathway that senses various cellular stresses such as DNA damage, oncogene activation, hypoxia, ribonucleotide depletion and telomere erosion<sup>15,17</sup>. Under stress, p53 is activated through various post-translational modifications and, in turn, it leads to up- or down-regulation of various genes functioning in cell-cycle arrest, DNA repair, senescence or apoptosis. Its transcriptional activities are tightly regulated through a complex network including its negative regulators; MDM2 and MDMX and various other signaling proteins<sup>12,18</sup>.

#### **1.1.2.1. Gene Structure and Protein Motifs of p53**

The human *TP53* gene resides on chromosome 17p13.1, consists of 11 exons, and transcribes a 2.8 kb mRNA<sup>19</sup> (Figure 1.1.A). In turn, this mRNA translates into a 393-residue p53 protein and it is active as a homo-tetramer<sup>18</sup>. Its complex domain organization contains 2 N-terminal transactivation domains (TAD1 and TAD2), a proline-rich region, a DNA-binding domain (DBD), a tetramerization domain, and finally a C-terminal regulatory domain (Figure 1.1.B)<sup>18</sup>. Three of these regions; TAD, Proline-rich region, and C-terminal regulatory domain are intrinsically disordered, whereas the remaining two domains are structured<sup>18,20</sup>. These natively unfolded structures are generally a feature of signaling proteins since they provide high conformational adaptability and plasticity in protein-protein interactions<sup>12</sup>.

A.



B.

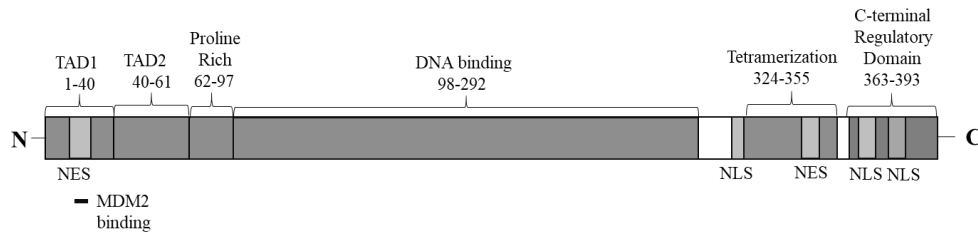


**Figure 1.1. Gene structure and Protein Motifs of p53.** (A) *TP53* gene consists of 11 exons. The full-length p53 is expressed from the P1 promoter and is translated from the first start codon in the exon 2. (B) Full-length p53's motifs are an N-terminal transactivation domain 1 and 2, an MDM2-binding site, a DNA-binding domain, a tetramerization domain, a C-terminal regulatory domain, and multiple nuclear localization and export signals.

p53 forms homo-tetramers from a dimer of dimers and each monomer consists of a tetramerization domain containing a  $\beta$ -sheet and an  $\alpha$ -helix<sup>21</sup>. Primary dimers are formed by the association of two monomers across an antiparallel  $\beta$ -sheet and antiparallel  $\alpha$ -helix interface and in turn, they form a tetramer through the association across a distinct parallel helix-helix interface<sup>21</sup>. Under normal conditions, p53 protein is found in a mixture of all three oligomeric states; monomers, dimers, and tetramers<sup>22</sup>. The balance between these forms does not simply depend on the concentration of p53 proteins in a cell. p53 tetramerization is triggered upon stress responses, such as DNA damage, without increasing protein concentration, which indicates that stabilization by post-translational modifications and accessory proteins is important for tetramer formation<sup>22</sup>. Moreover, DNA binding domain (DBD) of the p53 protein contains an immunoglobulin-like  $\beta$  sandwich formed by a loop-sheet-helix and two other loops and stabilized by a zinc ion to provide an extended DNA-binding surface<sup>23</sup>. The DBD binds in a sequence-specific manner to a double-stranded DNA containing two copies of a decameric motif separated by variable number of nucleotides. Stable p53-DNA complexes only form when four p53 subunits bind to two half sites<sup>24</sup>.

### 1.1.2.2. Tumor-suppressor pathways downstream of p53

Upon p53 activation, the most noticeable biological outcomes are cell-cycle arrest, apoptosis, and senescence, which are crucial for protecting the host from tumor development. Genotoxic stresses, such as ionizing radiation increase active p53 levels in a cell, which in turn, causes G1/S or G2/M phase arrests or apoptosis if DNA damage is irreparable. These outcomes are a result of p53-mediated transcriptional activation of cell cycle proteins, such as p21 and GADD45 or pro-apoptotic proteins, such as Bax and Puma<sup>25,26</sup>.

p53-mediated cell-cycle arrest is due to the transcriptional activation of the cyclin-dependent kinase inhibitor p21 through the direct binding of p53 to two upstream sites in the p21 promoter. p21, in turn, binds to cyclin E/Cdk2 or cyclin D/Cdk4 complexes and inhibits their phosphorylation of pRb, that results in G1/S arrest. Unphosphorylated pRb protein is a negative regulator of the growth-stimulatory transcription factor, E2F1, which plays a role in DNA synthesis and cell-cycle progression (Figure 1.2)<sup>26,27</sup>. p53 provides chromosomal integrity and damaged-cell survival by arresting the cells at the G1 phase and gives cells time to repair their double-stranded DNA breaks formed after ionizing irradiation<sup>28</sup>. Moreover, p53 activation leads to G2/M arrest through inhibition of Cyclin B/Cdc2 by p21 or through other p53 targets, such as 14-3-3<sup>26</sup>.

Cell-cycle arrest triggered by the activation of p53 is reversible when DNA damage is repaired. However, an excessive division of human fibroblasts leads to chronic p53 activation due to telomere erosion and constitutive DNA damage signaling, which in the end, causes p53-mediated irreversible arrest named replicative senescence. Because knock-down of p21 protects cells from p53-mediated senescence, p53's action on cell-cycle arrest is crucial for this type of senescence<sup>29,30</sup>. Moreover, senescence is considered as an irreversible outcome; however, after inactivation of p53, cells can re-enter the cell-cycle<sup>31</sup>. Although the action of p53 is important for the induction of senescence, activity of several other pathways, such as pRb, NFκB, or mTOR and their cross-talk with the p53 pathway are also required for the cell to choose between reversible cell-cycle arrest and senescence<sup>26</sup>.

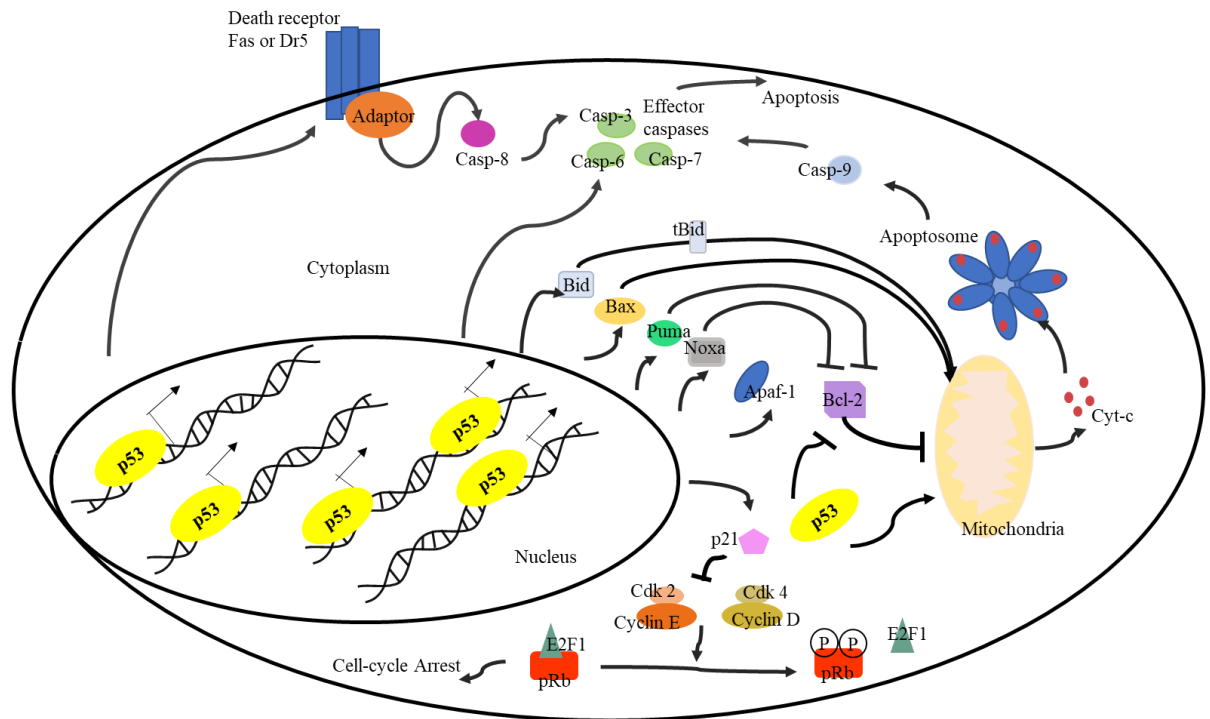


**Figure 1.2. Tumor suppressor pathways of p53.** Upon activation, nuclear p53 decides whether it activates apoptosis or cell cycle arrest related genes. p53 can activate both the intrinsic apoptotic pathway through the transactivation of pro-apoptotic genes and the interaction with mitochondria directly, and the extrinsic apoptotic pathway through the transactivation of death receptor genes. Moreover, p53 can activate cell-cycle arrest mostly through the transactivation of the p21 gene.

Upon p53 activation, certain cell types prefer to undergo apoptosis rather than to arrest the cell-cycle. Among p53's downstream targets, there are various genes playing a role in apoptosis signaling and its execution, which include proapoptotic proteins (Puma, Noxa, Bad, and Bid), death receptors (Fas and Dr5), and execution factors (Apaf1, and caspase 6)<sup>32</sup>. Death receptor induction by p53 activates the extrinsic apoptotic pathway; which involves death receptor dimerization and then activation of procaspase-8, and finally activation of executor caspases (caspase 3 and 7) and cell death, whereas the induction of BH3-only proteins by p53 activates the intrinsic pathway; which causes mitochondrial outer membrane permeabilization due to the pores generated by Bax and Bak, release of cytochrome c, forming apoptosome complex, activation of procaspase-9 and finally activation of executor caspases and cell death. In addition to p53-mediated transcriptional activation of apoptotic mechanisms, p53 can activate apoptosis in a transcription-independent way by directly interacting with Bak and Bcl-2 at the

mitochondria and activating one and inhibiting the other, respectively to lead to the loss of mitochondrial membrane potential and caspase activation, and at the end, cell death (Figure 1.2)<sup>33</sup>.

### 1.1.2.3. Modes of p53 regulation

The classical view of p53 activation consists of three steps; p53 stabilization affected by ATM/ATR-mediated phosphorylation, and subsequent MDM2 dissociation, DNA-binding in a sequence-specific manner, and transcription activation<sup>34,35</sup>. Since there are more than 36 conserved amino acids (serine, threonine, and lysine residues) that have been shown to be modified *in vitro* experiments, p53 post-translational modifications have been thought to play a crucial role in p53 activation<sup>34,35</sup>. However, when this classical mode of p53 activation has been tested in knock-in mutant mouse models, the finding challenged the importance of traditional regulation events<sup>34,35</sup>. For example, phosphorylation of mouse Ser18 or Ser23 after DNA damage by various kinases was thought to stabilize p53 by inhibiting the MDM2 interaction; however, the S18A or S23A point mutant knock-in mouse model showed no difference in stress-induced p53 stabilization between various cells, such as thymocytes and fibroblasts derived from wild-type and mutant mice<sup>36,37</sup>. Although more extreme defects in apoptosis-related p53 function were observed in certain tissues, such as thymocytes of S18/23A double mutant mice, no other tissues or embryonic fibroblasts showed a difference in p53 stability<sup>37</sup>. Because p53 can be activated regardless of whether it is phosphorylated or not, phosphorylation may not be critical for p53 activation, thereby the classical model is not sufficient for explaining every aspect of p53 stabilization<sup>34,36</sup>.

In addition to their role in transcriptional regulation by transferring an acetyl group to a lysine residue on histones, histone acetyltransferases also play an important part in p53 regulation. A histone acetyltransferase, p300/CBP acetylates p53 to recruit cofactors and activates p53 target genes. Moreover, when p300/CBP is localized at target promoter regions, it acetylates histones to make DNA more accessible<sup>38,39</sup>. There are several acetylation sites mostly in the C-terminal domain of p53, but also in the DNA-binding domain and by combinational knockin mutant models, these acetylation events were shown to be essential for p53-related tumor suppression activities<sup>40</sup>. The consequences of lacking p53 acetylation indicate that specific acetylation of different regions of p53 may

be important for cell-fate determination<sup>34</sup>. For example, there is no need for acetylation to activate the *MDM2* gene. On the other hand, activation of apoptosis-related target genes, such as Puma requires p53 modification at multiple sites<sup>34,40</sup>. Methylation, sumoylation and neddylation also occur at specific sites of p53 to contribute p53 promoter specificity<sup>39</sup>.

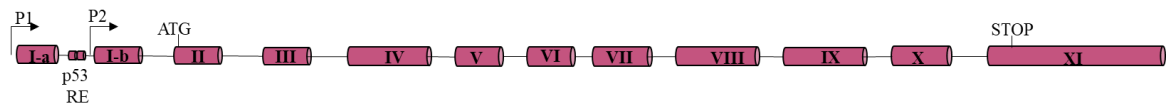
Under stress, post-transcriptionally modified and activated p53 binds to specific target promoter sequences. However, a great proportion of p53 is already bound to DNA in unstressed cells<sup>41</sup>. It is thought that although p53 is capable of binding to DNA under no stress conditions, it is inactive, which is probably a result of repression provided by its antagonists, MDM2 and MDMX. Therefore, it has been proposed that the release of p53 from the inhibition of MDM2/X in the DNA bound form is the significant step for its activation<sup>34</sup>.

### **1.1.3. MDM2 Biology**

#### **1.1.3.1. Gene Structure and Protein Motifs of MDM2**

The *Mdm2* gene was originally identified as an amplified-gene on double-minute chromosomes responsible for the transformation of mouse fibroblasts<sup>42</sup>. The *MDM2* gene is located on chromosome 12q13-14 and consists of 11 exons. It produces various proteins under the control of two different promoters (P1 and P2)<sup>35,43</sup>. Among these two promoters, P2 is the p53-responsive one and from these promoters, the full-length protein of 491 amino acids, p90 is produced (Figure 1.3.A)<sup>43,42</sup>. In many human tumors, the production of short proteins through alternative splicing occurs and it has been reported that the major ones; MDM-A and MDM-B, which lack the p53-binding domain, bind to the full-length MDM2 protein and lead to its sequestration in the cytoplasm<sup>44</sup>. The N-terminal region of the MDM2 protein, where the p53-binding domain resides, binds to the N-terminal transactivation domain of the p53 protein<sup>43</sup>. The MDM2 protein also contains a) nuclear localization and export signals for shuttling back and forth between the cytoplasm and the nucleus, b) the central acidic and zinc-finger domains for interacting with various proteins to induce proteasomal degradation of p53, c) a nucleolus localization signal, and d) a C-terminal RING domain for its E3 ligase activity (Figure 1.3.B)<sup>43,13</sup>.

**A.**



**B.**

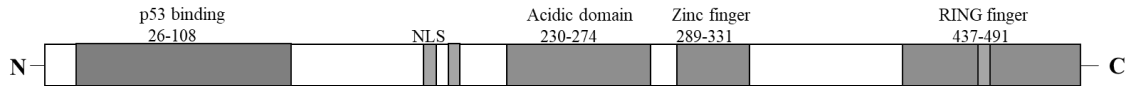


**Figure 1.3. Gene Structure and Protein Motifs of MDM2.** (A) The *MDM2* gene is encoded by 11 exons (2 alternative first exons). It is controlled by two p53 responsive elements in intron 1 and two promoters; P1 and P2 (shown by the arrows). The full-length MDM2 p90 is translated from the first ATG in exon 2. Both promoters can express MDM2 protein, but only P2 is under the control of p53. (B) Full-length MDM2 p90 contains the following motifs: An N-terminal p53-binding domain, nuclear localization and export signals, central acidic and zinc finger domains, a RING domain, and a nucleolus localization signal.

### 1.1.3.2. MDM2-p53 Regulation

Although MDM2 has several other p53-independent roles, its main oncogenic activity depends on its ability to inhibit the tumor suppressor, p53 through direct binding and blocking the transactivation domain of p53 and resulting in the further proteasomal degradation of p53 through E3 ubiquitin ligase activity (Figure 1.4)<sup>42</sup>. Ubiquitination of proteins occurs through a series of steps involving E1, E2, and E3 proteins<sup>45</sup>. First, an E1 enzyme binds to ubiquitin and activates it and then an E2 enzyme accepts that activated ubiquitin and transfers it to the E3 ligase enzyme, which in turn, covalently links this ubiquitin to lysine residues on the target protein<sup>45</sup>. MDM2's RING domain possesses this E3 ligase activity to ubiquitinate both p53 and also itself<sup>43</sup>. It was reported that MDM2 performs monomeric ubiquitination on p53, which does not result in proteasomal degradation. Later, it was found that p300/CBP interacts with MDM2 through its acidic domain to perform polyubiquitination and promotes the degradation of p53 on 26S proteasomes<sup>43,45,46</sup>. It was originally thought that MDM2 targeted p53 to the cytoplasm for degradation through its nuclear export signal (NES); however, it was later reported that only the RING domain that contains the E3 ligase activity, but not the NES is

essential for nuclear export<sup>46</sup>. Current thinking suggests that the nucleus is also a physiological site for p53 degradation, stemming from the observation of p53 degradation in cells treated with a specific nuclear export inhibitor<sup>47</sup>.

During stress responses, many layers of regulation connect MDM2 function to p53 stability and activation. One of the regulators of MDM2 is the tumor suppressor, ARF, which is an alternate reading frame expressed from the INK4a locus and functions as the inhibitor of MDM2-mediated proteasomal degradation of p53<sup>48</sup>. Even though under normal conditions, cellular levels of ARF are kept low, its levels are induced upon oncogenic stress and lead to suppression of cell proliferation by activating p53-mediated cell-cycle arrest or apoptosis. To activate the p53 pathway, ARF binds to MDM2, blocks its shuttling between the cytoplasm and the nucleus, and sequesters it in the nucleolus<sup>48,49</sup>. It is also reported that ARF blocks MDM2's E3 ligase activity to activate p53 (Figure 1.4)<sup>50</sup>.

The other important regulator of MDM2 is MDMX (also known as MDM4), which is another negative regulator of p53. In addition to its role in inhibiting p53-transactivation function by directly blocking its transactivation domain, MDMX can stabilize both p53 and MDM2. MDM2 and MDMX heterodimerize through their RING domains<sup>51,52</sup>. Moreover, MDMX also promotes the E3 ligase activity of MDM2 on p53 and causes an increase in the proteasomal degradation of p53. These findings make it a potential therapeutic target for cancer treatments (Figure 1.4)<sup>52,53,54</sup>.

MDM2 can be also regulated through post-translational modifications. There are multiple sites of phosphorylation and depending on the site and the kinase, phosphorylation can activate or inhibit MDM2's function. For example, ATM or c-Abl phosphorylates Ser395 and Tyr394, respectively to inhibit MDM2's activity<sup>55</sup>. Conversely, activated Akt kinase through PI3K pathway can phosphorylate MDM2 at serine residues 166 and 186 to induce the entry of MDM2 to the nucleus and promote p53 turnover (Figure 1.4)<sup>55</sup>. In addition to phosphorylation, MDM2 is also regulated by acetylation where p300/CBP acetylation inhibits MDM2's activity on p53<sup>56</sup>.

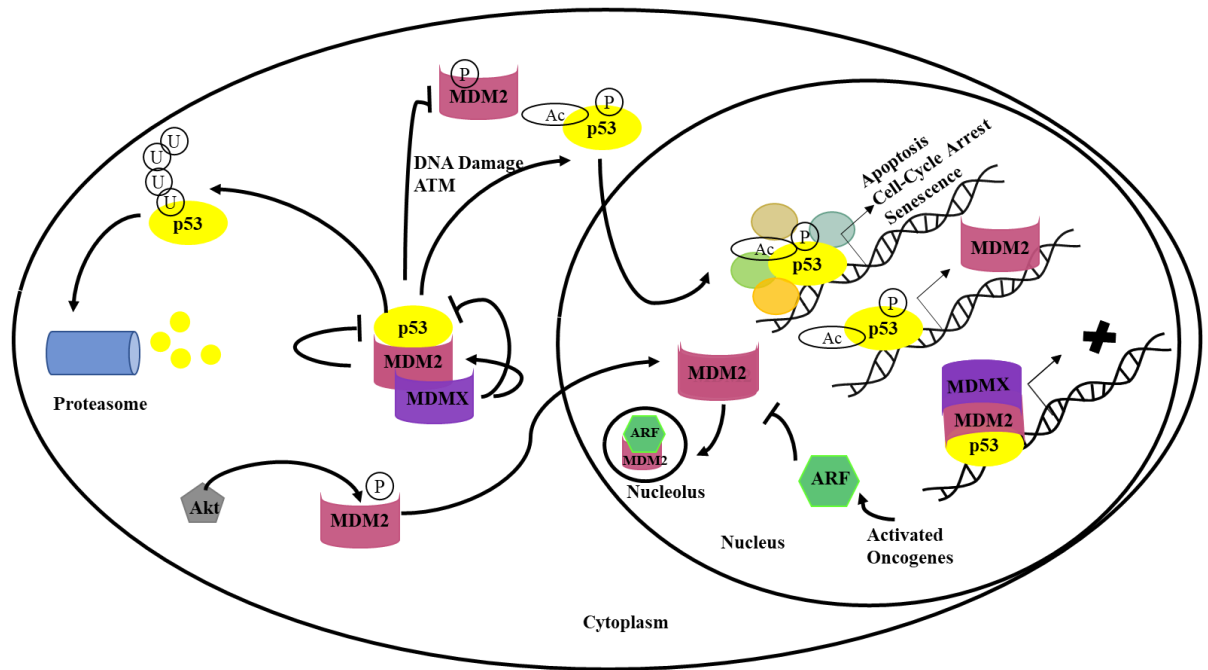


**Figure 1.4. Regulation of the p53-MDM2 pathway.** Under unstressed conditions, p53 protein levels are kept low due to its negative regulators; MDM2 and MDMX, which form heterodimers through their RING domains. MDM2/X binds to p53 to block its transactivation and by MDM2's E3 ligase activity, p53 is ubiquitinated and in turn, degraded in the proteasome. Under stress conditions, such as DNA damage, p53 is acetylated and phosphorylated to escape from MDM2/X inhibition. Later, p53 stimulates expression of its negative regulator, MDM2, and numerous anti-tumorigenic genes. Post-transcriptional modifications of p53 and various cofactors determine the fate of the cell. Moreover, MDM2 is also regulated by various proteins, such as ARF and by post-transcriptional modifications itself, for example, its phosphorylation by Akt.

Current studies suggested that the stabilization and activation by post-translational modifications are not sufficient for p53 activation because p53 needs to escape from the repressed state formed by its negative regulators, MDM2 and MDMX to be fully activated<sup>34</sup>. In addition to the N-terminal MDM2-binding domain, p53 also interacts with MDM2 through both its DNA-binding domain and its C-terminal domain, which indicates that post-translation modifications affecting these interactions can stabilize p53 and release it from repression (Figure 1.4)<sup>34,40</sup>. Different p53-dependent promoters have varying responsiveness to MDM2/X blockage of p53. For example, eliminating the repressed state may be sufficient for some highly responsive target genes, such as cell-cycle arrest genes, whereas for pro-apoptotic genes, in addition to removing the repressed state, some additional post-translational modifications are required<sup>34</sup>. These differences can be observed in the action of the small molecule MDM2 inhibitor, Nutlin-3a, which

can activate the genes functioning in the cell-cycle arrest pathway, but not pro-apoptotic p53 target genes in many tumor-derived cell lines<sup>57</sup>.

#### **1.1.4. Strategies targeting the p53-MDM2 pathway for cancer therapy**

##### **1.1.4.1. Targeting mutant-p53**

In more than 50% of human cancer, p53 is directly altered by a missense mutation, which is mostly located in the DNA-binding domain and rarely in intrinsically disordered regions<sup>58,59</sup>. Cancer-associated mutations in the DBD can be divided into two groups; contact mutations, which lead to the removal of desirable amino acids that interact with DNA, and conformational mutations, which play a role in the disruption of the p53 structure<sup>60,61</sup>. Contact mutations, such as R273C generally remove an interacting side chain from the p53-DNA interface, and they do not change the overall structure and stability of the DBD<sup>61,62</sup>. However, many conformational mutations, such as V143A or Y220C, make p53 unfolded and aggregated at body temperature by disrupting the hydrophobic interactions and lowering the stability of the DBD. These mutant p53 proteins in their folded state have the overall structure of wild-type p53<sup>61,63</sup>. Moreover, mutations causing a loss of the zinc ion, such as R175H, also destabilize the DBD and lead to impaired DNA binding<sup>64</sup>. In addition to DBD domain mutations, mutations in the tetramerization domain occur in human cancer. Although somatic mutations in this domain occur with low frequency, a pH-dependent tetramerization-domain mutation, R337H, is the most prevalent germ-line p53 mutation<sup>58,65</sup>.

Small-molecule stabilizers are designed against structural temperature-sensitive p53 mutants, which have a normal wild-type structure in their folded state<sup>63</sup>. These stabilizers may target a binding surface shared by wild-type p53 or may be mutant-specific targeting the region formed due to the mutation<sup>66,67</sup>. Using virtual screening and rational design, a carbazole-based molecule, PhiKan083 was discovered against the Y220C structural mutant. This mutation of a tyrosine to a cysteine gives rise to an external surface cavity, which in turn, causes the loss of hydrophobic interaction and instability of the DBD. The stabilizer targets specifically this cavity and shifts the protein structure from an unfolded state to a folded one<sup>67</sup>. Later, another Y220C stabilizer, PK7088 was discovered and preliminary results indicate it may cause p53 activation in various human cancer cell lines<sup>63</sup>.

The presence of tumorigenic mutations and the bioavailability of zinc affect the transcriptional activity of p53 because the lack of a coordinating zinc atom leads to the unfolding of the p53 protein<sup>64</sup>. The ZMC1 molecule, which acts as a metallochaperone, was discovered by screening novel compounds. This molecule has the ability to induce growth inhibition and apoptosis in the zinc-binding deficient R175H mutant cells. This metallochaperone increases intracellular zinc levels by transporting zinc ions from the cell membrane and allows the reformation of the unfolded zinc-binding site in these R175H mutant cells<sup>68</sup>.

About 10 percent of somatic p53 cancer mutations result in premature stop codons, which, in turn, leads to the degradation of their mRNAs by nonsense-mediated decay. R196X and R213X are the most frequently observed nonsense mutations in human cancers<sup>69</sup>. It is reported that aminoglycosides, such as gentamicin, which is used in the clinic against various bacterial infections, suppress the effects of premature stop codons and restore the translation of full-length proteins in mammalian cells<sup>70</sup>. For R213X mutant, mRNAs are stabilized after gentamicin treatment and cells can produce the full-length p53 protein, which results in decreased cell-viability<sup>69</sup>.

Gene therapy approaches targeting cancer with mutant p53 for restoring functional p53 have been another investigation area for years. One of the gene therapy strategies is to use a replication-deficient, *TP53* gene-containing adenovirus and introduce it into the tumor directly or into body cavities<sup>71</sup>. For example, one of these adenoviruses, Advexin has been used as a treatment for Li-Fraumeni syndrome, an inherited disorder that has a predisposition to various cancer types, such as sarcomas. Intratumoral injection of Advexin caused complete regression<sup>72,73</sup>. Although adenovirus containing *TP53* gene therapy is safe, feasible and has promising antitumor effects, its clinical efficacy has yet to be demonstrated<sup>11</sup>.

Another gene therapy approach is the Onyx-015 adenovirus, which lacks the *E1B-55K* gene. Viral replication induces p53 due to the expression of viral oncogenes, such as E1A, and the introduction of viral double-stranded DNA. During adenoviral infection, E1B-55K plays a role in degrading p53 and preventing p53-mediated cell-cycle arrest and apoptosis to allow viral replication<sup>74</sup>. Therefore, in normal p53 sufficient cells, the replication of ONYX-015 is restricted due to induced p53, whereas ONYX-015 virus can replicate in p53-mutant tumor cells, which results in the selective destruction of tumor cells<sup>74,75</sup>. Despite its safety, it is reported that ONYX-015 has a limited therapeutic

effect<sup>76</sup>. One of the potential problem for the use of p53 targeting gene therapy is due to the tetramerization domain because wild-type and mutant endogenous p53 proteins can form heterotetramers, which dominantly reduces p53 activity. Swapping the tetramerization domain of p53 with a modified coiled-coil domain of Bcr and generating a chimeric p53 protein was one of the strategies to overcome this problem<sup>77</sup>.

#### **1.1.4.2. Targeting Cancer with Wild-type p53**

In many human tumors containing wild-type p53, MDM2 and MDMX are generally overexpressed to effectively abrogate p53 function. Therefore, inhibiting MDM2 or MDMX interactions with p53 is a promising strategy to activate p53-mediated cell-cycle arrest and apoptosis and, in turn, regress tumor progression<sup>78</sup>. p53 interacts with MDM2 primarily through three hydrophobic pockets interacting with the amino acids; Phe19, Trp23, Leu26, which are well-studied and compact enough to design small molecule inhibitors binding in these pockets to block the p53-MDM2 interaction<sup>79</sup>.

Nutlins, a family of cis-imidazoline analogs, were reported as the first small-molecule antagonists of MDM2 that activate p53 by blocking the N-terminal p53-binding pocket of MDM2<sup>80</sup>. In the initial report, Nutlin-3a was one of the most potent inhibitors and it binds to MDM2 with IC<sub>50</sub>= 90nM and works synergistically with both adenovirus gene therapy and mutant p53 stabilizers<sup>79,63,81</sup>. Further studies have improved Nutlin's binding affinity, cellular potency, pharmacokinetics, and stability. More recent studies have discovered various other classes of small molecules targeting MDM2, such as pyrrolidine-containing compounds, spirooxindoles, and the piperidinone-containing compounds<sup>79</sup>. Structure-based design and extensive structure-activity optimizations resulted in the discovery of AMG 232 and, in turn, its modified version, AM-7209, which are the most selective and potent MDM2 inhibitors to date with the dissociation constants of 257 pM and 38 pM, respectively. They both have remarkable pharmacokinetics and antitumor activity *in vivo* in SJSA-1 osteosarcoma xenograft models. In addition to binding to p53-binding pockets, these compounds capture additional hydrophobic binding interactions and drive refolding of flexible N-terminal lid region of MDM2, which in turn, can achieve higher binding affinities compared to p53 binding<sup>82,83</sup>.

Many of the MDM2 inhibitors lack the ability to bind to MDMX due to the structural differences in their p53-binding pockets. However, because full activation of p53 antitumor pathways requires the inhibition of both MDM2 and MDMX in cancer with wild-type p53, a dual small-molecule targeting both MDM2 and MDMX is necessary<sup>78</sup>. One molecule that has dual activity is RO-5963, which results in homo- and heterodimerization of MDM2 and MDMX p53-binding pockets. In its binding mode, two inhibitor molecules stabilize MDM2 and MDMX by each inhibitor molecule covering the Phe19 pocket of one monomer and the Trp23 pocket of the other monomer<sup>84</sup>. Although it has poorer pharmacological properties compared to Nutlin-3a, it activates p53 pathways in cancer cell lines with both overexpressed MDM2 and MDMX<sup>78</sup>.

p53 has an extensive interactome and related regulatory pathways, which can be used as potential targets for anticancer therapy. For example, histone deacetylase SIRT1, which represses p53-dependent transcription activation, apoptosis and growth arrest by deacetylating Lys382 in the C-terminal regulatory domain of p53. Small-molecule screening for p53 activators resulted in the identification of tenovins, which are the compounds inhibiting these deacetylases<sup>85</sup>. It is reported that SIRT1 is overexpressed in various cancer cell lines, such as chronic myelogenous leukemia (CML) stem cells and SIRT1 inhibition by tenovin-6 in their corresponding mouse models results in selective regression of tumors formed by leukemia stem cells (LSC)<sup>86</sup>.

## **1.2. Genome Editing by Cluster Regularly Interspaced Short Palindromic Repeats (CRISPR)**

In recent years, new genome editing technologies have been developed to manipulate the genome. Among these are Zinc-finger nucleases (ZFNs), Transcription activator-like effector nucleases (TALENs) and most recently CRISPR/Cas9<sup>87,88</sup>. Generally, the manipulation of genomic information at the DNA level requires two major parts; a DNA-binding domain for sequence-specific DNA recognition and an effector domain for executing DNA cleavage<sup>88</sup>. ZFNs and TALENs consist of a transcription factor derived domains for sequence recognition and a nuclease domain derived from a restriction endonuclease for generating double-stranded breaks (DSBs) at the targeted locus. Conversely, the CRISPR/Cas9 system, which is originally an adaptive immune

mechanism present in bacteria and archaea against bacteriophage infection, targets specific DNA sequence by complementary RNA-DNA interactions and generate DSBs with an RNA-guided nuclease, the CRISPR-associated protein 9 (Cas9)<sup>87,88</sup>.

Creating DSBs in the genome by using these genome editing techniques stimulates DNA repair pathways, which in turn, results in two outcomes in the host cell: non-homologous end joining (NHEJ) where insertions and deletions (INDELS) occur at the targeted locus or homology-directed repair (HDR), where desired sequence replacement occurs at the DSB site through homologous recombination using a donor DNA (Figure 1.5.B)<sup>89</sup>. ZFNs and TALENs function by protein-DNA interactions, thereby re-engineering and cloning are required for targeting a new site. However, the CRISPR/Cas9 system requires only the cloning of a 20 nucleotide-long guide RNA sequence into Cas9-producing vector backbone for targeting a new site<sup>87,89</sup>.

The type II CRISPR-Cas9 system is the simplest among the other systems because of its compact enzymatic machinery and easily programmable DNA targeting, therefore it has been the top tool for genome engineering<sup>90</sup>. It simply contains a Cas9 protein and two RNA molecules; crRNA, which is complementary to the recognition site, and trans-activating crRNA (tracrRNA). After Cas9 binds to crRNA and then tracrRNA, it is recruited to the target site and generates DSBs<sup>91,88</sup>. One requirement for Cas9's activity is the existence of a protospacer adjacent motif (PAM) sequence, which is a short recognition motif found in the invading phage genome, but not in the host bacterial genome. The PAM sequence for Cas9 derived from *S. pyogenes* is an NGG at the 3' end of the target sequence and Cas9 cleaves the target DNA 3bp upstream of this PAM sequence<sup>88</sup>. For using this system as a tool, Cas9 was optimized and a single chimeric guide-RNA, which contains fused crRNA and tracrRNA, was formed (Figure 1.5.A)<sup>88,92</sup>. Moreover, new Cas9 homologs from other species, such as Cpf1 and the engineered Cas9 variants were developed, which allows genetic engineers to use various PAM sequences in the desired genome for the precise editing of targeted sequences<sup>88,93</sup>. The CRISPR/Cas9 system can be used for altering genes, generating knock-outs or knock-ins, large deletions or rearrangements, and gene activation<sup>87</sup>.



## 2. AIM OF THE STUDY

The p53 tumor suppressor is the most well-known transcription factor, which plays an important role in the protection from cancer by regulating DNA repair, cell cycle, and apoptosis pathways. In human cancers, p53 is either inactivated by a mutation or suppressed through the abrogation in one of its signaling or regulatory components. Therefore, the p53 pathway has been a primary target for novel cancer drug discoveries. One such approach is targeting the interaction between p53 and its negative regulator, MDM2 for activating the p53 pathway to promote tumor regression. In this project, we screened various compounds using distinct methods for identifying candidates that can block the interaction between the p53 and MDM2 proteins.

In the first part of the project, we aimed to generate a p53<sup>-/-</sup> MDM2<sup>-/-</sup> cell line for the screening of MDM2 targeting compounds. We planned to target the second exon of the *MDM2* gene by CRISPR/Cas9 genome editing system in the HCT116 p53<sup>-/-</sup> cell line to generate random INDEL mutations and shift the open reading frame of the *MDM2* gene. In the absence of these two proteins, the compounds, which are candidates for blocking the p53-MDM2 interaction should not affect the viability of the cell, whereas they should activate the p53 pathways in wild-type cells, and in turn, should result in cell-cycle arrest or apoptosis.

Secondly, we performed a fluorescent two-hybrid (F2H) assay for high-content screening the compounds targeting the p53-MDM2 interaction. In this assay, interacting domains of the p53 and MDM2 proteins were fused to two distinct fluorescent proteins. Interacting p53-MDM2 pairs formed two distinguishable fluorescent signals at the same spot in transfected Baby Hamster Kidney (BHK) cells. Upon the separation of MDM2 from p53, the colocalization of these two fluorescent foci should disappear in real time.

Finally, we wanted to express and purify the interacting domains of p53 and MDM2 proteins in bacteria and performed a surface plasmon resonance (SPR) experiment with the purified proteins for screening MDM2 targeting compounds *in vitro* and determined their effects on the kinetics of the p53-MDM2 interaction. In summary, we aimed to optimize three distinct methods for screening compounds targeting the p53-MDM2 interaction in order to discover novel cancer therapeutics for cancers with wild-type p53.

### 3. MATERIALS & METHODS

#### 3.1. Materials

##### 3.1.1. Chemicals

All the chemicals used in this thesis are given in Appendix A.

##### 3.1.2. Equipment

All the equipment used in this thesis are given in Appendix B.

##### 3.1.3. Solutions and Buffers

Calcium Chloride (CaCl<sub>2</sub>) solution: 60mM CaCl<sub>2</sub>(from 1M stock), 15% glycerol, 10mM PIPES pH 7.0 were mixed, completed to 500ml with ddH<sub>2</sub>O. The solution was sterilized with 0.22μM filter and stored at 4°C.

Agarose Gel: To prepare 100ml 1% w/v agarose gel, 1g of agarose powder was weighed and then dissolved in 100ml 0.5XTBE buffer by heating in a microwave.

Tris-Borate-EDTA (TBE) Buffer: For a 1L 5X stock solution, 54g Tris-Base, 27.5g boric acid, and 20ml 0.5M EDTA pH 8.0 were dissolved in 1L of ddH<sub>2</sub>O. The solution was diluted 1 to 10 with ddH<sub>2</sub>O to reach a working solution of 0.5xTBE.

Phosphate-buffered Saline (PBS): For 1L 1X PBS solution, 100mL 10X PBS was mixed with 900mL ddH<sub>2</sub>O and then 1X solution was filter-sterilized.

Polyethyleneimine (PEI) Solution: For 1mg/ml (w/v) working solution, 100mg polyethyleneimine powder was weighed and dissolved in 100ml of ddH<sub>2</sub>O. Then, the pH of the solution was adjusted to 7.0 by using HCl(33%). Finally, the solution was filter-sterilized and kept at -20°C.

SDS Separating Gel: For 10ml 10% separation gel, 2.5mL 1.5M Tris pH 8.3, 3.34ml Acrylamide: Bisacrylamide (37.5:1), 100μl 10% (w/v) SDS, 100μl 10% (w/v) APS and 10μl TEMED was mixed and the volume was completed to 10ml with ddH<sub>2</sub>O. In this study, in addition to 10% separating gel, 14%, and 18% separating gel were also prepared.

SDS Stacking Gel: For 5ml 4% stacking gel, 1.25ml 0.5M Tris pH 6.8, 1ml Acrylamide: Bisacrylamide (37.5:1), 50µl 10% SDS (w/v), 15µl 10% APS (w/v), and 7.5µl TEMED were mixed and the solution volume was completed to 5ml with ddH<sub>2</sub>O.

SDS Running Buffer: First, 1L 10X Tris-Glycine was prepared by weighing 40g Tris and 144g Glycine and adjusting pH to 8.3. Then, 100ml of 10X Tris-Glycine was mixed with 5ml of 20%(w/v) SDS and the total volume of the solution was completed to 1L.

Transfer Buffer: 100ml of 10X Tris-Glycine pH 8.3, 1.88ml of 20% (w/v) SDS and 200ml methanol was mixed and the volume was completed to 1L. The solution was stored at 4°C.

Protein Loading Buffer: For 4X protein loading buffer, 2.4mL Tris (1M pH 6.8), 0.8g SDS, 4ml glycerol (100%), 0.01% bromophenol blue, and 2ml β-mercaptoethanol were mixed and then the total volume was completed to 10ml.

Blocking Buffer: For 20ml of blocking buffer, 1g of skim milk powder was dissolved in 10ml of PBS-T buffer.

PBS-Tween20 (PBS-T) solution: For 1L 1X PBS-T solution, 0.5mL Tween20 was added in 1L of 1X PBS.

Antibody Dilution Solution: 10g BSA, 0.1g NaN<sub>3</sub> were weighed and added into 200ml PBS-T. The pH of the solution was adjusted to 7.5 and finally approximately 0.1g phenol red was added to the solution.

ECL solution: For a 5ml solution, 4.728ml ddH<sub>2</sub>O, 234µl 1.5M Tris pH 8.3, 25µl 250mM luminol (in DMSO), 12.5µl 90mM coumaric acid (in DMSO) and 1.5µl H<sub>2</sub>O<sub>2</sub> (30%) were mixed.

FACS Buffer: For 500 ml 1X solution, 0.5 g bovine serum albumin (BSA) and 0.5 g sodium-azide were weighed and then mixed in 500 ml 1X HBSS. The final solution was kept at 4°C.

Lysis Buffer: For 50ml 1X lysis buffer, 50mM HEPES, 250mM NaCl, 0.5mM TCEP, 10mM imidazole, EDTA-free protease inhibitor cocktail (Roche), and 10µl DNase I (100U/µl) were mixed and completed to 50ml with ddH<sub>2</sub>O.

Buffer IMAC-A: For 1L IMAC-A solution, 50mM HEPES, 250mM NaCl, and 10mM imidazole were mixed and then the total volume was completed to 1L with ddH<sub>2</sub>O. The

solution was filter-sterilized and stored at 4°C. 0.5mM TCEP was added fresh before using the solution.

Buffer IMAC-B: 50mM HEPES, 250mM NaCl, and desired concentration of imidazole were mixed. The solution was filter-sterilized, and 0.5mM TCEP was added fresh to the solution. The IMAC-B solution was used as the elution buffer of His-tagged affinity chromatography. In this study, IMAC-B with 100mM, 300mM, and 600mM imidazole concentrations were used.

Gel Filtration Buffer: For 1L gel filtration buffer, 20mM HEPES, and 250mM NaCl were mixed. 5mM TCEP or 0.05%  $\beta$ -mercaptoethanol was added to the solution and the volume was completed to 1L with ddH<sub>2</sub>O.

#### **3.1.4. Growth Media**

Luria Broth(LB): For each 1L 1X LB medium, 20g LB powder was weighed and completed to 1L with ddH<sub>2</sub>O. The medium was then autoclaved at 121°C for 15 minutes. After cooling the medium, for antibiotic selection, kanamycin at a final concentration of 50 $\mu$ g/ml, ampicillin at a final concentration of 100 $\mu$ g/ml or chloramphenicol at a working concentration of 34 $\mu$ g/ml was added to the liquid medium.

LB Agar: For each 1L 1X LB-agar medium, 35g LB-Agar already mixed powder was weighed and the mixture was completed to 1L with ddH<sub>2</sub>O. Then, the medium was autoclaved at 121°C for 15 minutes. After cooling down to 50°C, the antibiotic of interest at desired concentration was added. The working concentration of ampicillin, kanamycin, and chloramphenicol was 100 $\mu$ g/ml, 50 $\mu$ g/ml, and 34 $\mu$ g/ml, respectively. Approximately 15ml of LB-Agar solution was poured into a sterile petri dish under bacteria hood. Sterile agar plates were kept at 4°C.

DMEM: HCT116 WT, HCT116 p53<sup>-/-</sup> and BHK cells were maintained in culture in DMEM growth medium supplemented 10% heat-inactivated fetal bovine serum (FBS), 1% PenStrep (100U/mL Penicillin and 100 $\mu$ g/mL Streptomycin).

Freezing Medium: All the cell lines were frozen in heat-inactivated fetal bovine serum containing 10% DMSO (v/v).

Terrific Broth (TB): For 1L 1X TB medium, 47.6g TB powder was weighed, 8ml glycerol was added, and finally the mixture was completed to 1L with ddH<sub>2</sub>O. The medium was autoclaved at 121°C for 15 minutes. When antibiotic selection is required, antibiotics

were added with the desired working concentrations. Kanamycin at a final concentration of 50 $\mu$ g/ml or chloramphenicol at a working concentration of 34 $\mu$ g/ml was added to the liquid medium.

### **3.1.5. Molecular Biology Kits**

All the commercial molecular biology kits used in this thesis are given in Appendix C.

### **3.1.6. Enzymes**

All the restriction and modifying enzymes, polymerases, their corresponding buffers and PCR reaction supplements were obtained from either New England Biolabs (NEB) or Fermentas.

### **3.1.7. Antibodies**

All the antibodies used in this thesis are given in Appendix D.

### **3.1.8. Bacterial Strains**

*Escherichia coli* (*E. coli*) DH-5 $\alpha$  is used for general plasmid amplification and *cloning* applications and *E. coli* Rosetta 2 DE3 expression strain is used for mammalian protein production and purification.

### **3.1.9. Mammalian Cell Lines**

HCT116 and HCT116 p53<sup>-/-</sup>: Human colorectal carcinoma cell line and its p53-null derivative.

BHK: BHK21 cell line was derived from the kidneys of Syrian hamsters. The cell line we used was a modified derivative. Lac operator repeats have been embedded into the genome<sup>94</sup>.

### **3.1.10. Plasmid and Oligonucleotides**

All the plasmids and oligonucleotides used in this thesis study are listed in Table 3.1 and Table 3.2, respectively.

<b>OLIGONUCLEOTIDE NAME</b>	<b>SEQUENCE</b>	<b>PURPOSE OF USE</b>
MDM2-sgRNA-top	CACCGAGGGTCTCTTGTTC CGAAGC	pSpCas9(BB)-2A-Puro cloning
MDM2-sgRNA-bottom	AAACGCTTCGGAACAAGAGACCCTC	pSpCas9(BB)-2A-Puro cloning
Cas9 reverse	TATGTAACGGGTACCTCTAGAGCC	pSpCas9(BB)-2A-Puro sequencing
MDM2-RFLP-Forward	GACGCACGCCACTTTTTCTCT	RFLP analysis
MDM2-RFLP-Reverse	TACGCCAGAGGTAGCACACTT	RFLP analysis
GBP-NheI-Forward	TCAGCTAGCATGGCCGATGTGCA GCTGGT	pcDNA3.1/myc-His(-)B cloning
LacI-BamHI-Reverse	ATTGGATCCTCATCGGGAAACCT GTCGTGC	pcDNA3.1/myc-His(-)B cloning
TagGFP-SmaI-Forward	TGGACCCGGGGTGAGCGGGGGC GAGGAGCT	pET-47(b)+ cloning
P53-NotI-Reverse	GGACGCGGCCGCCTATGTAGG AGCTGCTGGTGCAGG	pET-47(b)+ cloning
MDM2-SmaI-Forward	TGGACCCGGGATGTGCAATACC AACATGTCTGTACC	pET-47(b)+ cloning
MDM2-NotI-Reverse	GGACGCGGCCGCCTAGTGAC ACCTGTTCTCACTCACAG	pET-47(b)+ cloning

**Table 3.1. List of oligonucleotides**

<b>PLASMID NAME</b>	<b>PURPOSE OF USE</b>	<b>SOURCE</b>
pSpCas9(BB)-2A-Puro	The mammalian expression plasmid for the CRISPR/Cas9 system with puromycin resistance gene	Addgene (#48139)
MDM2-pSpCas9(BB)-2A-Puro	Mammalian expression plasmid with MDM2-targeting CRISPR/Cas9 expression and puromycin resistance gene	Lab construct
pcDNA3-GFP	GFP expressing plasmid for transfection control	Lab construct

pcDNA3-flag-p53	The mammalian expression plasmid for human p53 protein expression with N-terminal FLAG-tag	Addgene (#10838)
pcDNA3.1/myc-His (-) B	Mammalian expression plasmid with a CMV promoter	Thermo Fischer Scientific, (V85520)
pcDNA3.1/myc-His (-) B-GBP-LacI	Mammalian expression plasmid with GBP-LacI fusion protein expression for F2H assay	Lab construct
pET-47b (+)	The bacterial expression plasmid for expressing fusion proteins with an N-terminal His-tag	Merck Millipore, (71461)
pET-47b (+)-TagGFP-p53	Bacterial expression plasmid for expressing TagGFP-p53 fusion protein with an N-terminal His-tag	Lab construct
pET-47b (+)-MDM2	The bacterial expression plasmid for expressing the MDM2 protein with an N-terminal His-tag	Lab construct

**Table 3.2. List of plasmids.**

### **3.1.11. DNA and Protein Molecular Weight Markers**

DNA ladder and protein standard used in this thesis are given in Appendix E.

### **3.1.12. DNA Sequencing**

Sequencing analysis services were provided in this study by McLAB, CA, USA. (<https://www.mclab.com/home.php>)

### **3.1.13. Software, Computer-based Programs, and Websites**

Software, computer-based programs, and websites which are used in this thesis are given in Table 3.3.

<b>SOFTWARE, PROGRAM, WEBSITE NAME</b>	<b>COMPANY/WEBSITE</b>	<b>PURPOSE OF USE</b>
CLC Main Workbench v7.9.4	QIAGEN Bioinformatics	Primer design, Molecular cloning, analysis of sequence data, DNA sequence alignment
FlowJo v10	FlowJo, LLC	Flow cytometry data analysis
BD FACSDiva	BD Biosciences	Acquiring flow cytometry data
NCBI BLAST	<a href="https://blast.ncbi.nlm.nih.gov/Blast.cgi">https://blast.ncbi.nlm.nih.gov/Blast.cgi</a>	The basic local alignment tool
Ensembl Genome Browser	<a href="http://www.ensembl.org">http://www.ensembl.org</a>	Human genome sequence information
CRISPR Design, Zhang Lab, MIT	<a href="http://crispr.mit.edu">http://crispr.mit.edu</a>	CRISPR design tools for sgRNA design and off-target analysis
CRISPOR	<a href="http://crispor.tefor.net">http://crispor.tefor.net</a>	CRISPR design tools for sgRNA design and off-target analysis
Addgene	<a href="https://www.addgene.org">https://www.addgene.org</a>	Plasmid map information
RTCA Software 2.0	ACEA Biosciences	Real-time cell growth analysis
UNICORN 7.1	GE Healthcare Life Sciences	Chromatography operation
ExPASy	<a href="https://www.expasy.org/">https://www.expasy.org/</a>	Protein translation and parameter tool
IN Cell Developer software	GE Healthcare Life Sciences	Dot analysis
BIACORE T200 software v3.0	GE Healthcare Life Sciences	Operating and evaluating SPR experiments

**Table 3.3. List of software and computer-based programs and websites.**

## **3.2. Methods**

### **3.2.1. Bacterial Cell Culture**

#### **3.2.1.1. The growth of Bacterial Culture**

*E. coli* DH5 $\alpha$  and Rosetta2 DE3 strain were cultured in LB with desired antibiotic selection for overnight (12-16 hours) at 37°C with vigorous shaking (221rpm). For single bacterial colony, bacterial culture was spread onto LB-Agar plates with antibiotic selection by using glass beads and the plates were incubated overnight at 37°C. For long-term storage, glycerol at a final concentration of 10% (v/v) was added to the bacterial culture for a total volume of 1ml under bacteria hood. Glycerol stocks were stored in cryovials at -80°C.

#### **3.2.1.2. Preparation of competent bacteria**

Previously prepared competent *E. coli* DH5 $\alpha$  was added into 40ml LB in a 250ml flask without adding any antibiotic selection and incubated overnight at 37°C by vigorous shaking (For Rosetta2 DE3, chloramphenicol with a final concentration of 34 $\mu$ l/ml was added). The next day, 4ml of overnight-grown culture was transferred into 400ml LB in a 2L flask without any antibiotics and then the culture was incubated at 37°C with 221rpm shaking until the optical density (OD) of the culture at 590nm reached around 0.375. The 400ml culture was aliquoted into eight sterile 50ml tubes and incubated on ice for 10 minutes. Then, the prechilled bacterial culture was centrifuged at 1600xg for 10 minutes at 4°C. The supernatant was discarded, and each bacterial pellet was resuspended in 10ml ice-cold CaCl<sub>2</sub> solution and then centrifuged at 1100xg for 5 minutes at 4°C. Again, the supernatant was removed, and each bacterial pellet was resuspended in 10ml ice-cold CaCl<sub>2</sub> solution. Cells were kept on ice for 30 minutes and then centrifuged at 1100xg for 5 minutes at 4°C. Bacterial pellets were resuspended in 2ml ice-cold CaCl<sub>2</sub> solution and finally, all the suspensions were combined into one 50ml tube and divided into 200 $\mu$ l aliquots into pre-chilled microcentrifuge tubes, which were immediately flash-frozen in liquid nitrogen at -80°C. Before using them, their transformation efficiency was determined by transforming different concentration of pUC19 plasmid.

### **3.2.1.3. Transformation of competent bacteria**

200µl of frozen competent bacteria were thawed on ice and plasmid DNA at desired amount was added to competent bacteria. Then, the bacteria-DNA mixture was incubated on ice for 30 minutes. Cells were heat-shocked at 42°C for 90 seconds and immediately put back on the ice for 2 minutes. 800µl of LB was added to each tube and competent bacteria were incubated in a water bath already heated to 37°C for 45 minutes. After incubation, they were centrifuged at 13,200rpm for 30 seconds and bacterial pellet was resuspended in 100µl of LB. Finally, cells were spread onto an LB-agar plate with the appropriate antibiotic selection and the plates were incubated at 37°C overnight.

### **3.2.1.4. Plasmid DNA isolation**

Alkaline lysis protocol as described in Molecular Cloning: A Laboratory Manual (Sambrook et al.) was followed for pDNA isolation from *E. coli* DH5α. In addition to alkaline lysis protocol, PureLink HiPure Plasmid Midiprep and ZymoPure Plasmid Maxiprep commercially available kits were applied according to manufacturer's protocols. The acquired pDNA's concentration and purity were analyzed by a NanoDrop spectrophotometer.

## **3.2.2. Mammalian Cell Culture**

### **3.2.2.1. Maintenance of cell lines**

HCT116, HCT116 p53<sup>-/-</sup> and BHK cells were maintained in complete DMEM medium in sterile 10cm tissue culture plates at an incubator set to 37°C and 5% CO<sub>2</sub>. When the cells reached 70-80% confluency, they were split. Cells were washed with serum-free DMEM or 1X PBS and then trypsin was added and incubated at an incubator set to 37°C and 5% CO<sub>2</sub> for 5 minutes. Then, the cells were resuspended in complete DMEM and split to a new sterile 10cm tissue plate at 1:10 ratio. The cells were split every 2-3 days.

### **3.2.2.2. Cryopreservation of the cells**

Cells were split to become 30-40% confluent one day before freezing for HCT116, HCT116 p53<sup>-/-</sup> and BHK cells. In the following day, cells were counted and 1-5x10<sup>6</sup> cells were centrifuged at 300xg for 5 minutes. Cell pellets were resuspended in 1ml freezing medium and put into a cryovial. Cryovials were then transferred into a freezing container

containing isopropanol and placed into a -80°C fridge. For long-term storage, cryovials were transferred into the liquid nitrogen.

### 3.2.2.3. Thawing of frozen mammalian cells

Cryovials were first taken out of liquid nitrogen tank and quickly thawed by diluting it with 9 ml of complete DMEM. Then, cells were centrifuged at 300xg for 5 minutes to get rid of DMSO. The cell pellet was resuspended in fresh complete DMEM, and finally, cells were put into a sterile 10cm tissue culture plate and incubated at 37°C with 5% CO<sub>2</sub>. In the next day, the culture medium was changed to fresh one to check the condition of cells and remove dead ones.

### 3.2.2.4. Transient Transfection of Mammalian Cell Lines using Polyethyleneimine (PEI)

One day before transfection, the required number of cells were seeded depending on the plate type. On the day of the transfection, the desired amount of DNA was mixed with a calculated amount of serum-free phenol red-free DMEM in a sterile microcentrifuge tube. Next, PEI (1µg/µl) solution, which was vortexed well, was added to DNA-DMEM mix (the ratio of PEI (1µg) to total plasmid DNA (µg) should be 3:1 or 5:1). The solution was mixed immediately by vortexing. After incubation at room temperature for 15 minutes, the mixture was added dropwise onto cells. The list of PEI transfection conditions based on plate type is shown in Table 3.4.

Plate Type	Cell number seeded	DMEM amount in which cells were seeded.	Total DNA amount	The DMEM amount in which transfection was performed	PEI: DNA ratio
6-well plate	1-3x10 <sup>5</sup>	2ml	3µg	200µl	1:3 or 1:5
24-well plate	5x10 <sup>4</sup>	500µl	900ng	50µl	1:3
96-well plate	5-10x10 <sup>3</sup>	200µl	300ng	20µl	1:3 or 1:4

**Table 3.4. List of PEI transfection conditions depending on the plate type.**

### **3.2.2.5. Genomic DNA isolation**

PureLink Genomic DNA Mini Kit was followed according to manufacturer's protocol for genomic DNA isolation.

### **3.2.2.6. Cell Lysis, SDS Gel, Transfer, and Western-Blot**

$7.5 \times 10^6$  cells were harvested from their culture plates by using trypsin and then the cells were centrifuged at 300xg for 5 minutes and the supernatant was discarded. The cells were washed with 1X PBS and sedimented again at 300xg for 5 minutes. The pellet was dissolved in 90-120 $\mu$ l of 1XPBS and then the required amount of 4X Laemlli dye was added to make the dye concentration 1X. The mixture was then boiled at 95°C for 10 minutes. The lysates were either stored at -20°C for further use or immediately used. The SDS gels prepared in this study were mostly 10% separating gel and 4% stacking gel. After sample loading, the SDS gels were run with 1X running buffer at a constant voltage of 80V. When the milliamperage value for two gels dropped to approximately 35mA, the voltage was increased until the voltage reached a maximum value of 140V. The gels were run generally for 1.5-2 hours using BIORAD Mini Protean Tetra Cell. After running, the gels were transferred to 0.45 $\mu$ m PVDF membranes in 1X transfer buffer at a constant current of 250mA for 1.5-2 hours at 4°C by using BIORAD Mini Trans-Blot. Then, each membrane was blocked in 10ml of PBS-T with 5% skim milk (w/v) at room temperature for 1 hour with continuous shaking. After washing with 10ml PBS-T for 10 minutes 3 times, primary antibody incubation was done overnight at 4°C with constant shaking. After the previous washing step repeated, secondary antibody incubation was done at room temperature for 1 hour. After the same washing protocol was performed, ECL solution was added onto the membrane and the analysis of membrane was performed by ImageQuant LAS100 Biomolecular Imager.

### **3.2.3. Vector Construction**

#### Restriction enzyme digestion

A digestion reaction, which contains the template DNA, the required enzyme, and its compatible buffer, was incubated for 30 minutes to 2 hours at the optimum temperature depending on the enzyme. Digested DNA was run on an agarose gel for further cloning procedures.

### Dephosphorylation of 5' phosphate groups

Alkaline phosphatase enzyme (calf intestinal alkaline phosphatase, CIP) was used to remove 5' phosphate groups of linearized vectors to prevent recirculation of vector during ligation.

### Agarose gel electrophoresis and DNA purification from the gel

CIP-treated vector DNA or digested insert DNA was run on an agarose gel. Based on the DNA fragment size, 0.7-2% agarose gels were used. The agarose gel with different concentration was prepared by dissolving the desired amount of agarose in 100ml of 0.5X TBE solution and then the solution was heated up by a microwave. After cooling down the solution, 0.0002% ethidium bromide was added. Digested DNA samples were loaded into a solidified agarose gel and electrophoresis was performed with a constant voltage of 100V. When the electrophoresis is done, the desired DNA band was extracted from the gel using a blade under the UV light quickly to minimize the dangerous effects of UV light. Finally, extracted DNA was purified by commercial gel purification kits according to the manufacturer's protocol.

### Ligation

100ng vector DNA was used for ligation reactions with the required amount of insert. The molar ratio of vector to insert should be 1:3. T4 Ligase enzyme (NEB) was used for ligation reactions and the reaction mixture was incubated with the enzyme at 16°C for 16hours or at room temperature for 4 hours. A ligation reaction lacking an insert molecule was also used as a ligation control. The ligation reaction was transformed into competent *E. coli* DH5 $\alpha$ .

## **3.2.4. CRISPR/Cas9 Genome Editing**

sgRNA targeting *MDM2* gene and Cas9 protein expressing pSpCas9(BB)-2A-Puro plasmid was used in this study. The plasmid was transiently transfected into HCT116 p53<sup>-/-</sup> cells.

### **3.2.4.1. sgRNA design and off-target analysis**

The sgRNA was designed by using human genome sequence and possible CRISPR/Cas9 targeting sites on the second exon of the *MDM2* gene was determined by CRISPR design tool (Zhang Lab, [www.crispr.mit.edu](http://www.crispr.mit.edu)) and CRISPOR (<http://crispor.tefor.net/>). The

sgRNA was chosen depending on the highest score provided by these tools and off-target sites of each sgRNA were also considered.

### 3.2.4.2. Phosphorylation and annealing of top and bottom oligonucleotide pairs

sgRNA sequence provided by the tool was synthesized as complementary top and bottom single-stranded oligonucleotides. Flanking ends of the oligonucleotides were compatible with BbsI-digested ends of pSpCas9(BB)-2A-Puro plasmid. First, top and bottom oligonucleotides were diluted to 100 $\mu$ M concentration and then the following reaction was used for annealing reaction:

MDM2-sgRNA Top Oligonucleotide (100 $\mu$ M)	1 $\mu$ l
MDM2-sgRNA Bottom Oligonucleotide (100 $\mu$ M)	1 $\mu$ l
10X T4 Ligase Buffer	1 $\mu$ l
T4 PNK Enzyme	1 $\mu$ l
ddH <sub>2</sub> O	Completed to 10 $\mu$ l

Top and bottom oligonucleotides were annealed in a thermocycler using the following parameters:

37°C	30 minutes
95°C	5 minutes
Ramp down to 25°C	5°C/minute

### 3.2.4.3. pSpCas9(BB)-2A-Puro plasmid digestion and ligation

Digestion of pSpCas9(BB)-2A-Puro plasmid with BbsI enzyme and ligation of the annealed oligo duplex into the digested vector backbone were performed in the same following reaction:

pSpCas9(BB)-2A-Puro Plasmid (100ng)	1 $\mu$ l
Previous annealed oligonucleotide duplex (1:200 dilution)	1 $\mu$ l
10X T4 Ligase Buffer (NEB)	2 $\mu$ l
DTT (10 mM)	1 $\mu$ l
ATP (10 mM)	1 $\mu$ l

BbsI (10,000 U/ml) (NEB)	1 $\mu$ l
T4 Ligase (400,000 U/ml) (NEB)	0.5 $\mu$ l
ddH <sub>2</sub> O	Completed to 20 $\mu$ l

The reaction was incubated in a thermocycler at the following conditions:

37°C	5 minutes
21°C	5 minutes
Go to step 1	5 times

The reaction mixture was then incubated with an exonuclease:

Previous reaction mixture	20 $\mu$ l
10X Buffer 4 (NEB)	3 $\mu$ l
ATP (10 mM)	3 $\mu$ l
Exonuclease V (10,000 U/ml) (NEB)	1 $\mu$ l
ddH <sub>2</sub> O	To 30 $\mu$ l

Incubate the reaction at the following conditions:

37°C	30 minutes
70°C (for inactivation)	30 minutes

This final reaction mixture was finally transformed into *E. coli* DH5 $\alpha$  competent bacteria.

#### **3.2.4.4. Transformation of pSpCas9(BB)-2A-Puro**

The final ligated and exonuclease-treated reaction mixture was transformed into *E. coli* DH5 $\alpha$  competent cells and when single bacterial colonies were obtained, several single colonies were picked and their pDNAs were isolated. The cas9-reverse primer was used for sequencing and sequencing services of MDM2-pSpCas9(BB)-2A-Puro plasmid was provided by McLAB, CA, USA.

#### **3.2.4.5. Transfection with Cas9 expressing plasmids**

HCT116 p53<sup>-/-</sup> cells were transiently transfected with MDM2-pSpCas9(BB)-2A-Puro according to PEI transfection protocol. The pcDNA3-GFP plasmid was used as a transfection control and for optimizing the transfection efficiency, which was analyzed based on GFP expression 36 hours after transfection. On the next day after transfection, cells medium was changed to a medium containing 1µg/µl puromycin to enrich the concentration of cells containing Cas9 plasmid. Puromycin selection continued for 3 days.

#### **3.2.4.6. Flow Cytometry**

To determine the transfection efficiency of HCT116 p53<sup>-/-</sup> cell line transfected with pcDNA3-GFP, flow cytometry technique was performed. 36 hours after transfection pcDNA3-GFP transfected cells were washed and resuspended in FACS buffer. Cells then were acquired by BD FACS Canto and finally analyzed by FlowJo software.

#### **3.2.4.7. Preparation of clonal cell lines**

After puromycin selection, single cell clones were generated by limiting dilution. First, cells were counted and diluted in complete DMEM medium to reach a final concentration of 0.3-0.5cells per 200µl for each well of 96-well plate. Cells were expanded for 2-3 weeks. When the cell number of a single cell clone reached 2-3millions, its genomic DNA was isolated, and it was frozen for further processes.

#### **3.2.4.8. Determination Genome Targeting Efficiency**

##### Restriction Fragment Length Polymorphism (RFLP) assay

First, a PCR reaction was performed by using genomic DNAs of single cell clones and all the required PCR additives. PCR reaction was performed according to Phusion DNA Polymerase (NEB) protocol. Then, the half of the PCR product was further digested with a restriction enzyme, BsaI or AluI for 2hours at 37°C. Each PCR product and its digested product were run on a 1% agarose gel side-by-side and RFLP results were used for the identification of mutant single cell clones. If the recognition sites of BsaI or AluI were disrupted, it was expected to see a clear uncut band.

### Sequencing of PCR products from genomic DNA of single cell clones

Mutations at the site of double-stranded breaks introduced by Cas9 enzyme was analyzed by sequencing. 380bp-region covering the second exon of the *MDM2* gene was amplified for each desired single cell clone by PCR. Then, blunt-end PCR product was cloned into pCR4-Blunt-TOPO vector backbone (Zero Blunt TOPO PCR Cloning Kit for Sequencing) according to the manufacturer's protocol. The ligated product was transformed into *E. coli* DH5 $\alpha$  competent cells. Plasmid DNA was isolated from single bacterial colonies and finally sequenced.

#### **3.2.4.9. Determination of Cell Viability by MTT assay**

One day after seeding  $1 \times 10^4$  cells into each well of 96-well plate, the medium was changed to the medium with compounds. The cells were treated with compounds for 72 hours. Next, cell viability was determined using Cell Proliferation Kit I (MTT) according to the manufacturer's protocol.

#### **3.2.4.10. Real-Time Cell Growth**

Cell proliferation was measured in real time with xCELLigence RTCA DP system. First, 10,000 cells were seeded in each well of an E-Plate VIEW 16 and then incubated inside the xCELLigence station at an incubator set to 5% CO<sub>2</sub> and 37°C. The cell index was monitored every 15 minutes for at least 5 days. Medium only wells were also included in the experiments as a negative control. The experiments were performed as triplicates.

#### **3.2.5. Fluorescent two-hybrid (F2H) assay**

##### **3.2.5.1. pcDNA3.1/myc-His(-)B-GBP-LacI Vector Construction**

pcDNA3.1/myc-His (-) B mammalian expression vector was selected since it had NheI and BamHI recognition sites in the correct order. GFP-binding protein(GBP)- LacI fusion protein was obtained from Platf-p53-Mdm2 mixture (Chromotek) by PCR by using Phusion Polymerase (NEB) according to the following reaction conditions:

5X Phusion GC Buffer (NEB)	5 $\mu$ l
10 mM dNTPs	0.5 $\mu$ l
10 $\mu$ M forward primer (GBP-NheI-forward)	1.25 $\mu$ l
10 $\mu$ M reverse primer (LacI-BamHI-reverse)	1.25 $\mu$ l

Template DNA (1ng)	1 ul
Phusion HF DNA Polymerase (2,000 U/ml) (NEB)	0.25 $\mu$ l
ddH <sub>2</sub> O	To 25 $\mu$ l

For cloning of the insert, forward primer with NheI and a reverse primer with BamHI recognition site was used for PCR amplification. Then, PCR product was cleaned up by NucleoSpin Gel and PCR Clean-up kit and cloned into pCR4-Blunt-TOPO vector backbone using Zero Blunt TOPO PCR Cloning Kit for Sequencing according to manufacturer's protocol. The ligated vector was then transformed into *E. coli* DH5 $\alpha$  competent cells. Single bacterial colonies were picked and their pDNAs were isolated. After confirming whether the pDNAs had the insert or not, one of the positive pDNA was selected for further steps. To construct the vector, pcDNA3.1/myc-His (-) B vector and pCR4-Blunt-TOPO- GBP-LacI were digested with NheI-HF and BamHI-HF enzymes (NEB) for 2hours by using a thermocycler.

	Insert	pcDNA3.1/myc-His (-) B
DNA	2ug	2ug
CutSmart Buffer (NEB)	5 $\mu$ l	3 $\mu$ l
NheI-HF (20,000 U/ml) (NEB)	1 $\mu$ l	1ul
BamHI-HF (20,000 U/ml) (NEB)	1 $\mu$ l	1 $\mu$ l
ddH <sub>2</sub> O	To 50 $\mu$ l	To 30 $\mu$ l

The digested vector was then incubated at 37°C for 30 minutes with CIAP enzyme (Fermentas) for dephosphorylation of 5' ends.

Double-digested vector	30 $\mu$ l
10X CIAP Buffer (Fermentas)	5 $\mu$ l
CIAP Enzyme (20,000U/ml) (Fermentas)	3 $\mu$ l
ddH <sub>2</sub> O	To 50 $\mu$ l

Afterward, the digested and CIAP-treated vector and the insert were run on a 1% agarose gel for the separation of digested DNA bands from uncut ones. The correct insert and vector DNA bands were extracted from the gel and then the extracted DNA was purified

by NucleoSpin Gel and PCR Clean-up kit. Insert to vector molar ratio was 3:1 for setting up the ligation reaction. After transforming the ligation mixture into DH5 $\alpha$  competent cells, single colonies were picked and their pDNAs were isolated. After the control digestion with selected enzymes with their appropriate conditions and buffers, positive colonies were selected and sequenced.

### **3.2.5.2. PEI transfection of F2H-assay plasmids and Compound Treatment**

On the day before transfection, depending on the type of tissue culture plate, BHK cells were seeded. On the day of transfection, equal amounts of three plasmids; TagGFP-p53, TagRFP-MDM2, and pcDNA3.1/myc-His(-)B-GBP-LacI, were transfected into BHK cells. 16-24 hours after transfection, culture media was changed to that with the desired amounts of compounds.

### **3.2.5.3. Live Cell Imaging**

After compound treatment, culture plates were placed into live cell imaging microscopy (IN cell analyzer 2500S). Several regions were selected for each well for each drug and pictures of each region was snapped with 10-20 minutes intervals using GFP and RFP channels. Each experiment lasted for 3-4 hours. The results were analyzed using IN Cell Developer software.

## **3.2.6. Protein purification**

### **3.2.6.1. Vector Construction**

pET-47b (+) bacterial expression vector with an N-terminal His-tag was used as vector backbone. TagGFP-p53 and MDM2 inserts were obtained as PCR products by using Phusion Polymerase (NEB) according to its suggested reaction conditions. For the amplification of inserts, the forward primers with SmaI and the reverse primers with NotI recognition site were used. Since NotI-HF and SmaI enzymes were not worked in Phusion GC buffer, PCR Clean-up was performed before digesting the PCR products. Appropriate annealing temperature was determined by performing a gradient PCR. PCR reactions were performed in a thermal cycler by using Phusion polymerase according to the following reaction:

5X Phusion GC Buffer (NEB)	5 $\mu$ l
10 mM dNTPs	0.5 $\mu$ l
10 $\mu$ M forward primer (TagGFP-SmaI-forward or MDM2-SmaI-forward)	1.25 $\mu$ l
10 $\mu$ M reverse primer (p53-NotI-reverse or MDM2-NotI-reverse)	1.25 $\mu$ l
Template DNA (1ng)	1 $\mu$ l
Phusion HF DNA Polymerase (2,000 U/ml) (NEB)	0.25 $\mu$ l
ddH <sub>2</sub> O	To 25 $\mu$ l

To construct the vector, first, we digested vector backbone and inserts with SmaI at 25°C for 2 hours and then with NotI-HF at 37°C for 30 minutes.

	Insert	pET-47b (+)
DNA	PCR product	2 $\mu$ g
CutSmart Buffer (NEB)	5 $\mu$ l	3 $\mu$ l
SmaI (20,000 U/ml) (NEB)	1 $\mu$ l	1 $\mu$ l
NotI-HF (20,000 U/ml) (NEB)	1 $\mu$ l	1 $\mu$ l
ddH <sub>2</sub> O	To 50 $\mu$ l	To 30 $\mu$ l

Then, the digested pET-47b (+) vector backbone was treated with CIAP enzyme (Fermentas) to block recyclization of vector backbone.

SmaI and NotI-HF digested pET-47b (+)	30 $\mu$ l
10X CIAP Buffer (Fermentas)	5 $\mu$ l
CIAP Enzyme (20,000U/ml) (Fermentas)	3 $\mu$ l
ddH <sub>2</sub> O	To 50 $\mu$ l

The CIAP enzyme was incubated at 37°C for 30 minutes and then digested vector was run on a 1% agarose gel to separate the double-digested vector from the uncut one. The correct band was extracted from the gel and its DNA purified. For the digested insert, the reaction mixture was cleaned up by using NucleoSpin Gel and PCR Clean-up. The ligation reaction was performed according to 3:1 insert to vector ratio by using general ligation method. After transforming ligation reaction into *E. coli* DH5 $\alpha$  competent cells, single bacterial colonies were picked and their pDNAs were isolated. After checking

whether ligation worked or not by performing control digestions, correct pDNAs were sequenced.

### 3.2.6.2. His-tagged protein expression

pET-47b (+) plasmid contains all the features for protein expression and purification; T7 promoter, lac operator, LacI gene, N-terminal His-tag, 3C protease recognition site, and finally kanamycin resistance gene for selection. LacI generally binds to lac operator and blocks the transcription of the protein from the T7 promoter; however, when IPTG is added to the medium, it competes with LacI and removes the blockage. N-terminal His-tag was necessary for affinity chromatography and 3C protease recognition site was useful when N-terminal His-tag required to be removed.

pET-47b (+)-TagGFP-p53 and pET-47b (+)-MDM2 plasmids were first transformed into the expression strain of *E. coli*, Rosetta2 DE3, which is the derivate of BL21 strain and designed to express eukaryotic proteins containing codons rarely used in bacteria. This strain supplies tRNAs for rare codons and their native promoters on a plasmid containing chloramphenicol resistance gene. DE3 represents that the strain is a lysogen of  $\lambda$ DE3, which means a prophage exists as DNA expressing T7 RNA polymerase gene under the control of the lacUV5 promoter and protein production takes place when the Rosetta2 DE3 cells are induced with IPTG.

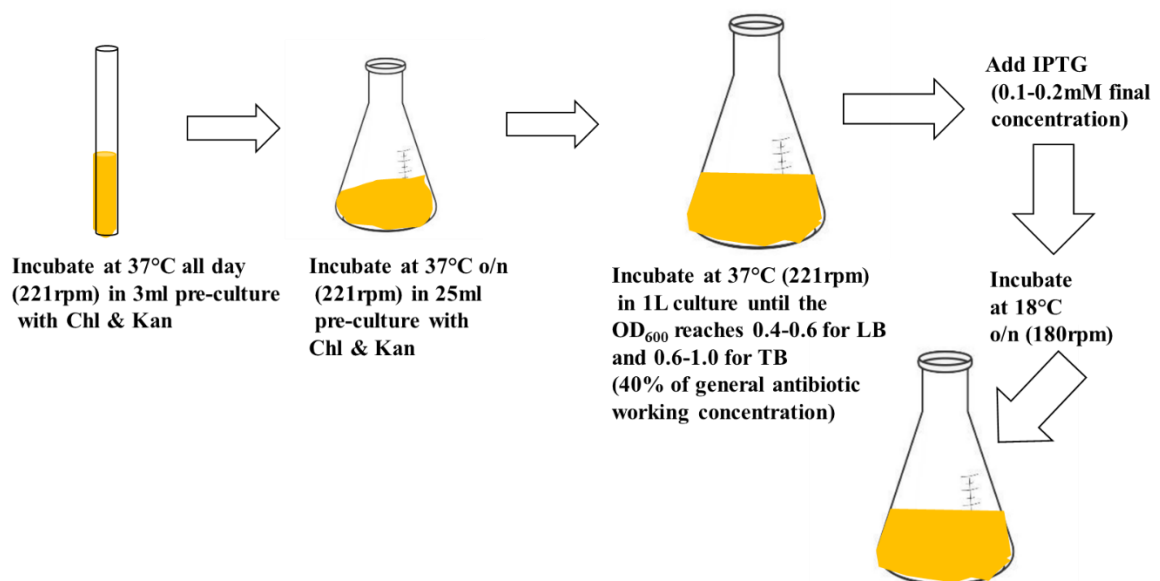


**Figure 3.1. Bacterial expression and induction of His-tagged proteins.**

After transformation, a single colony was picked and inoculated into 3ml LB containing selecting antibiotics (Chl and Kan). After incubating 3ml pre-culture at 37°C for 6-8 hours (221rpm), the pre-culture was transferred to 25ml LB culture with the desired concentration of antibiotics and incubated overnight at 37°C (221rpm). Finally, 25ml pre-culture was transferred to 1L LB or TB medium with 40% of general antibiotic concentration and 1L culture was incubated at 37°C (221rpm) until the optical density at 600nm reached 0.4-0.6 for LB and 0.6-1.0 for TB. In this step, antibiotic concentration dropped to 40% of their general working concentration to decrease the resistance on the cells and promote growth and protein production at further steps. IPTG was added to the culture with a final concentration of 0.1-0.2mM and the protein induction was performed by incubating the culture at 18°C overnight in a shaker incubator (180rpm) (Figure 3.1).

### **3.2.6.3. Affinity chromatography of His-tagged proteins**

Cells were harvested at 2700xg for 15 minutes and the supernatant was discarded. Afterward, the bacterial pellet was dissolved in 25ml of lysis buffer and the cells were lysed at 4°C in a box full of ice by sonication using Qsonica Q500. For sonication procedure, total elapsed time was 6 minutes and 30 seconds, and pulse was on for 5 seconds and off for 10 seconds. The cell lysate was then centrifuged at 27,000xg for 45 minutes at 4°C.

Meanwhile, the column was washed with ddH<sub>2</sub>O and then with 20% EtOH and finally with ddH<sub>2</sub>O again. For the cell lysate coming from 1L culture, 3ml HisPur Cobalt Superflow Agarose was added onto the column. Since the resin solution was diluted 1:1 in EtOH, 1.5ml actual resin was added. The resin was first washed with ddH<sub>2</sub>O 2 times to remove EtOH and then washed with 10ml of IMAC-A 2 times for equilibration. When the centrifuge is finished, the supernatant, which contains soluble proteins, was poured into the column and resin-protein mixture was incubated with end-to-end rotation for 30 minutes at 4°C.

After incubation is finished, the flow-through was collected in a 50ml tube and stored at 4°C for further analysis. This flow-through was named non-retained fraction since it was generally composed of proteins lacking His-tag. Then, the resin-protein complex was washed with 10ml of IMAC-A three times. Finally, the His-tagged protein was eluted using IMAC-B solutions with different concentrations. With starting from the lowest one, the concentration of imidazole was increased and the elution with the same concentration

was performed at several cycles. The elutes of each imidazole concentration was collected in the same 15ml tube and stored at 4°C (Figure 3.2).

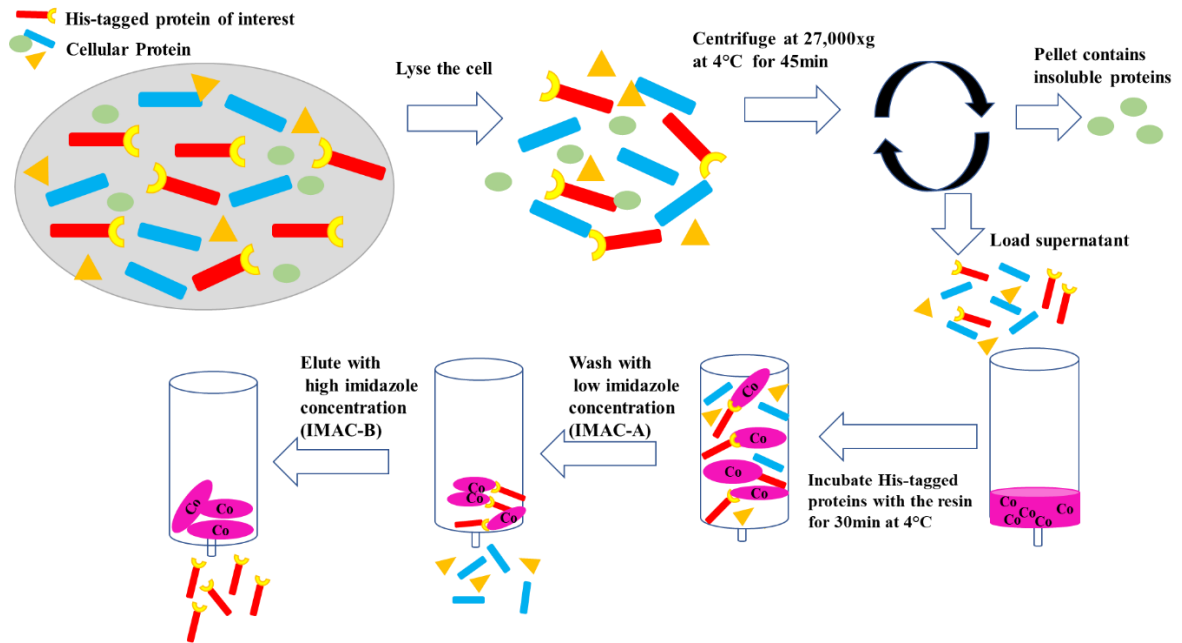


**Figure 3.2. Affinity chromatography steps of His-tagged proteins.**

#### 3.2.6.4. SDS-PAGE gel and Coomassie Blue Staining

14% separating gel and 4% stacking gel were poured and the samples from each step of protein purification; sonicated cell lysate, pellet, non-retained fraction and elutes were mixed with 4X protein loading buffer and denatured at 95°C for 10 minutes. After the samples were loaded into the gel, it was run with 1X running buffer for 2-2.5 hours.

When the run was over, the gel was removed from the glasses. The stacking part was also discarded. Then, the gel was put into Coomassie staining solution and heated up by using a microwave. The gel was incubated in the staining solution for 2-3 hours and then the staining solution was changed to the destaining solution. The gel was incubated in the destaining solution overnight.

#### 3.2.6.5. Concentrating Protein

If the protein is too diluted, concentrator tubes with a specific molecular weight cut-off were used to concentrate the protein. If the protein's size is smaller than the cut-off value, it will pass to the bottom part. First, ddH<sub>2</sub>O was added into the concentrator falcon and

centrifuged at 3000xg until the all the water passed. Then, the protein was added and centrifuged for 1 minute and the concentration of the protein was measured by Nanodrop. The liquid passed to the bottom part was used as a blank. Concentrator falcon was centrifuged for several rounds at 3000xg until the protein concentration or the volume reached desired values. Concentrator tubes used in this study had 10kDa or 5kDa MWCO.

#### **3.2.6.6. Size-exclusion chromatography**

If the protein eluted after His-tag affinity chromatography had other non-specific proteins, size exclusion chromatography was performed to separate the desired protein from non-specific ones by their size. AKTA pure was used for size exclusion chromatography with a HiLoad 16/60 Superdex p75 column. Gel Filtration buffer was used to equilibrate the column; however, before equilibration, firstly the pumps and the column were washed with autoclaved filtered ddH<sub>2</sub>O with at least 1 column volume (CV). Afterward, the column and the system were equilibrated with at least 1.5 CV of Gel Filtration Buffer before starting the experiment. To inject the protein sample to AKTA pure, its volume should be lower or equal to 1ml. Therefore, size exclusion chromatography was performed after concentrating the protein. For injecting the sample, first, the loop was washed with 10ml Gel Filtration Buffer by using a syringe. Then, the protein sample was injected into the loop with a syringe and the experiment started. After protein passed in front of a UV detector, they were collected in a 96-well collector plate. There was 1ml buffer in each well and depending on the UV absorbance at 280nm the desired protein's location was determined later. After selecting the samples from different peak positions of UV absorbance graph, the samples were loaded in the SDS-PAGE gel to determine which samples had the pure desired protein and what the boundaries of purity were.

#### **3.2.6.7. Dialysis**

To provide buffer exchange and remove contaminants with a new buffer composition, we used Slide-A-Lyzer Dialysis Cassette G2. This dialysis cassette has a semipermeable membrane with 10kDa protein MW cut-off. After the addition of sample into the cassette, it floated inside a beaker containing the desired buffer. The beaker should contain 300 times more amount than the sample amount added inside the cassette. After dialyzed for 2 hours at 4°C, the buffer was changed and waited for another 2 hours at 4°C. After

changing the buffer again, it was dialyzed overnight at 4°C. Finally, the sample was removed from the cassette using a syringe.

### **3.2.6.8. 3C Protease Digestion and GST pull-down**

3C 'Prescission' protease was used to remove His-tags for further steps. In pET-47b (+) plasmid, after His-Tag sequence and before the protein sequence, there was 3C protease recognition sequence, which was LEVLFQGP. When 3C protease recognizes this sequence, it digests between Q and G. Therefore, after 3C digestion, two amino acids (GP) are left in the final polypeptide sequence. 100µl of 3C protease (2mg/ml) was added into 1ml of the concentrated protein in a 1.5ml Eppendorf tube and the mixture was incubated overnight at 4°C with end-to-end rotation. After digestion, SDS-PAGE (18%) was performed to check whether the enzyme worked or not.

3C 'Prescission' protease had a GST-tag, and therefore GST pull-down was performed to remove the enzyme and eliminate the risk of nonspecific degradation of our protein. First, the desired amount of Glutathione Sepharose 4 Fast Flow was added into a 1.5ml Eppendorf tube and sedimented at 500xg for 5 minutes at 4°C. After removing the supernatant carefully, 5 ml 1X filtered PBS for each 1ml original slurry was added for washing and the mixture was sedimented at 500xg for 5 minutes at 4°C. After repeating the washing step, the protein-enzyme containing mixture was added onto the Glutathione Sepharose 4 Fast Flow and they were incubated for 2 hours at 4°C with end-to-end rotation. Then, the mixture was sedimented at 500xg for 5 minutes at 4°C and the supernatant, which contained the digested protein was collected into a 1.5ml Eppendorf tube carefully. After three washing steps, 3C protease was eluted with a buffer containing 50mM Tris-HCl and 10mM reduced glutathione pH 8.0 for further analysis.

### **3.2.6.9. His pull-down**

To remove the free His-tags formed after digestion and eliminate the undigested His-tagged proteins, His pull-down was performed by using HisPur Cobalt Superflow Agarose. First, the desired amount of HisPur Cobalt Superflow Agarose resin was added into a 1.5ml Eppendorf tube and centrifuged at 700xg for 2 minutes at 4°C. After removing the supernatant carefully, IMAC-A buffer with a greater volume than the resin bed volume was added onto the resin and centrifuged at 700xg for 2 minutes at 4°C. After repeating the washing steps once more, the protein sample added onto the resin and the

mixture was incubated at 4°C for 0.5-1 hour with end-to-end rotation. When the incubation was finished, the mixture was centrifuged at 700xg for 2 minutes at 4°C. The supernatant was removed carefully and collected in a 1.5ml Eppendorf tube. After washing 3 times with IMAC-A buffer and eluting with the desired amount of IMAC-B buffer, the eluted content was analyzed in the SDS-PAGE gel.

### **3.2.7. Surface Plasmon Resonance**

We performed our surface plasmon resonance (SPR) experiments by using BIACORE T200. Our experiment design required a chip that was able to capture His-tagged proteins. Therefore, we preferred Series S Sensor Chip NTA. The surface of this chip contained a carboxymethylated dextran matrix consisting of nitrilotriacetic acid (NTA), which was used to immobilize nickel to the chip. Since nickel had an affinity for His-tags, after immobilizing nickel on the chip, His-tagged proteins could be captured. 1X PBS containing 0.05% P-20 and 50µM EDTA was used for running buffer to prime the chip and the system. Moreover, all the proteins and certain chemicals were diluted in this buffer. First, the conditioning step was performed with a regeneration solution containing 350mM EDTA to remove nickel and all immobilized molecules from the surface. The flow rate of this step was 30µl/min and the contact time was 1 minute. Then, 0.5mM NiCl<sub>2</sub> in running buffer was used with a flow rate of 10µl/min for 1 minute for activating the surface. After activating the chip, 0.6-2.0µg/ml His-tagged protein was passed on the chip. Contact time for capturing ligand was 1 minute and the flow rate was 10 µl/min. Next, for binding assay, analyte was passed with varying concentrations with a flow rate of 30µl/min for 2 minutes on the chip with immobilized His-tagged protein. For regeneration, again 350mM EDTA solution was used to start over a new experiment. Between the steps, if necessary a washing step was also performed by using 3mM EDTA solution with a flow rate of 30µl/min.

## 4. RESULTS

### 4.1. Generation of the p53<sup>-/-</sup> MDM2<sup>-/-</sup> Cell Line for Testing the Activity of Compounds

#### 4.1.1. CRISPR/Cas9 targeting the Human *MDM2* gene

In this study, we aimed to screen compounds that disrupt the interaction between p53 and MDM2 proteins. To test the specificity of these compounds, we wanted to screen them in the absence of these two targeted proteins. For this reason, we intended to knock out the *MDM2* gene through CRISPR/Cas9 genome editing in the HCT116 p53<sup>-/-</sup> cell line for the generation of a p53<sup>-/-</sup> MDM2<sup>-/-</sup> double knock-out cell line. It was expected that after the introduction of a double-stranded break by the Cas9 enzyme, the break repaired through non-homologous end joining (NHEJ) system would result in INDEL mutations that could shift the open reading frame of the *MDM2* gene. We designed an sgRNA, which targeted the second exon of the *MDM2* gene because this region was present in all alternatively spliced transcripts of the *MDM2* gene (Figure 4.1).

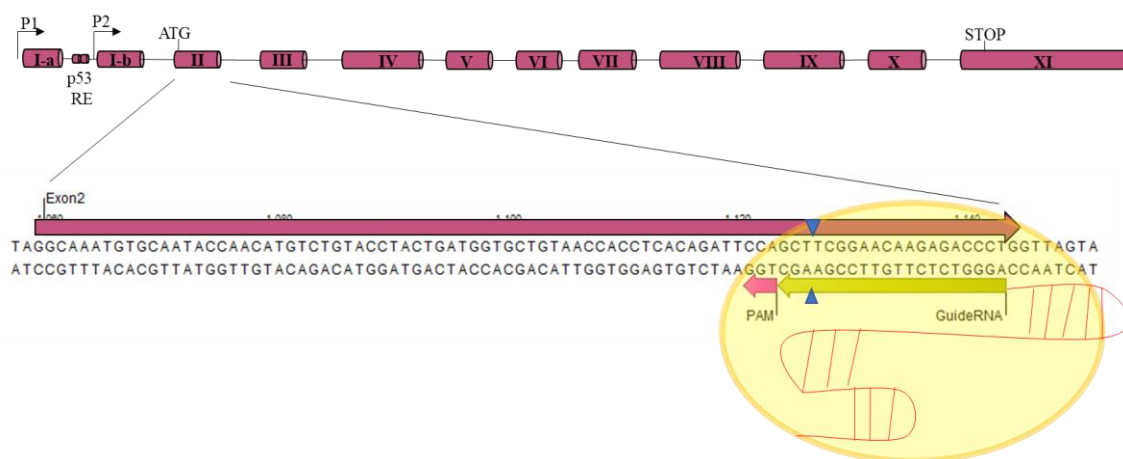


**Figure 4.1. MDM2-sgRNA design.** The sgRNA (yellow) targeted 3' ends of the second exon of the *MDM2* gene (purple). DSB (blue arrows) occurred 3bp upstream of PAM sequence (pink).

First, we annealed oligonucleotides that encode the top and bottom stands of the guide RNA and cloned that oligo duplex into the pSpCas9(BB)-2A-Puro backbone. This constructed CRISPR/Cas9 vector containing guide RNA was verified by sequencing and it

was transfected into the HCT116 p53<sup>-/-</sup> cell line by PEI transfection. Appropriate transfection conditions were determined by using a preexisting GFP-encoding plasmid, pcDNA3-GFP and by optimizing DNA amount and DNA to PEI ratio. For transfection efficiency, the expression of GFP was assessed 36 hours after transfection. For a 6-well plate, the highest transfection efficiency was 39% obtained with 3 $\mu$ g DNA and 1:5 DNA to PEI ratio, so the further transfection of MDM2-pSpCas9(BB)-2A-Puro was performed using this condition. Later, we initiated puromycin selection 24 hours after transfection and aimed to enrich the cell population containing the CRISPR/Cas9 plasmid. After three consecutive days of puromycin selection, we removed the selection to minimize the off-target effects of the Cas9 enzyme. This pool of transfected cells theoretically contained four different types of cells; wild-type cells, heterozygous mutants, and homozygous mutants, which have the same mutation on both allele or different mutation on each allele (Figure 4.2).

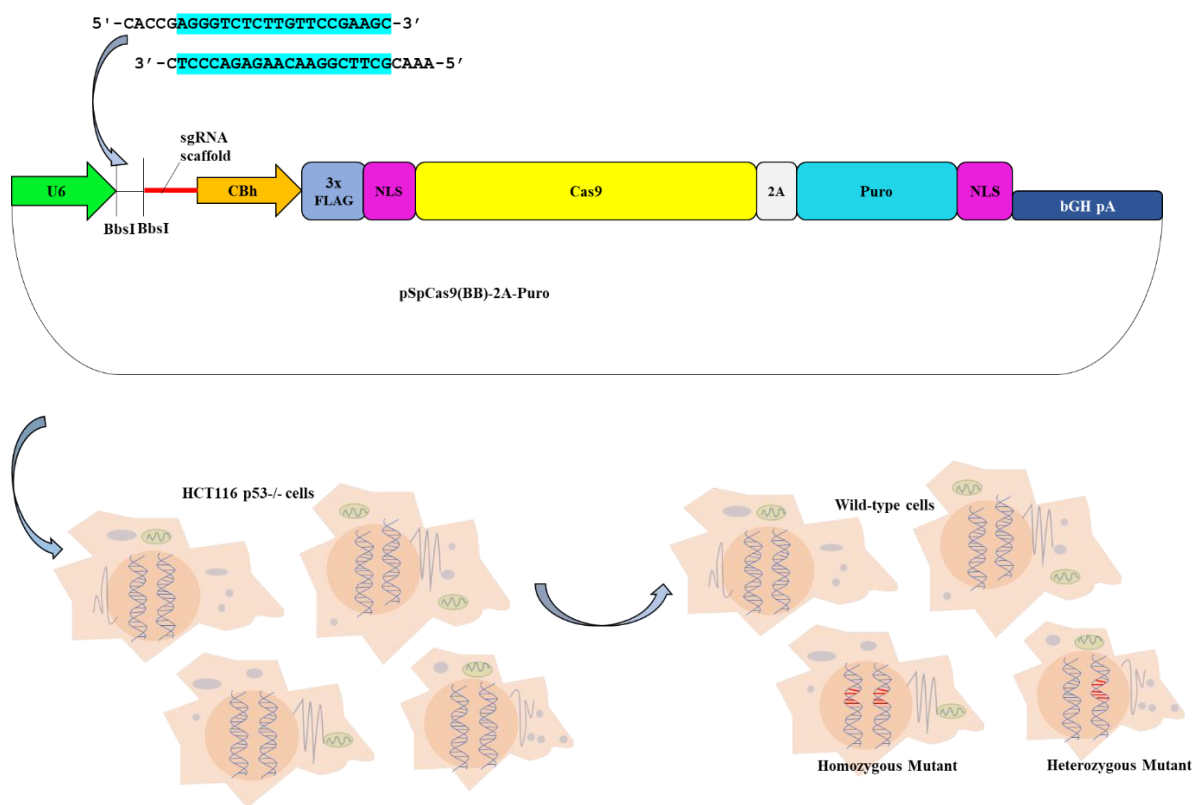


**Figure 4.2. Experimental design of the CRISPR/Cas9 system targeting the *MDM2* gene using pSpCas9(BB)-2A-Puro.** First, complementary top and bottom oligonucleotides with flanking sequences suitable for cloning were annealed. Annealed oligo duplex then inserted into pSpCas9(BB)-2A-Puro vector backbone, which was digested with BbsI enzyme. Finally, HCT116 p53<sup>-/-</sup> cells were transfected with the ligated plasmid expressing Cas9 enzyme and the sgRNA targeting *MDM2* gene to make random INDEL mutations.

To show the existence of mutant cells in a pool, the pools were expanded, and their genomic DNAs were isolated. Restriction Fragment Length Polymorphism (RFLP) assay was used to identify the mutant cells, which included the amplification of the region of interest by PCR and then the digestion with a restriction enzyme. In our case, we used two different restriction enzymes; BsaI and AluI because their recognition sites were very close to the double-stranded break formed by the Cas9 enzyme. A 380bp region was amplified with RFLP primers and then digested with BsaI or AluI enzyme (Figure 4.3.A). Mutant cells were observed in the RFLP analysis as a faint uncut band. Out of four transfected pools, in the second and third pools, there were clear uncut bands. Therefore, we continued with these pools for further steps (Figure 4.3.B).

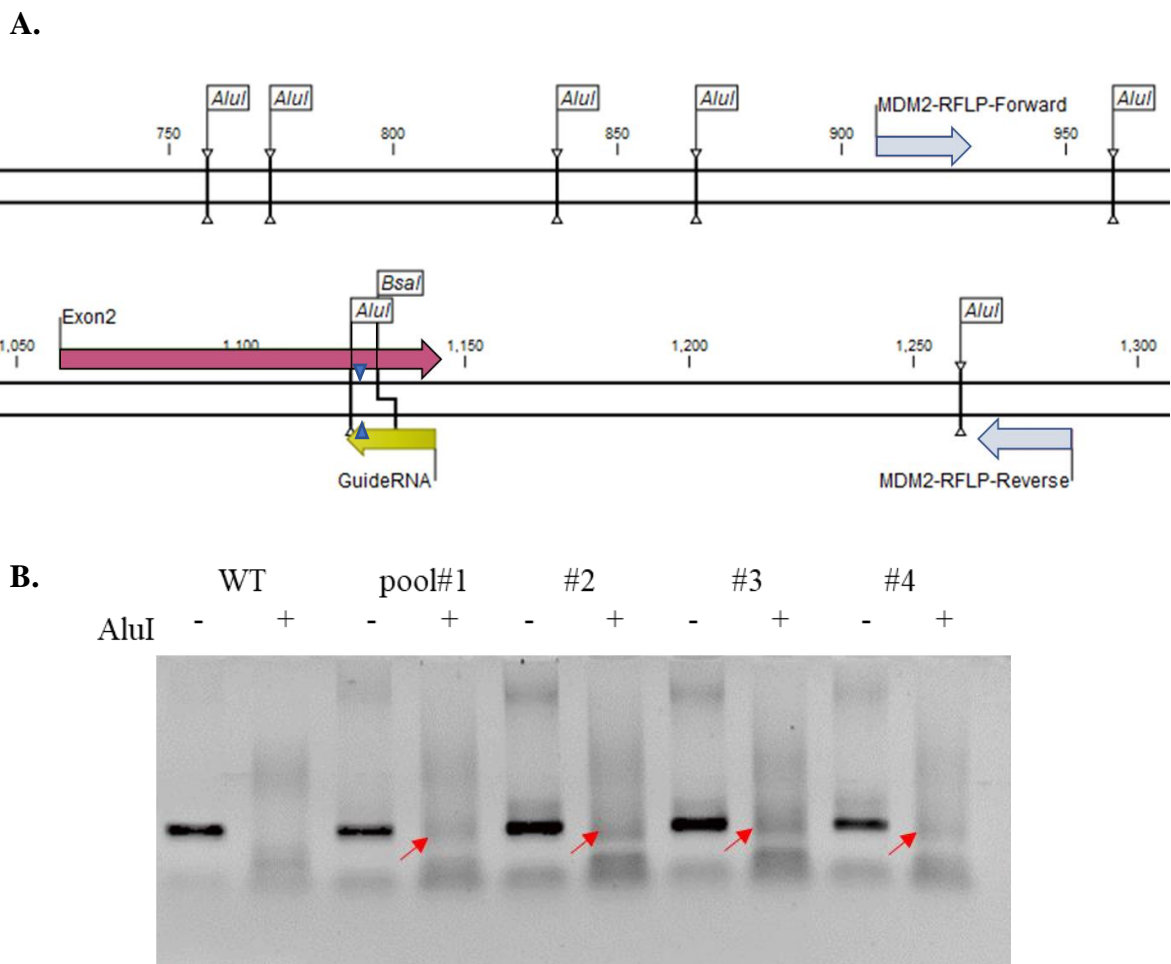


**Figure 4.3. Mutation analysis of MDM2-sgRNA mediated mutations. (A)** RFLP forward and reverse primers (light blue) amplified the region covering the second exon of *MDM2* gene (purple), which was targeted by a sgRNA (yellow). Dark blue arrows represented DSB generated by the Cas9 enzyme. To identify the existence of mutations, RFLP assay using AluI or BsaI enzyme was performed. **(B)** MDM2-sgRNA targeted HCT116 p53<sup>-/-</sup> transfection pools were subjected to the RFLP assay by AluI enzyme. Undigested bands (shown with red arrows) represented the presence of mutant cells.

After confirming the presence of mutant cell population in our transfected cell pool, the single cell populations in a 96-well plate were generated by limiting dilution. We gave single cell clones three to five weeks to expand. Then, their genomic DNAs were isolated and the same RFLP analysis was performed to identify the mutant single cells. Among 48 single cell clones we screened, the mutant cells with insertions drew our attention. We selected the clones with big insertions and the clones with undigested PCR products for the further steps (Figure 4.4).

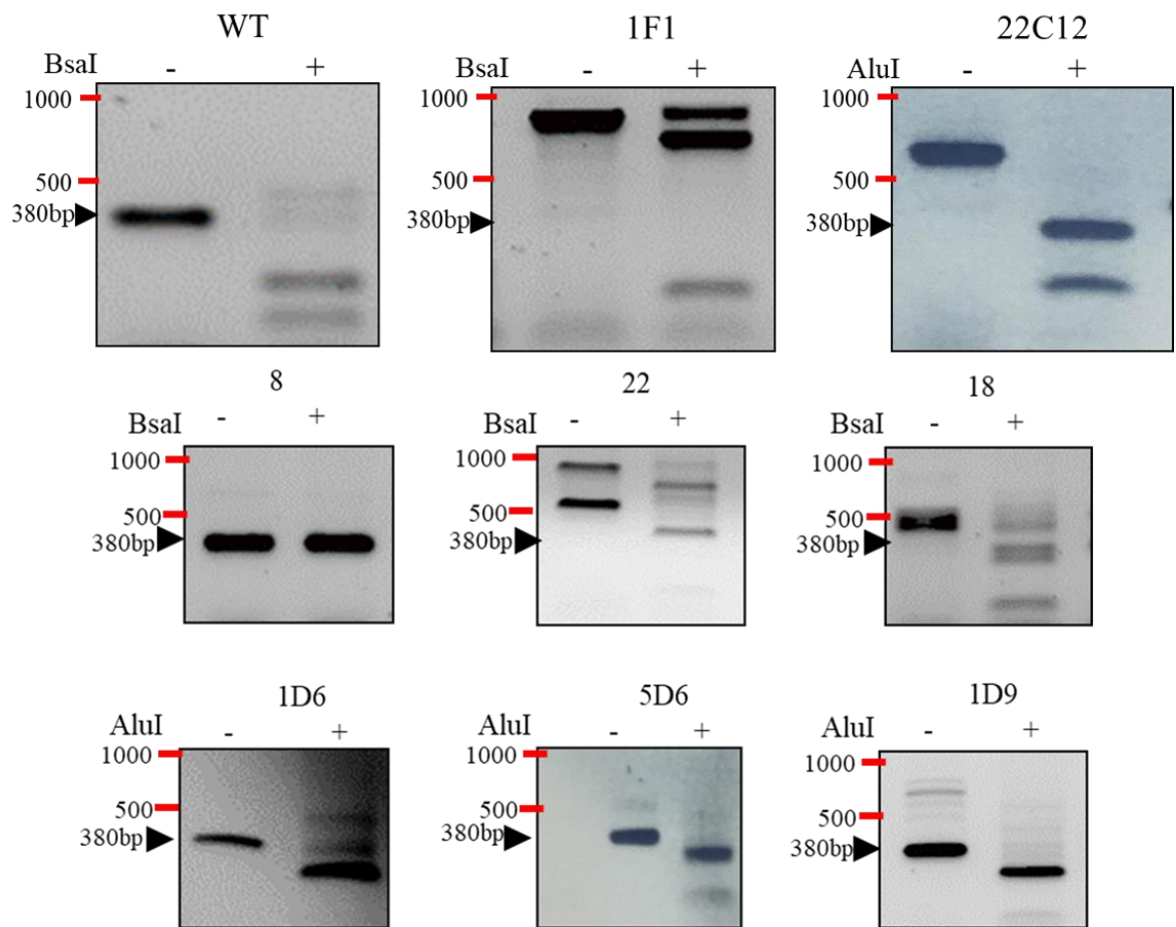


**Figure 4.4. Detection of CRISPR/Cas9 induced mutations in single cell clones.** Single cell clones isolated from MDM2-pSpCas9(BB)-2A-Puro transfection pools were examined by RFLP assay. The PCR products from Clone-8, -18, -22 and -1F1 were digested with BsaI enzyme. The remaining PCR products were digested with AluI enzyme for RFLP analysis. Red lines represented 500bp and 1000bp.

For selected positive clones, we amplified the 380bp fragment that contained the region of interest with the same primers we used for RFLP analysis and then we cloned their uncut PCR products into the pCR4-TOPO-Blunt vector backbone (Zero TOPO Blunt Kit). These ligated vectors were transformed into *E. coli* DH5 $\alpha$  competent cells and then

pDNAs were isolated and analyzed by Sanger sequencing to identify their mutations. We observed that big insertions came from mainly two sources; *Escherichia coli* genomic DNA or pSpCas9(BB)-2A-Puro plasmid backbone. Moreover, the disruption of recognition site could be clearly seen in the sequencing results of clones that had an uncut band after BsaI or AluI digestion. For most of the single cell clones, we observed two alleles for our region of interest. This was expected because the HCT116 p53<sup>-/-</sup> cell line is known to be near-diploid<sup>95,96</sup>. However, for Clone-1F1 and Clone-1D9, we observed only one allele, and for Clone-5D6, we observed 3 different alleles. More than 2 alleles indicated that this clone did not originate from a single cell, therefore we eliminated Clone-5D6 from further analysis (Figure 4.5).

Clone Name	WT		Allele	INDELS	Insert Origin
	ACCTCACAGATTCCAGCT	TCGGAACAAGAGACCCTGGT			
	AluI	BsaI			
1F1	ACCTCACAGATTCCAGCTTCTGGTGGCGCGTGAAC	TCGGAACAAGAGACCCTGGT	Allele 1	+484nts	<i>E.coli</i>
22C12	ACCTCACAGATTCCAGCTGTGGAAGAAGCTGTCGT	TCGGAACAAGAGACCCTGGT	Allele 1	+181nts	pSpCa9
	ACCTCACAGATTCCAGCTACATAATTTTAAACTGC	----AACAAGAGACCCTGGT	Allele 2	+131nts, -4nts	pSpCa9
22	ACCTCACAGATTCCAGCTAACAGTCAGGCTGAATA	TCGGAACAAGAGACCCTGGT	Allele 1	+500nts	<i>E.coli</i>
	ACCTCACAGATTCCAGCTTTCCGCGTGATCGTCAA	TCGGAACAAGAGACCCTGGT	Allele 2	+199nts	<i>E.coli</i>
18	ACCTCACAGATTCCAGCTTTGCGTCTTTAACGGTCA	TCGGAACAAGAGACCCTGGT	Allele 1	+86nts	<i>E.coli</i>
	ACCTCACAGATTCCAGCTACATAATTTTAAACTGCA	----AACAAGAGACCCTGGT	Allele 2	+131nts, -4nts	pSpCa9
8	ACCTCACAGATTCCAGCT	-----AGACCCTGGT	Allele 1	-10nts	
	ACCTCACAGA-----	-----CCCTGGT	Allele 2	-21nts	
1D9	ACCTCACAGATTCC---	TCGGAACAAGAGACCCTGGT	Allele 1	-4nts	
1D6	ACCTCACAGATT-----	TCGGAACAAGAGACCCTGGT	Allele 1	-6nts	
	ACCTCACAGATTCCAGC-	-----ACAAGAGACCCTGGT	Allele 2	-6nts	
5D6	ACCTCACAGATTCCAGCT	-----GT	Allele 1	-18nts	
	ACCTCACAG-----	TCGGAACAAGAGACCCTGGT	Allele 2	-9nts	
	ACCTCACAGATTCCAGCT	--GGAACAAGAGACCCTGGT	Allele 3	-2nts	

**Figure 4.5. Sequencing Analysis of MDM2-sgRNA targeted genome of single cell clones.** Mutations in the exon 2 region of the *MDM2* gene were detected by sequencing. Yellow arrow showed the sgRNA binding site and theoretically, Cas9 enzyme cut the DNA between two thymine bases. Pink and orange boxes showed the recognition sites of AluI and BsaI enzymes, respectively. Deletions in some single cell clones removed these recognition sites, which in turn, resulted in their detection by RFLP assay. The origin of the sequence inserted into single cell clones' genome was either *Escherichia coli* genomic DNA or pSpCas9(BB)-2A-Puro plasmid backbone.



**Figure 4.6. Early stop codon formation due to CRISPR-Cas9 mediated mutations.** (A) After Cas9 generated DSBs in the exon 2 of *MDM2* gene, for several single cell clones, DNA repair system gave rise to big insertions in the targeted region, which, in turn, changed the open reading frame of *MDM2* gene and resulted in an early stop formation either inside the insert sequence or inside the following exon sequence. Blue arrows represented DSB generated by the Cas9 enzyme. (B) For Clone-21D9, 4nts-deletion also resulted in an early stop codon in the exon 3.

Some mutations in the exon 2 region of the *MDM2* gene after targeting by CRISPR/Cas9 resulted in a shift in the open reading frame of the *MDM2* gene. Based on our sequencing analysis, 5 out of 8 single cell clones contained an early stop codon either in the insert sequence or in the following exon sequence, which should result in no MDM2 protein production due to nonsense-mediated decay (Figure 4.6). To determine if we could detect MDM2 proteins in these clones, we performed western blotting with an anti-MDM2 monoclonal antibody (Clone IF2) recognizing an epitope located between amino acids 26-169 encoded by the human *MDM2* gene. In addition to recognizing the full-length 90kDa main isoform of MDM2, alternative isoforms with molecular weights of 57kDa and 74kDa could also be observed using this antibody.

The cell line we used was p53<sup>-/-</sup>, so the feedback loop between p53 and MDM2 was disrupted and the general MDM2 protein level in this cell line was low. We aimed to increase MDM2 protein levels by transfecting the cells with a pcDNA3-flag-p53 plasmid. By increasing p53 protein levels in the cell, we expected to reactivate the feedback loop between these two proteins. Firstly, on the day before transfection, 3x10<sup>5</sup> cells were seeded per well in a 6-well tissue culture plate. 36 hours after transfecting each single cell clone and the parental HCT116 p53<sup>-/-</sup> cell line with the pcDNA3-flag-p53 plasmid, we prepared lysates from 1 million cells. Then, anti-FLAG and anti-MDM2 antibodies were used to detect cellular p53 and MDM2 levels, respectively, and anti-βactin antibody was used as a loading control. As we expected, MDM2 protein levels in the HCT116 p53<sup>-/-</sup> cell line was induced after the introduction of p53 protein. A doublet MDM2 band was visible with a molecular weight of approximately 90kDa. This doublet could be a result of a difference between two alleles of the *MDM2* gene affecting its further post-translational modifications.

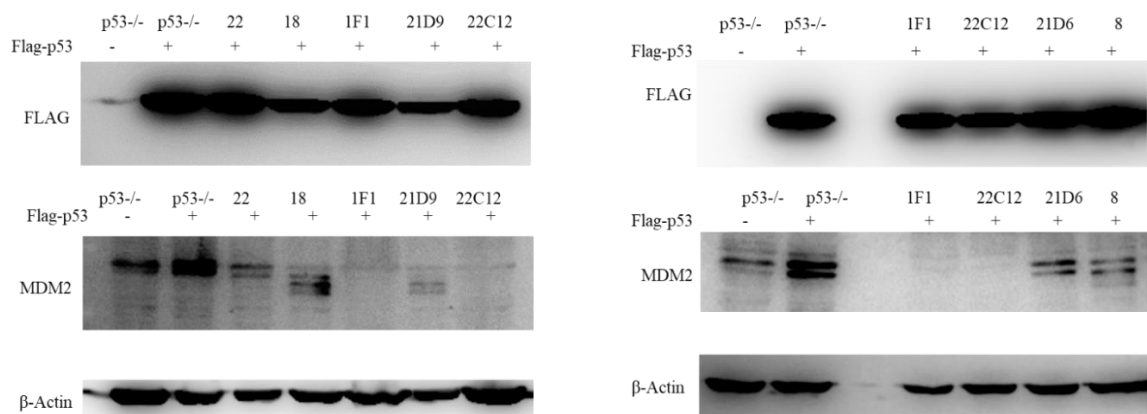


**Figure 4.7. Analysis of MDM2 protein expression in single cell clones by western blotting.** 36 hours after pcDNA3-flag-p53 transfection, cell lysates were prepared from the HCT116 p53<sup>-/-</sup> cell line and from single cell clones. Western blotting was performed with anti-FLAG and anti-MDM2 antibodies to see cellular p53 and MDM2 protein levels. β-Actin was used as a loading control.

It was expected to observe almost the same amount of MDM2 protein levels in the single cell clones after transfection if they were expressing the *MDM2* gene. Anti-MDM2 blotting results of Clone-1F1 and Clone-22C12 showed no visible MDM2 protein band. Therefore, we considered them as an *MDM2* knockout. MDM2 protein bands of Clone-18 and Clone-1D9 were truncated (Figure 4.7).

Although the sequence analysis of 5 single cell clones showed an early stop codon in the *MDM2* gene locus, for 3 of them, we observed an MDM2 protein band. Two of them had truncated MDM2 protein bands, and one of them had the same band with the parental HCT116 p53<sup>-/-</sup> cell line. There could be more alleles, which were not identified with sequencing analysis, thereby these clones could originate from multiple cells. For Clone -18, one of the alleles was the same with Clone-22C-12, therefore Clone-18 could originate from Clone-22C12 and another cell.

#### **4.1.2. Analysis of Compounds by using HCT116 p53<sup>-/-</sup> MDM2<sup>-/-</sup> cell line**

Later, we examined the effects of the compounds on the growth and viability of double knockout cell lines; Clone-1F1 and Clone-22C12. Because these compounds should target the p53-binding pocket of MDM2 protein, in the absence of p53 and MDM2 proteins, our compounds should not affect the cell viability. Conversely, in the wild-type cell (p53<sup>+/+</sup> MDM2<sup>+/+</sup>), our compounds should activate cell-cycle arrest or apoptosis through the blockage of the interaction between p53 and MDM2 and the activation of p53. After seeding four different cell lines: HCT116 WT, p53<sup>-/-</sup>, Clone-1F1 and Clone-22C12, different concentrations of the compounds were added and incubated for 72 hours, and then the cell viability and the growth were analyzed by MTT assay.

From our previous analysis, one of the MDM2 inhibitor candidates was 4A1-AN and we compared its effect on the cell viability of these 4 different cell lines with the effect of our positive control, Nutlin-3a<sup>80</sup>. The cell viability was decreased in HCT116 WT after addition of Nutlin-3a, whereas Nutlin-3a did not enhance apoptosis in HCT116 p53<sup>-/-</sup>, Clone-1F1, and Clone-22C12 as expected. Like Nutlin-3a, 4A1-AN decreased the cell viability in HCT116 WT. However, unlike Nutlin-3a, it also decreased the cell viability in HCT116 p53<sup>-/-</sup>, Clone-22C12, and Clone-1F1, especially with high doses (Figure 4.8). This could mean that 4A1-AN resulted in DNA damage, which, in turn, led to p53 activation and cell death. Because we were interested in the compounds blocking the binding of MDM2 to p53 without causing any DNA damage, we concluded that 4A1-AN was not a good candidate. Screening of compounds by using these cell lines and searching for the desired results based on their corresponding cell viability could be a good way to find new candidates.

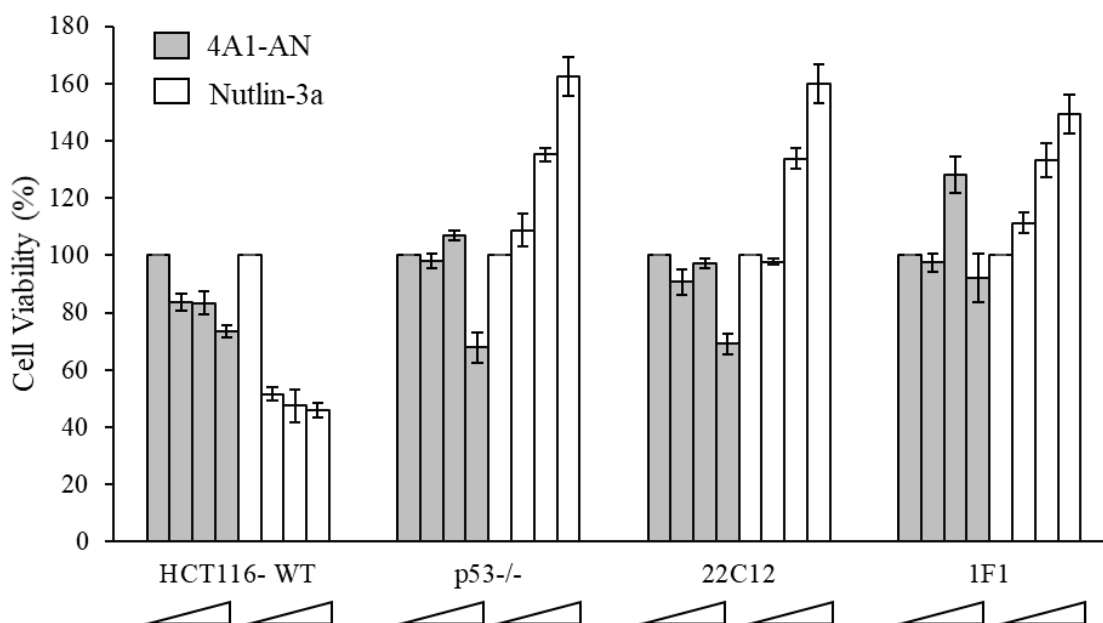


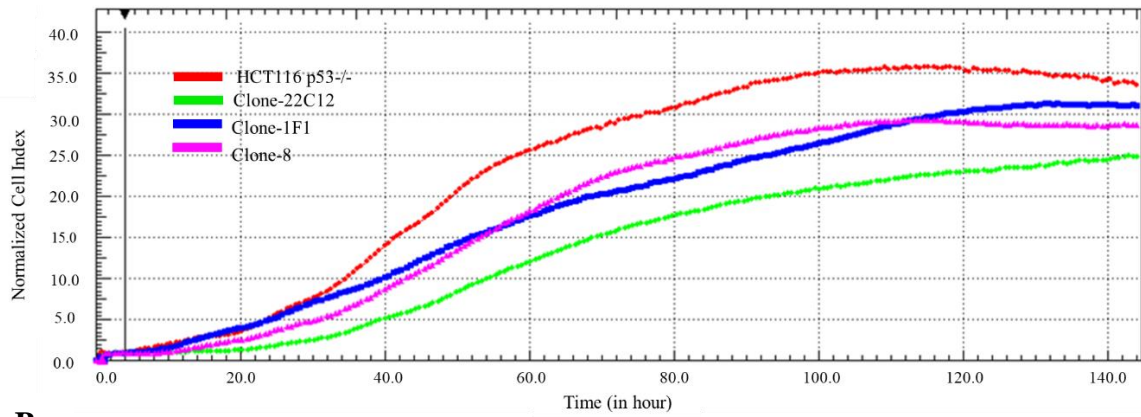
**Figure 4.8. Cell viability analysis of a compound.** Increasing concentrations of compounds (1 $\mu$ M, 5 $\mu$ M, and 10 $\mu$ M) were added onto the HCT116 WT, p53<sup>-/-</sup>, Clone-22C12, and Clone-1F1. After incubating for 3 days, their cell masses were analyzed colorimetrically by MTT assay kit (Roche). Average absorption values normalized to untreated control (DMSO) were displayed after multiplication with 100.

#### 4.1.3. Effect of MDM2 in Cellular Growth Rate Independently of p53

MDM2 expression is required for cell survival in p53<sup>-/-</sup> cells and its absence negatively affects the cell through the activation of p73<sup>97</sup>. Moreover, it also reported that MDM2 plays an oncogenic role in serine/glycine metabolism and redox homeostasis in a p53-independent manner, which promotes the growth of cancer cells<sup>98</sup>. Based on these previous findings, we examined the effect of the absence of MDM2 on cellular proliferation rates in the HCT116 p53<sup>-/-</sup> cell line. We compared 4 different cell lines; HCT116 p53<sup>-/-</sup>, Clone-1F1, Clone-22C12 and Clone-8 and measured their growth curves and determined their doubling times. Their cell indexes were monitored every 15 minutes in real time for over 5 days using the xCELLigence RTCA-DP system. The cell indexes were normalized to the point when the cells settled down (4 hours 11 minutes after seeding). The doubling times for 4-hours intervals were calculated from these normalized cell indexes. In the beginning of exponential phase, HCT116 p53<sup>-/-</sup> cell line displayed a shorter doubling time compared to the mutant ones. We reported that there was a clear difference between the HCT116 p53<sup>-/-</sup> and the double knockout cell line, Clone-1F1 as expected. Unlike Clone-1F1, although the other double knockout cell line, Clone-22C12

started slow, later it displayed shorter doubling time compared to the parental p53<sup>-/-</sup> cell line. Clone 8 had only one allele expressing the *MDM2* gene. We observed an expected result because its growth rate was the intermediate one (Figure 4.9).

**A.**



**B.**

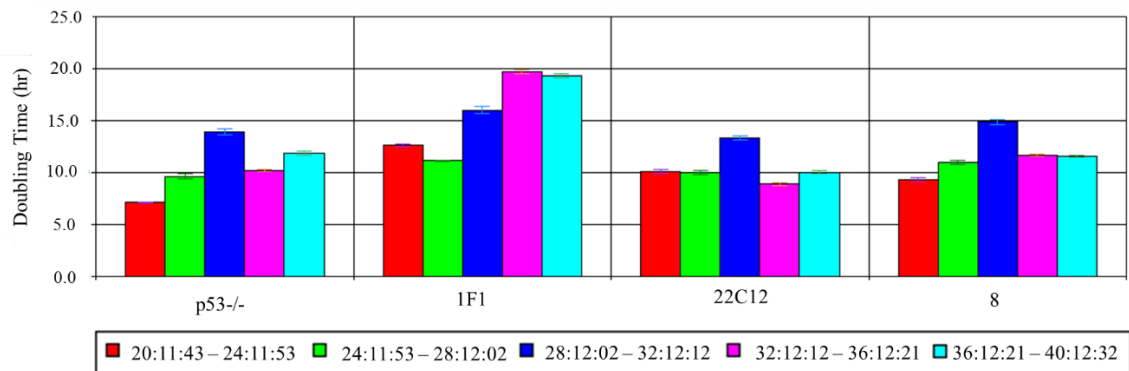


**Figure 4.9. Growth rate analysis of double knockout HCT116 cells.** (A) The cell indexes of HCT116 p53<sup>-/-</sup> (red), Clone-1F1 (blue), Clone-8 (pink) and Clone-22C12 (green) were measured by xCELLigence RTCA-DP system every 15 minutes for over 5 days. The cell indexes were normalized to 4 hours 11 minutes after seeding. Black arrow represented the normalization point. Clone-1F1 and -22C12 were the double knockout cell lines and Clone-8 had one allele expressing the *MDM2* protein. (B) The doubling times of different 4-hour intervals were calculated by using RTCA 2.0 software.

## 4.2. Fluorescent two-hybrid (F2H) assay for screening the compounds

We constructed and optimized a fluorescent two-hybrid (F2H) assay for the high-content screening of the compounds. The F2H assay is a useful method for investigating protein-protein interactions by using fluorescent live cell microscopy because one can detect the disruption of protein-protein interactions after the introduction of a compound in living cells in real time. In this system, two different proteins tagged with two distinct fluorescent proteins; green or red, are localized on the lac operator sites integrated into the baby hamster kidney (BHK) cells' genome and form green and red foci in the nucleus.

For this project, p53 was fused to TagGFP protein and MDM2 was fused to TagRFP protein. This system also included another fusion protein, LacI-GFP binding protein(GBP). These 3 fusion protein containing plasmids were introduced into BHK cells by transfection and 16-24 hours after transfection, the cells were observed under the fluorescent microscope (Figure 4.10.A). LacI part of GBP-LacI fusion protein was localized to the lac operator sites found in BHK cell's genome and its GBP part was bound to the TagGFP-p53 fusion protein, which led to a green focus formation in the BHK cell nucleus. With the interaction between p53 and MDM2 proteins, the TagRFP-MDM2 fusion protein was also localized to these regions, which resulted in a red focus at the same place. If the compounds, we screened, disrupted the interaction between these two proteins, after the introduction of compounds, it was expected to observe the disappearance of red foci (Figure 4.10.B).

The plasmids containing TagRFP-MDM2 and TagGFP-p53 were isolated from the Pltf-p53-Mdm2 mix (Chromotek). The plasmid containing GBP-LacI was constructed by the amplification of GBP-LacI sequence from the same mix by PCR and its cloning into pcDNA3.1/myc-His(-)B vector backbone. We tested the functionality of the constructed pcDNA3.1/myc-His(-)B-GBP-LacI plasmid by transfecting these 3 plasmids with different combinations. By only using TagGFP-p53 and TagRFP-MDM2 plasmids, we did not observe any green or red focus formation and when we used TagRFP-MDM2 and pcDNA3.1/MycHisB(-)-GBP-LacI together, we did not observe any red foci in the nucleus. Moreover, when we used TagGFP-p53 and pcDNA3.1/myc-His(-)B-GBP-LacI plasmid together, the green foci formation in the nucleus was recorded, which indicated pcDNA3.1/myc-His(-)B-GBP-LacI plasmid was required for the focus formation.

Finally, using all three of the plasmids generated both green and red foci at the same place and set up the experiment (Figure 4.11).

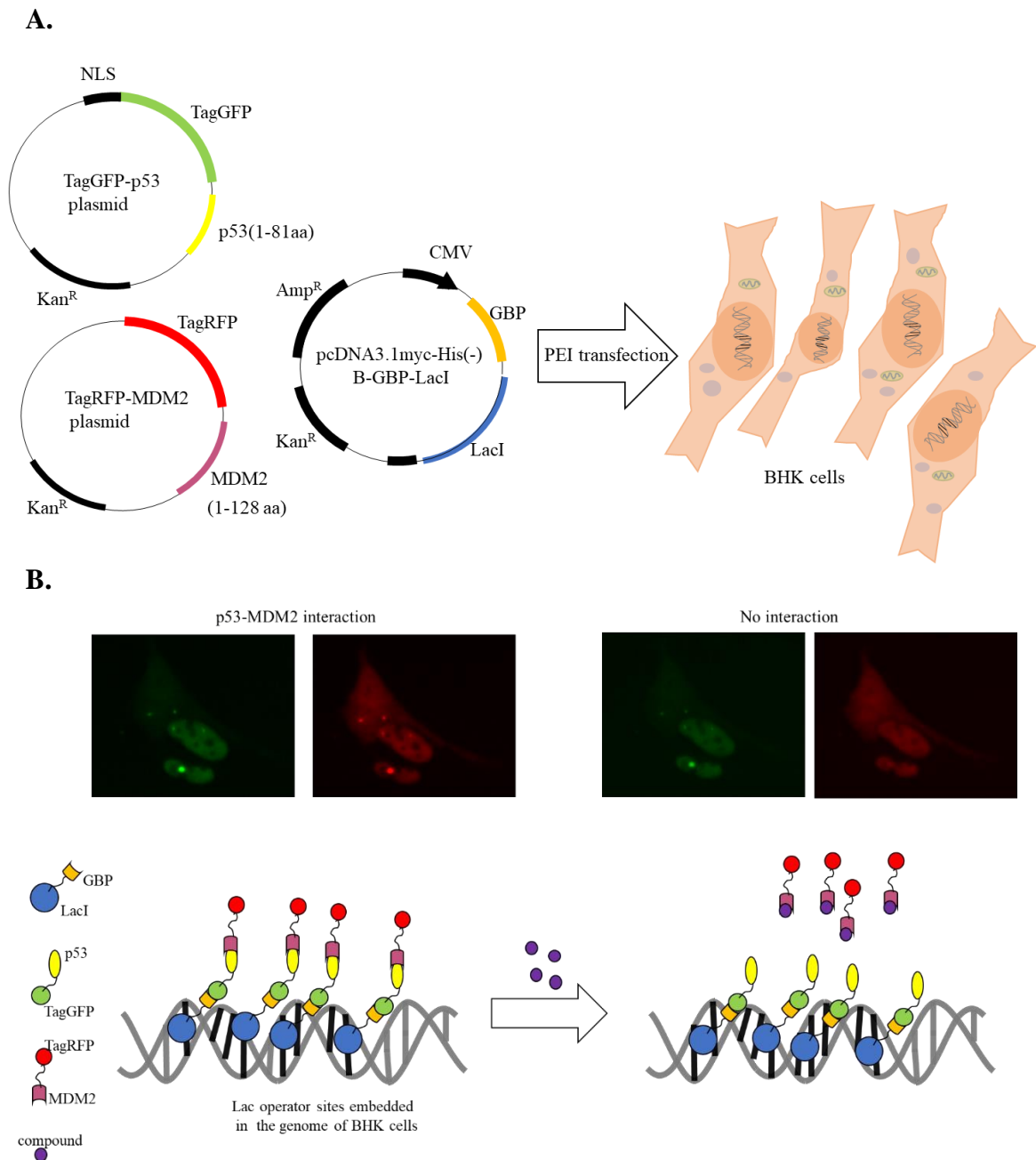


**Figure 4.10. Experimental design of fluorescent 2 hybrid (F2H) assay.** (A) 3 plasmids containing TagGFP-p53, TagRFP-MDM2, and GBP-LacI fusion proteins were transfected into BHK cells. (B) There were lac operator sites embedded in the genome of BHK cells and GBP-LacI fusion protein localized to these regions. Through the interactions between GBP and TagGFP proteins, and p53 and MDM2 proteins, TagGFP-p53 and TagRFP-MDM2 fusion proteins were also localized to these regions, which resulted in the formation of green and red foci in the nucleus. If the compound blocked the interaction between p53 and MDM2 proteins, the disappearance of the red foci would be observed.

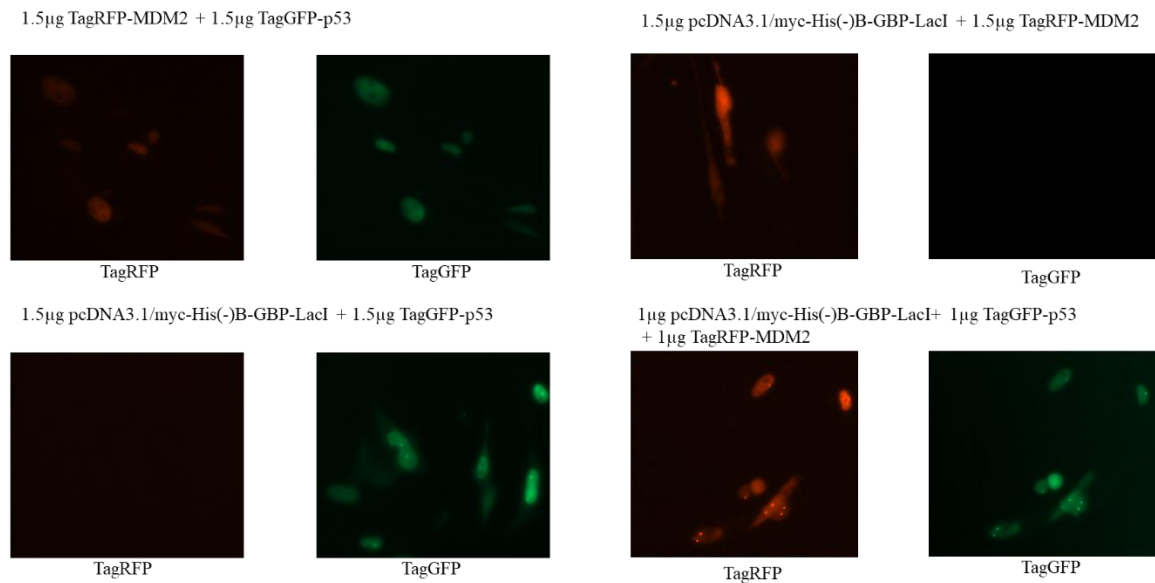


**Figure 4.11. Verification of F2H assay.** Three plasmids were transfected into BHK cells with different combinations. Red and green foci at the same place only formed when three plasmids were transfected together, which represented the system was working.

After we set up the experiment, we tested how the assay worked with a positive control. Because Nutlin-3a is a widely known compound that disrupts p53-MDM2 interaction, we used it as our positive control<sup>80</sup>. We used two different concentrations of Nutlin-3a; 1µM and 10µM. After our first trials with this compound, we observed how fast it acted. Therefore, after we added Nutlin-3a, we started the experiment immediately. We used IN Cell Analyzer 2500HS for running our live-cell imaging experiments. After setting up the parameters and adjusting the laser autofocus, we took out the plate, added the desired dose of Nutlin-3a and then started the experiment with already determined parameters.

First, we tested 1µM Nutlin-3a and we set up the experiment with the lowest exposure time possible for both green and red channels. We selected 25 distributed tile regions and there was 1 minute between each cycle. The experiment lasted for approximately 15 minutes and we observed the disappearance of some of the red foci and then after some time, the reappearance of some of the red foci by eye. We also quantified the disappearance and the reappearance of the red foci using IN Cell Developer software (Figure 4.12.A). Dot-analysis graphs showed the total number of green foci, the total number of red foci and the total number of yellow foci, where green and red foci met.

The analysis of foci in the nucleus generally includes a nuclear stain, such as Hoechst stain, to determine the boundaries of the nucleus with a different wavelength channel,

such as blue in the case of Hoechst stain, which makes the analysis much easier. We did not stain the nucleus with a nuclear dye, and therefore we analyzed the foci with a vesicle-analysis strategy. This strategy had a higher error rate because it also counted some cellular contents as dots. However, from the analysis of 1 $\mu$ M Nutlin-3a, we observed the activity of the compound even if the analysis included some percentage of false dots.

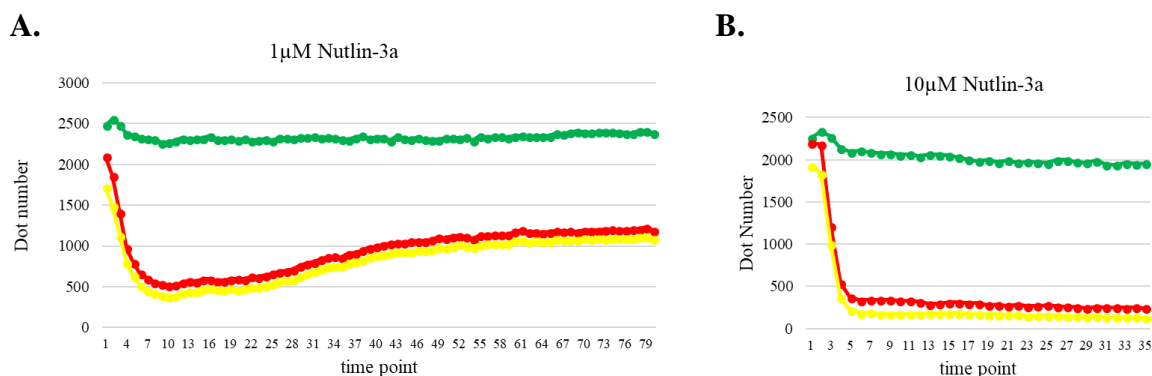


**Figure 4.12. The disappearance of red foci in F2H assay using our positive control, Nutlin-3a.** (A) 16-24 hours after transfection of BHK cells with our three plasmids, 1 $\mu$ M Nutlin-3a was added onto cells. Cells were immediately monitored by using IN Cell Analyzer 2500HS. After the experiment, dot analysis was performed by using IN Cell Developer Software. The disappearance and the reappearance of red dots were observed after the introduction of 1 $\mu$ M Nutlin-3a. (B) 10 $\mu$ M Nutlin-3a was added to cells. They were monitored by IN Cell Analyzer 2500HS and analyzed by IN Cell Developer Software. While the experiment, the disappearance of the red foci was observed; however, they did not come back.

Next, we analyzed the response to 10 $\mu$ M Nutlin-3a, and again after the introduction of the compound, we started the experiment immediately. We used the same parameters and the same number of regions with the previous 1 $\mu$ M Nutlin-3a experiment; however, the only difference was that we selected ‘fast as it can’ option, which meant that the microscope worked without any stop. We observed the disappearance of red foci quickly and they did not come back during the experiment. Vesicle-like particle analysis also met the expectations and showed the fast disappearance of the red and yellow foci with a stable total number of green foci (Figure 4.12.B).

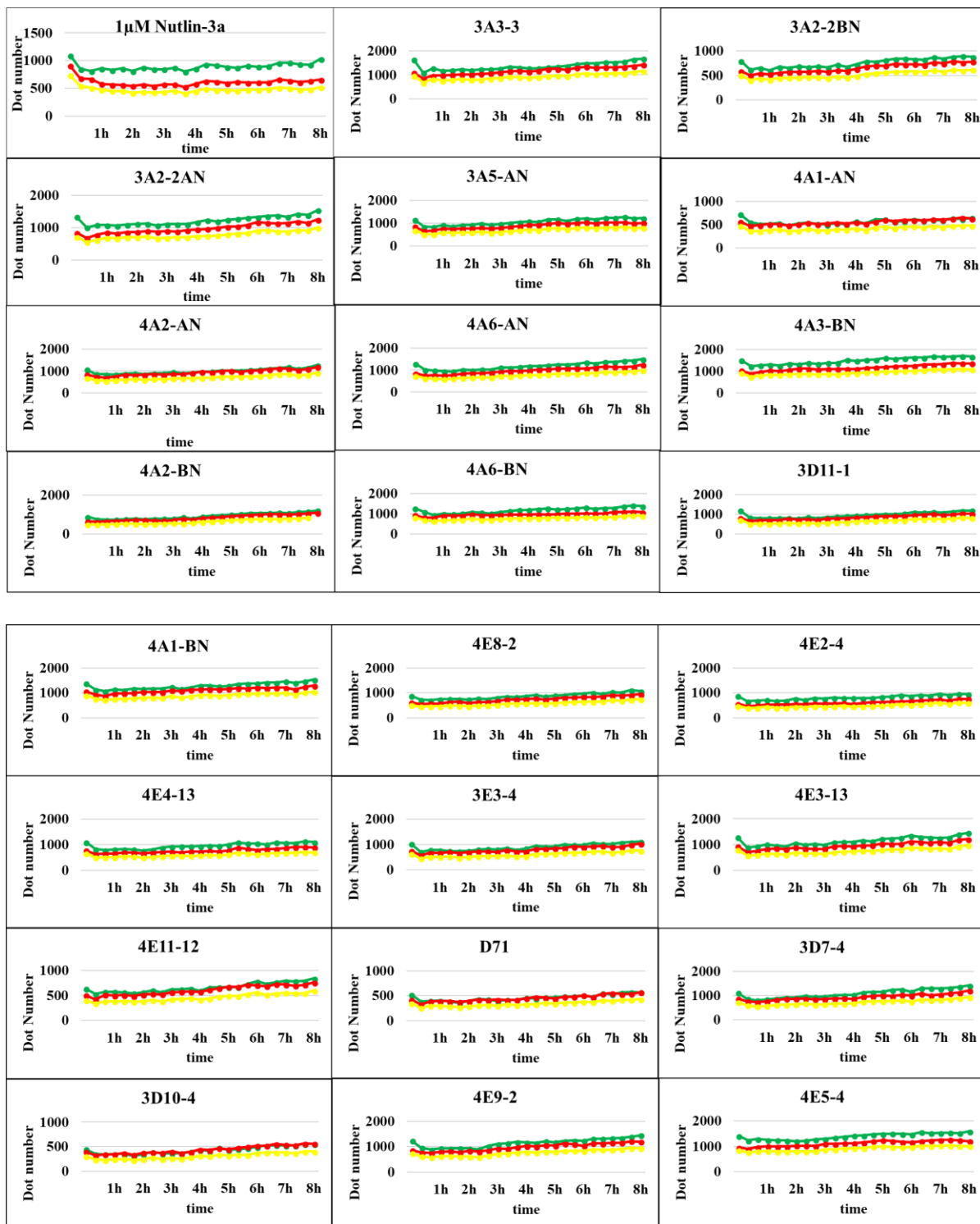


**Figure 4.13. Screening of 1µM compounds in F2H assay.** After the addition of compounds, in a 24-well plate, we monitored the cells by using IN Cell Analyzer 2500HS. We selected 9 regions and there were 20 minutes between each cycle. After the eight-hour experiment, the red and green foci were counted by using IN Cell Developer software.

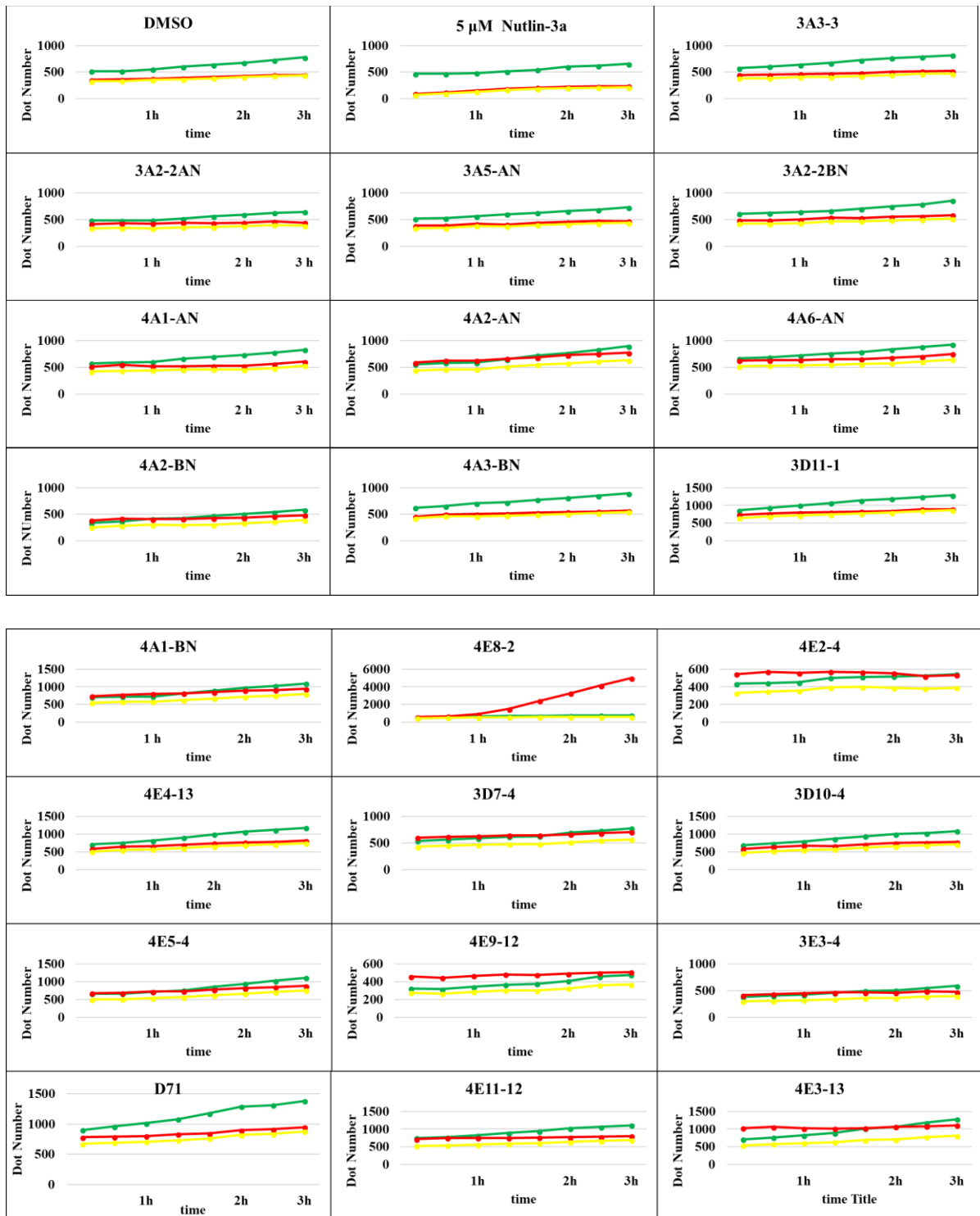
Afterward, because the first trials with our positive control were done, we started screening of our novel compounds. We had two different settings for screening; a 24-well plate and a 96-well plate setting. The 96-well plate setting was advantageous for screening more compounds; however, to screen one 96-well plate lasted more. Moreover, cells tended to go to the edges of the well in a 96-well plate, which sometimes led to poor quality data. First, in a 24-well plate setting, we screened the compounds with 1 $\mu$ M concentration and the experiment lasted for 8 hours. After analyzing the green and red foci in IN Cell Developer software, we did not determine any compound with a stable green focus count and decreasing red and yellow focus counts (Figure 4.13).

Software counted green and red foci similar in number and they generally remained stable or increased. This increase was due to the long duration of the experiment. The intensities of red and green fluorescent proteins increased during the experiment, which led software to analyze more features as dots. Moreover, because there was 20 minutes time interval between two cycles, we could not catch the disappearance of the red foci in Nutlin-3a well; however, the low number of red dots could mean the disappearance of the red foci in the first minutes of the experiment.

We then screened 10 $\mu$ M compounds in a 96-well plate. After setting up the same parameters as the previous experiments and adjusting the laser autofocus, we started the experiment with 9 distributed regions (closed to the edges) and 20 minutes time interval between each cycle. The experiment lasted for 3 hours. After finishing the experiment, we analyzed our raw data in IN Cell Developer software with the same vesicle-like particle analysis. We could not observe any compound with a stable green dot number and decreasing red and yellow dot numbers. Generally, dot counts were stable or even increasing. Like our previous experiment, towards the end of the experiment, the green and red fluorescent proteins' intensities increased, which misled the software.

It was expected to observe a stable green dot count and decreased red and yellow dot counts. Because false dots due to the intensity increase generally affected the total dot number in both green and red channels, they did not affect the analysis badly. Moreover, because some compounds led to cell death, these apoptotic cells caused more features counted as dots by the software. For example, for 4E8-2, cellular debris was counted in the red channel as dots, therefore, we observed a sharp increase in the red dot number in the software analysis. We used 5 $\mu$ M Nutlin-3a as our positive control and although we could not catch the initial disappearance of red foci, the red and yellow dot numbers were

lower than green dot number, which indicated the initial disappearance of red foci (Figure 4.14).



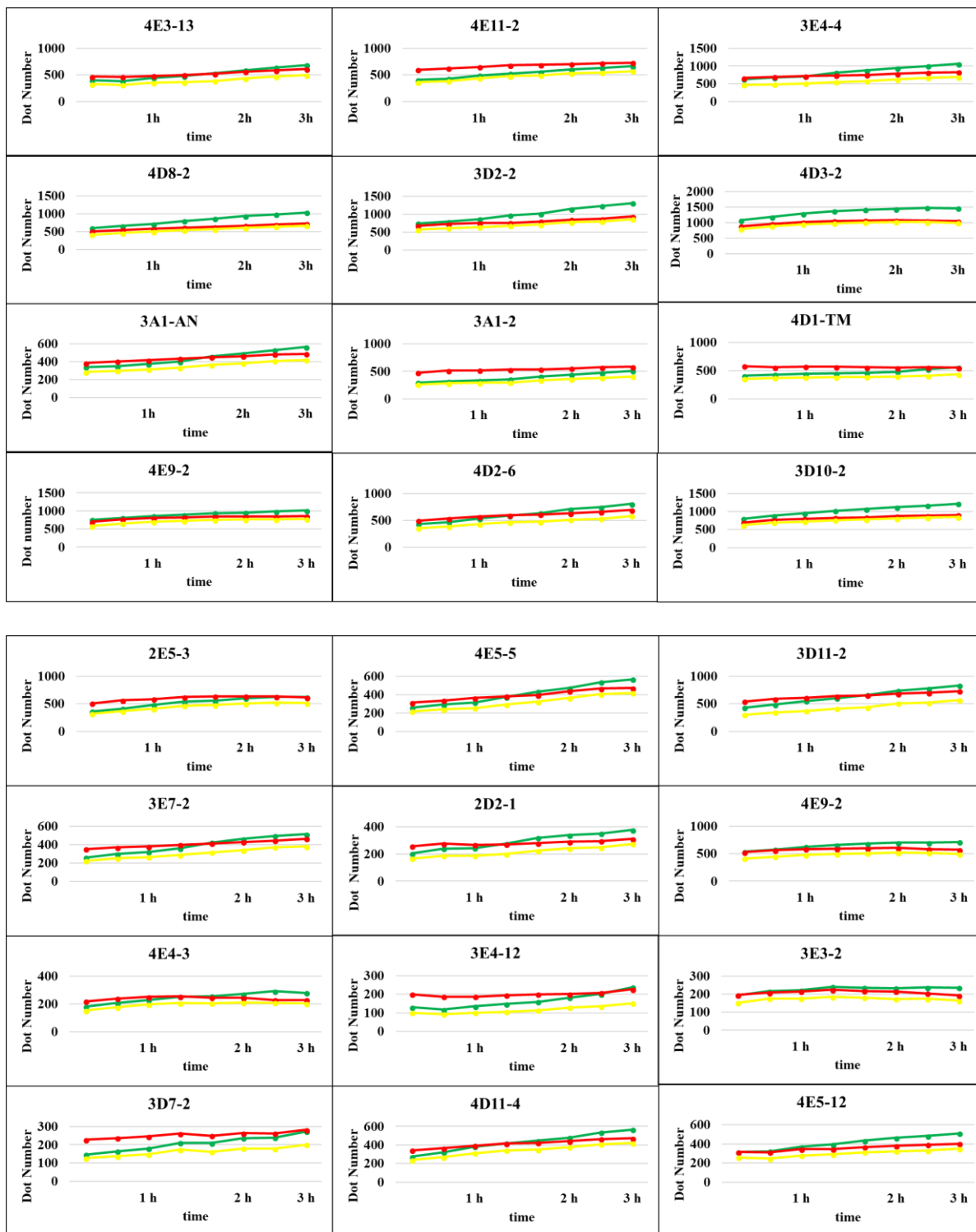


**Figure 4.14. Screening of 10 $\mu$ M compounds in F2H assay.** After addition of compounds, in a 96-well plate, we monitored the cells by using IN Cell Analyzer 2500HS. We selected 9 regions close to the edges and then we started the experiment with approximately 20 minutes between each cycle. After the three-hour experiment, the experiment was analyzed by using IN Cell Developer software.

### **4.3. Protein purification of TagGFP-p53 and MDM2 proteins and screening compounds *in vitro* by surface plasmon resonance (SPR)**

Our novel compounds did not give any positive results in F2H assay, and therefore we aimed to observe simple p53-MDM2 interaction *in vitro* by using a surface plasmon resonance system and checked whether the compounds disrupt the interaction *in vitro*. We designed a surface plasmon resonance experiment, where His-tagged TagGFP-p53 fusion protein was bound onto a nickel-activated NTA chip. Next, we passed the MDM2 protein in the presence or absence of the compounds to analyze the p53-MDM2 interaction. Our first experiment design constituted TagGFP-p53 and TagRFP-MDM2 fusion proteins; however, TagRFP-MDM2 fusion protein caused some problem during purification, thereby we switched to produce only MDM2 protein. The p53 and MDM2 proteins we planned to use in this experiment were their domains necessary for the interaction between two proteins.

#### **4.3.1. Protein purification of TagGFP-p53 and MDM2 proteins**

We then first intended to purify the proteins, therefore we constructed two bacterial expression plasmids expressing His-tagged TagGFP-p53 and His-tagged MDM2 proteins. TagGFP-p53 fusion protein sequence and MDM2 protein sequence were amplified by PCR from TagGFP-p53 and from TagRFP-MDM2 plasmids used in F2H assay, respectively. The sequences were amplified using a forward primer with a SmaI recognition site and a reverse primer with a NotI recognition site. These SmaI and NotI digested PCR products were cloned into pET-47b (+) vector backbone, which was digested with the same enzymes (Figure 4.15).

We transformed pET-47b(+)-TagGFP-p53 and pET-47b(+)-MDM2 plasmids into Rosetta2 DE3, bacterial expression strain of *E. Coli*. This Rosetta 2 strain designed to express eukaryotic proteins because it contained a chloramphenicol-resistant plasmid containing tRNAs for rare codons. The pET-47b (+) bacterial expression vectors expressed fusion proteins with an N-terminal His-tag for further affinity chromatography purification. Protein expression under the control of T7 promoter was blocked because LacI protein expressed from the same plasmid was bound to a Lac operator site. When the cells were induced with IPTG, which competed with LacI proteins on the Lac

operators, the blockage of RNA transcription was removed, and the protein was produced constitutively.

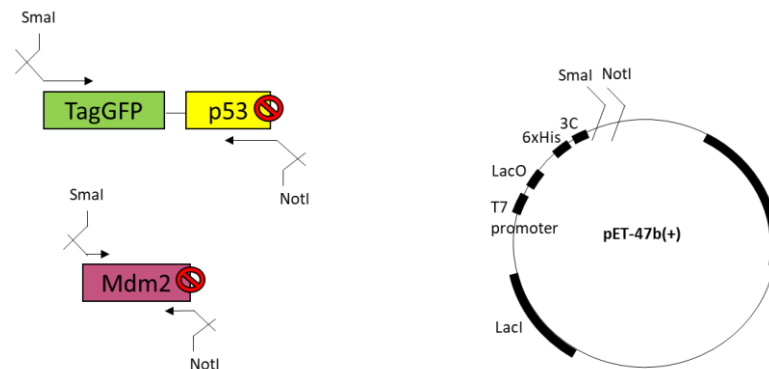


**Figure 4.15. Vector construction design of bacterial expression plasmids.** TagGFP-p53 and MDM2 sequences were amplified by using primers with suitable restriction enzyme recognition sites (SmaI and NotI). There were stop codons after p53 and MDM2 sequences. The digested PCR products were then cloned into the bacterial expression vector, pET-47(b) digested with the same enzymes.

We first purified His-tagged TagGFP-p53 fusion protein. Its green fluorescent part made protein induction and further affinity purification easier because the green fluorescent protein gave a visible green color to the culture and to every solution containing the protein. We picked up a single Rosetta2 colony containing pET-47b(+)-TagGFP-p53 and grew 1L TB culture at 37°C (221rpm) until the optical density at 600nm reached between 0.6-1.0. Generally, we stopped the incubation at the lowest value around 0.6. Then, 0.2 mM IPTG was added to the culture and IPTG induction was performed overnight at 18°C (180rpm). After induction, the protein production was confirmed by checking the green fluorescent color (Figure 4.16.A).

We harvested the cells at 2700xg for 15 minutes and then resuspended in lysis buffer, which was used to protect the proteins from the degradation. After sonication for mechanical lysis and centrifugation at 27,000xg for 45 minutes at 4°C for precipitating cell wall and non-soluble proteins, the supernatant was added onto 3ml already equilibrated HisPur Cobalt Superflow Agarose resin (Thermo Fisher Scientific) and incubated for 30 minutes at 4°C with end-to-end rotation to provide binding between His-tags and the resin. Afterward, we allowed it to flow and this flow-through was named non-retained fraction because it contained all the soluble proteins without any His-tags and our protein should not be found in this fraction. After washing the resin-protein complex with wash buffer containing low imidazole concentration to remove any non-

specific proteins, we eluted the His-tagged TagGFP-p53 with an elution buffer containing 300mM imidazole concentration. We took samples from every step; sonicated lysate, pellet, non-retained fraction and elutes for further SDS-PAGE gel analysis.

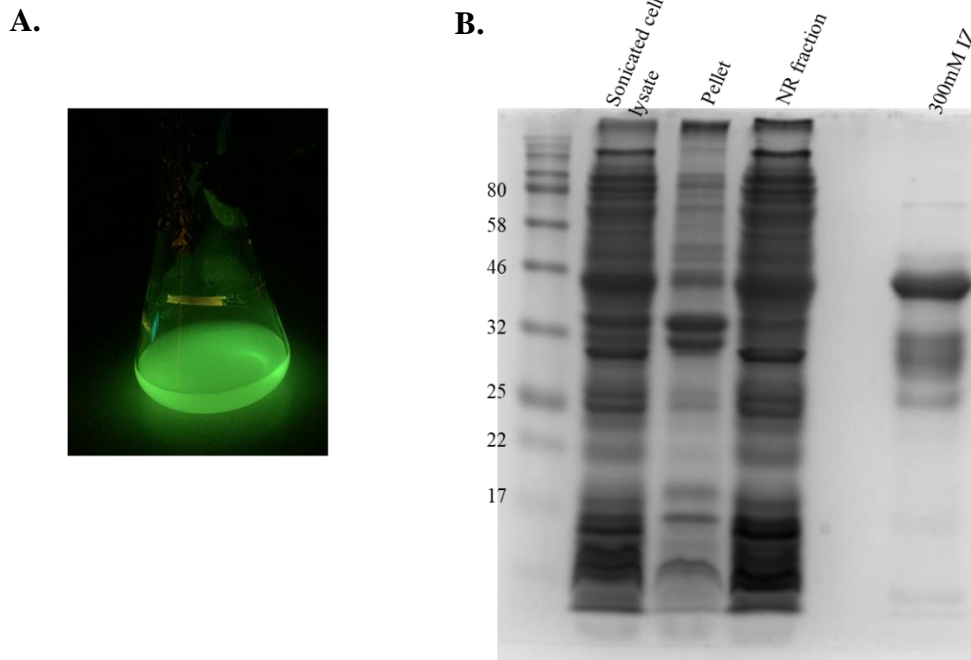
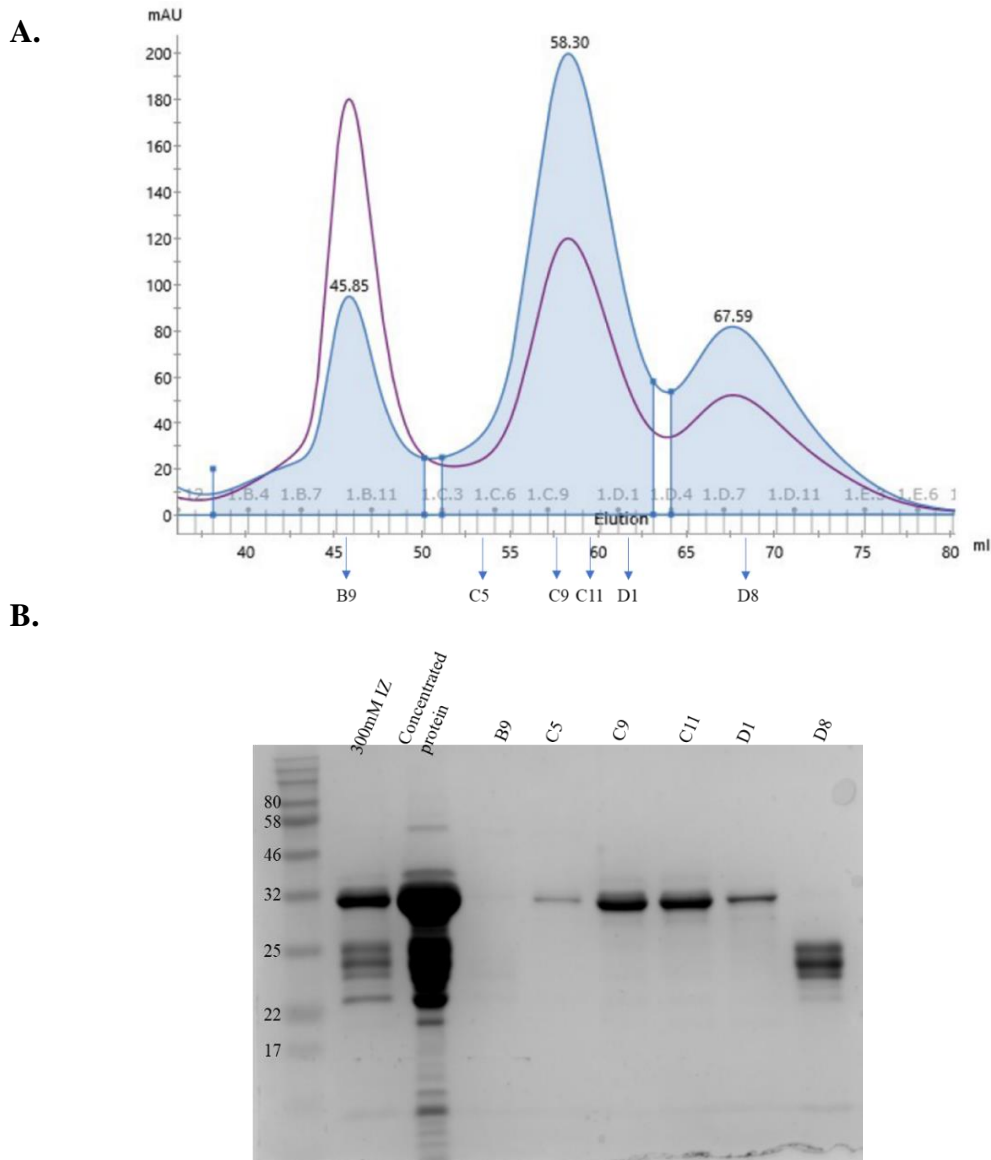


**Figure 4.16. Bacterial expression and affinity purification of His-tagged TagGFP-p53 fusion protein.** (A) 18h after IPTG induction, the culture expressing TagGFP-p53 fusion protein emitted green color when it was excited with blue light. (B) We performed the affinity purification of His-tagged TagGFP-p53 fusion protein by using HisPur Cobalt Superflow Agarose resin (Thermo Fisher Scientific). We collected the samples from every step of our protein purification protocol and loaded into an SDS-PAGE gel (14%). Expected protein size was 38kDa.

The expected size for His-tagged TagGFP-p53 was 38kDa and with 300mM imidazole, we purified the desired protein; however, the eluted protein was not pure and there were other contaminant proteins, which were smaller than our protein (Figure 4.16.B). Moreover, the same protein band was visible in the sonicated lysate and the non-retained fraction samples; however, not in the pellet, which meant the protein was soluble. Finding the protein in NR led to a problem because we could not collect all the expressed protein. Other contaminant proteins that eluted with high-imidazole concentration could have an affinity for the resin and could block the binding of the desired His-tagged protein.

Then, we concentrated our protein sample by using a concentrator tube with 10kDa MWCO to a volume that was less than or equal to 1ml, which was required to load the sample into AKTA pure for size-exclusion chromatography and for removing

contaminant proteins. At 750 $\mu$ l, the protein concentration was 25mg/ml and then we injected the sample to AKTA pure. Before injection, the column was already washed with water and then equilibrated with Gel Filtration buffer. After the size-exclusion chromatography was finished, depending on the UV absorbance at 280nm, we collected the samples from all the peaks (Figure 4.17.A).

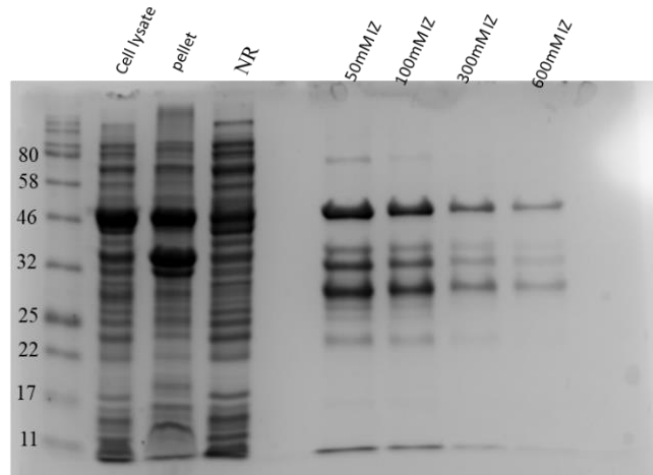
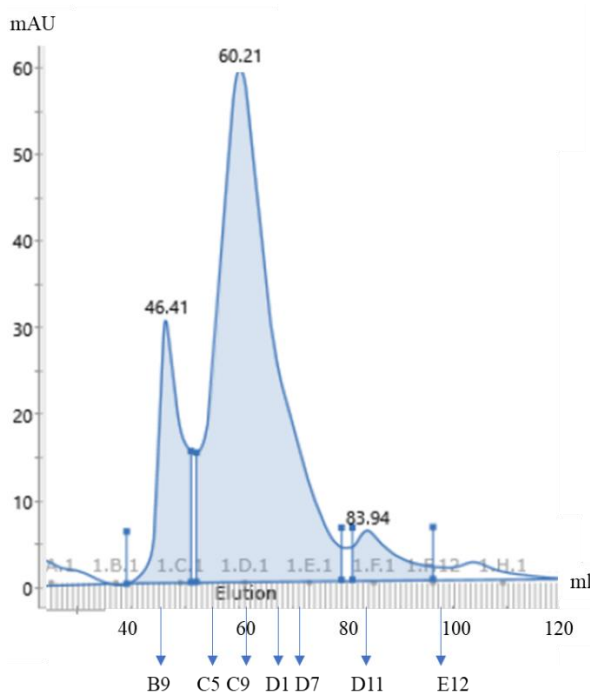
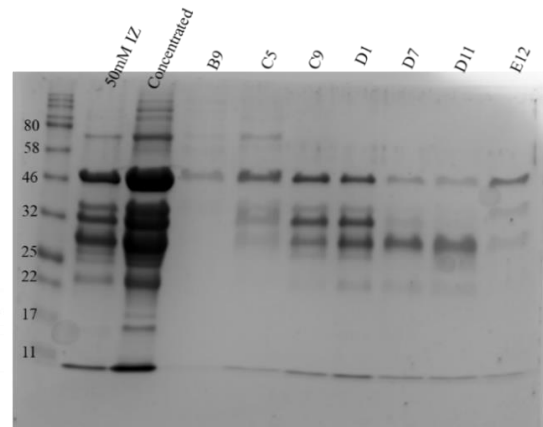


**Figure 4.17. Size exclusion chromatography of His-tagged TagGFP-p53 fusion protein.** (A)The graph showed absorbance (mAU) versus elution volume (ml) graph for His-tagged TagGFP-p53 fusion protein. We performed size exclusion chromatography by using AKTA Pure to remove the contaminant proteins. The blue graph showed absorbance at 280nm, which represented the presence of proteins, whereas the purple graph showed absorbance at 254nm, which represented DNA contamination. (B)The samples from both the previous steps (from elution step and concentration step) and the size exclusion step were loaded into an SDS-PAGE gel for analysis. The expected size for His-tagged TagGFP-p53 was 38kDa.

We prepared samples from B9 (first peak), C5, C9, C11, D1 (second peak) and D8 (third peak). Because the second peak was the peak where the desired protein was eluted, we collected more samples from this peak to understand the boundaries of the pure protein. After analyzing these samples with SDS-PAGE (14%), we observed that the desired protein was found between C5 and D1 and in the third peak, there were all the unwanted proteins (Figure 4.17.B). Because C5 was very diluted, from C6 to D1 the elutes were collected in the same 15-ml tube and the concentration of the protein was 0.75mg/ml. His-tagged TagGFP-p53 protein was then concentrated again to reach a concentration of more than 1mg/ml, and flash-frozen in liquid nitrogen for further SPR experiments.

Before purifying the His-tagged MDM2 protein, we tried to purify the His-tagged TagRFP-MDM2 protein. Again, we grew 1L TB culture for purification of the protein and performed the same steps we performed for the His-tagged TagGFP-p53 fusion protein. However, the protein degraded during every purification trial (Figure 4.18). Therefore, we had to switch to produce only MDM2 portion of the protein.

For producing His-tagged MDM2 protein, we also grew 1L LB culture containing Rosetta2 DE3 with pET-47b(+)-MDM2 and induced it with the same workflow we performed previously. Then, the protein was purified again using 3ml HisPur Cobalt Superflow Agarose resin; however, we eluted this protein with 3 different imidazole concentrations; 100mM, 300mM, and 600mM. After we analyzed all the samples obtained from the previous affinity purification steps in SDS-PAGE, we observed that we purified the protein without any contaminant proteins. The expected His-tagged MDM2 protein size was 17kDa and we got the protein almost the exact size. In the pellet, there was also a band with the same size, therefore some of the protein could be insoluble (Figure 4.19).

**A.****B.****C.**

**Figure 4.18. Affinity and Size-exclusion chromatography of His-tagged TagRFP-MDM2 fusion protein.** (A) SDS-PAGE gel result of affinity chromatography of His-tagged TagRFP-MDM2. We performed multiple elution steps with increasing imidazole concentrations. The expected size for His-tagged TagRFP-MDM2 was 44kDa. (B) Size-exclusion chromatogram of His-tagged TagRFP-MDM2 protein. We collected samples from three peaks for further analysis steps. (C) SDS-PAGE gel result of size-exclusion chromatography of His-tagged TagRFP-MDM2 fusion protein.

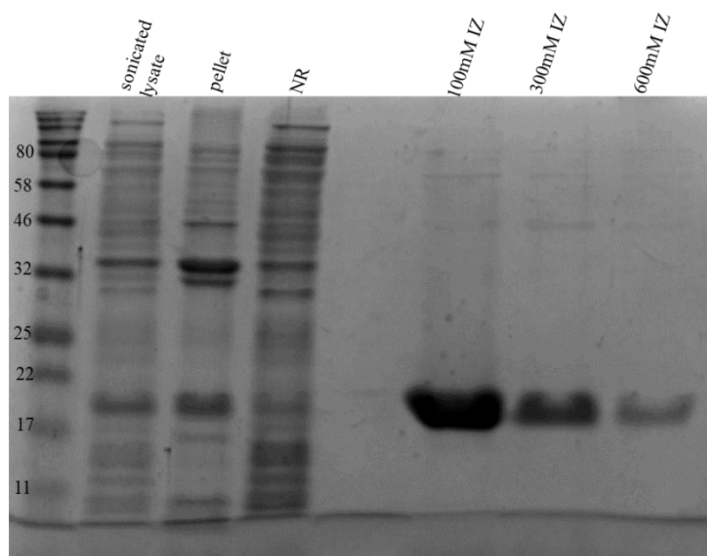


**Figure 4.19. Affinity purification of the His-tagged MDM2 protein.** SDS-PAGE gel result of affinity chromatography of His-tagged MDM2 protein. We performed multiple elution steps with increasing imidazole concentrations; 100mM, 300mM, and 600mM imidazole concentrations. The expected protein size was 17kDa.

Because there was no other contaminant protein, we continued without performing a size exclusion chromatography step. Based on our SPR experiment design, we required to get rid of the His-tag of MDM2 protein because it would also bind to nickel activated NTA chip. There was a 3C protease recognition site before the *MDM2* sequence and after His-tag sequence, therefore we then digested His-tagged MDM2 with 3C ‘Prescission’ protease. We continued with the His-tagged MDM2 eluted with 100mM imidazole and at 7ml, the protein concentration was 1.4mg/ml. Before digestion, we concentrated the protein sample to a volume, which was less than or equal to 1ml. At 900 $\mu$ l of the concentrated protein sample, the protein concentration was 12.2mg/ml. After adding 100 $\mu$ l of 3C protease (2mg/ml), the mixture was incubated overnight at 4°C with end-to-end rotation. On the next day, SDS-PAGE (18%) was performed to check whether His-tags were digested or not. It was observed that after 3C protease digestion, the protein size got smaller, therefore we could say that the digestion worked. Moreover, we observed 3C ‘Prescission’ protease (46kDa) band in the SDS-PAGE gel (Figure 4.20).

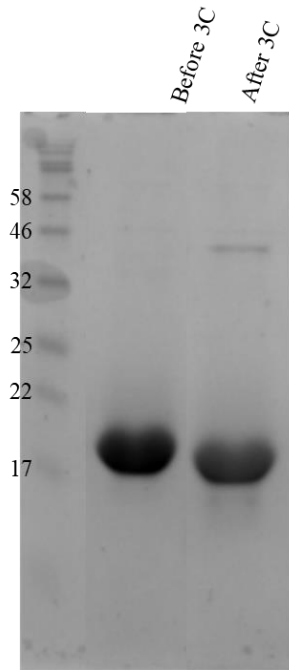


**Figure 4.20. 3C ‘Precission’ protease digestion of His-tagged MDM2 proteins.** To cleave His-tag, the His-tagged MDM2 protein was incubated with 3C protease overnight at 4°C with end-over-end rotation. To observe the size difference, the samples before and after the digestion were loaded into an SDS-PAGE gel (18%). The expected sizes of the 3C protease and MDM2 were about 46kDa, and 16kDa, respectively.

Later, it was required to remove this protease to minimize its non-specific degradation of the MDM2 protein. This protease consisted of a GST-tag, and therefore we performed GST pull-down to eliminate the protease. After adding the desired amount of Glutathione Sepharose 4 Fast to the protein sample and incubating the mixture at 4°C for 2 hours with end-to-end rotation, we sedimented at 500xg for 5 minutes and took out the supernatant carefully. The supernatant part theoretically contained MDM2 protein and free His-tags only. We also eluted fraction retained on Glutathione Sepharose 4 Fast Flow with a buffer containing 10mM reduced glutathione for further analysis steps.

Afterward, we also required performing a His pull-down to eliminate free His-tags and undigested His-tagged MDM2 proteins, which could bind to nickel activated NTA chip and led to false binding results. To perform His pull-down, first, we performed dialysis. We eluted His tagged-MDM2 protein with elution buffer containing 100mM imidazole, therefore the protein sample still consisted of a high imidazole concentration, which could block further His pull-down step. We dialyzed the sample buffer to Gel filtration buffer, which lacked imidazole. Then, we performed His pull-down by using HisPur Cobalt Superflow Agarose resin. After adding the resin on the protein sample and incubating the mixture at 4°C for 30 minutes with end-to-end rotation, we sedimented at 700xg for 5 minutes and took out the supernatant carefully and collected. The fraction resided in the resin was also eluted with IMAC-B buffer for further analysis steps.

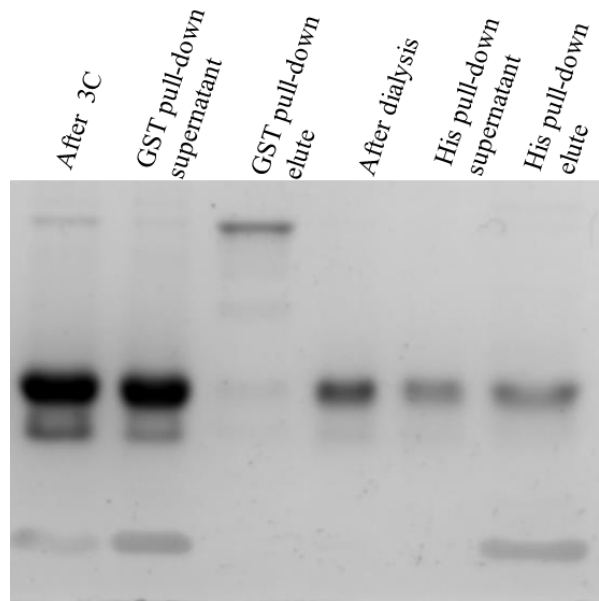


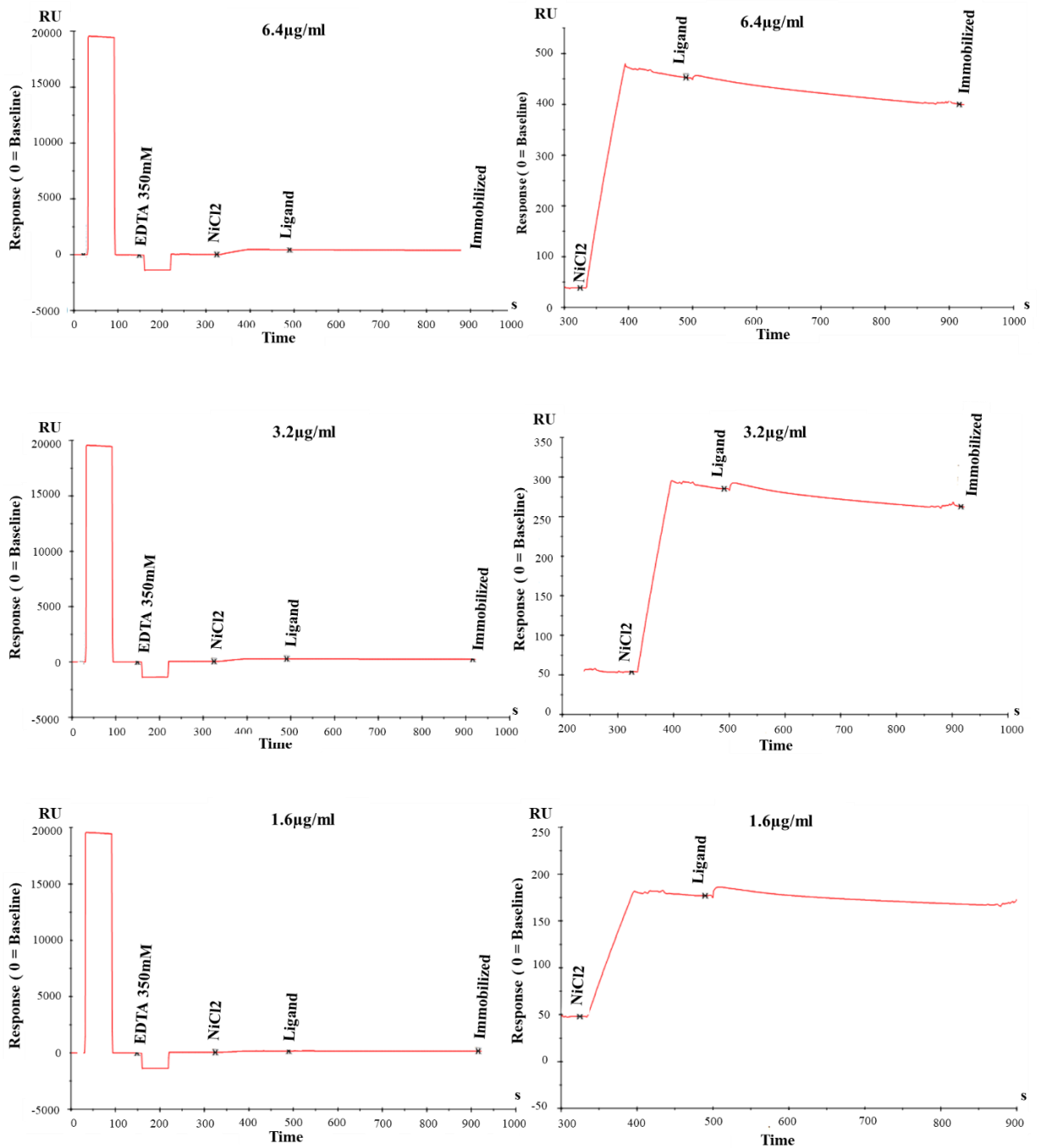
**Figure 4.21. Purification of MDM2 protein after 3C protease digestion.** To get rid of the protease, first, we performed GST pull-down. Then, to remove free His-tags, we performed dialysis and His pull-down. The samples collected from each step were analyzed in an SDS-PAGE gel (14%).

We observed that there was some degradation after 3C digestion, therefore we should be fast after 3C digestion for removing the protease. After GST pull-down, we removed the protease effectively because the protease remained bound to the Glutathione Sepharose 4 Fast resin and then eluted with reduced glutathione later. We lost some amount of protein every step, therefore purification steps should be optimized. Especially, we lost the protein during His pull-down because a great portion of the protein remained with HisPur Cobalt Superflow Agarose resin and eluted with the elution buffer (Figure 4.21).

#### 4.3.2. Surface Plasmon Resonance Assay

With these reagents, we performed surface plasmon resonance experiments by using a BIACORE T200. First, we aimed to determine the concentration of the His-tagged TagGFP-p53 protein required to immobilize to the NTA chip for further binding assays. High concentrations of His-tagged proteins on an NTA chip tended to become unstable and dissociated from the chip. Therefore, we immobilized different concentrations of His-tagged TagGFP-p53 protein and checked whether it was stable or not. For an immobilization experiment, first, we performed conditioning the NTA chip with 350mM EDTA and then activated it with 0.5mM NiCl<sub>2</sub> with a flow rate of 10μl/min for 1 minute, which resulted in approximately 50 response unit (RU). Later, we passed our His-tagged

TagGFP-p53 protein with varying concentrations with a flow rate of 10 $\mu$ l/min for 1 minute. After passing running buffer for 5 minutes to see the stability of the protein, we regenerated the chip with 350mM EDTA solution.



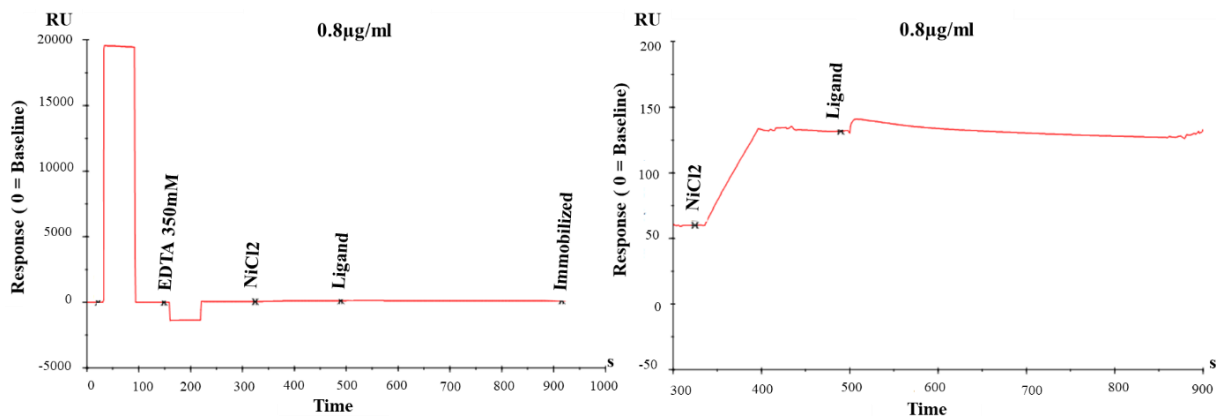


**Figure 4.22. Immobilization of His-tagged TagGFP-p53 onto NTA chip at different concentrations.** After the activation of NTA chip with a NiCl<sub>2</sub> solution, we passed various concentrations of our His-tagged protein on the chip. After passing running buffer for 5 minutes, we checked whether the His-tagged TagGFP-p53 protein was stable or not. At high concentrations (6.4 and 3.2 µg/ml), the protein dissociated slowly, whereas, at low concentrations (1.6 and 0.8 µg/ml), the protein was more stable.

At the concentrations of 6.4 µg/ml and 3.2 µg/ml, we observed approximately 400RU and 250RU, respectively; however, His-tagged TagGFP-p53 protein was not stable on the chip and dissociated slowly. At lower concentrations; 1.6 µg/ml and 0.8 µg/ml, although there was some dissociation, the protein was more stable, and we obtained 130RU and 70 RU, respectively (Figure 4.22). We decided to continue the further experiments with the concentration of 1.6 µg/ml because we got higher response unit.

Later, we wanted to check whether MDM2 protein without any His tag could bind to the NTA chip or not. After activating the chip with a 0.5mM NiCl<sub>2</sub> solution, we passed 60nM MDM2 protein on the chip with a flow rate of 10 µl/min for 1 minute. We observed a non-specific binding and later a quick dissociation when the running buffer was passing; however, in the end, there was approximately 10RU binding to the chip. Therefore, we understood that only MDM2 protein could bind to the chip non-specifically at some level and resulted in a binding response. Moreover, although the MDM2 protein was diluted in the running buffer, there was a sharp decrease after the introduction of MDM2 protein, which could be the result of an air bubble or the aggregates of MDM2 proteins (Figure 4.23).

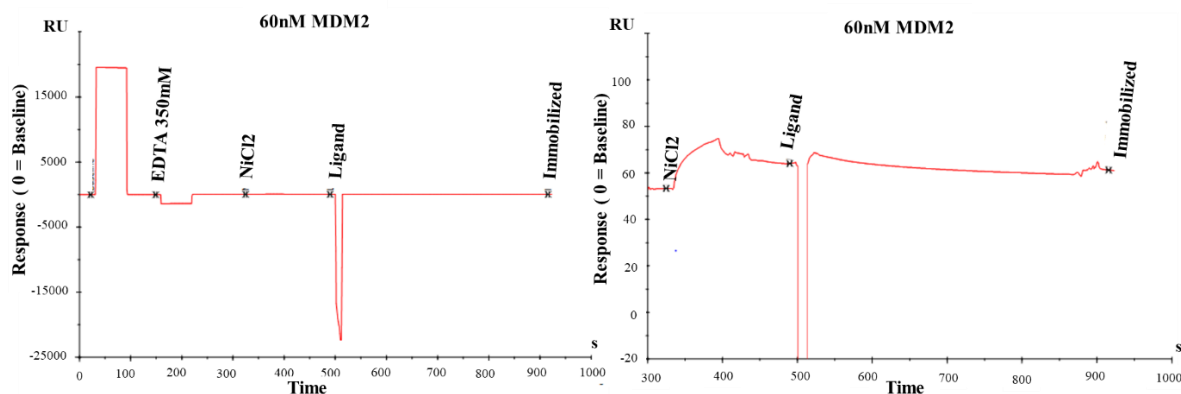


**Figure 4.23. The binding ability of MDM2 protein without the His-tag to the NTA chip.** We passed 60nM MDM2 protein on the activated NTA chip with a flow rate of 10 $\mu$ l/min for 1 minute as we passed His-tagged TagGFP-p53 protein previously. Then, we passed running buffer for 5 minutes to observe the dissociation of the protein.

Next, we performed a binding assay, where we immobilized His-tagged TagGFP-p53 protein and later passed MDM2 protein to see if there was a binding between them or not. After activating the NTA chip, we first passed 1.6 $\mu$ g/ml His-tagged TagGFP-p53 protein with a flow rate of 10 $\mu$ l/min for 1 minute and then we passed 60nM MDM2 protein with a flow rate of 30 $\mu$ l/min for 2 minutes. After passing His-tagged TagGFP-p53 protein, we got again approximately 130RU, which led to providing approximately 50RU binding capacity based on the molecular weight of the two proteins. Therefore, we expected to observe a binding response of approximately 50RU after passing the MDM2 protein. When we set the immobilization of His-tagged TagGFP-p53 as a baseline, after passing MDM2 protein, we got a binding response of approximately 40RU. Moreover, the binding was not stable and there was a quick dissociation of the MDM2 protein. This sharp dissociation could be a result of the non-specific interaction of the MDM2 protein with NTA chip. Moreover, we observed a sharp increase after the injection of MDM2 protein, which could be due to some air bubbles or the aggregates of MDM2 proteins (Figure 4.24).

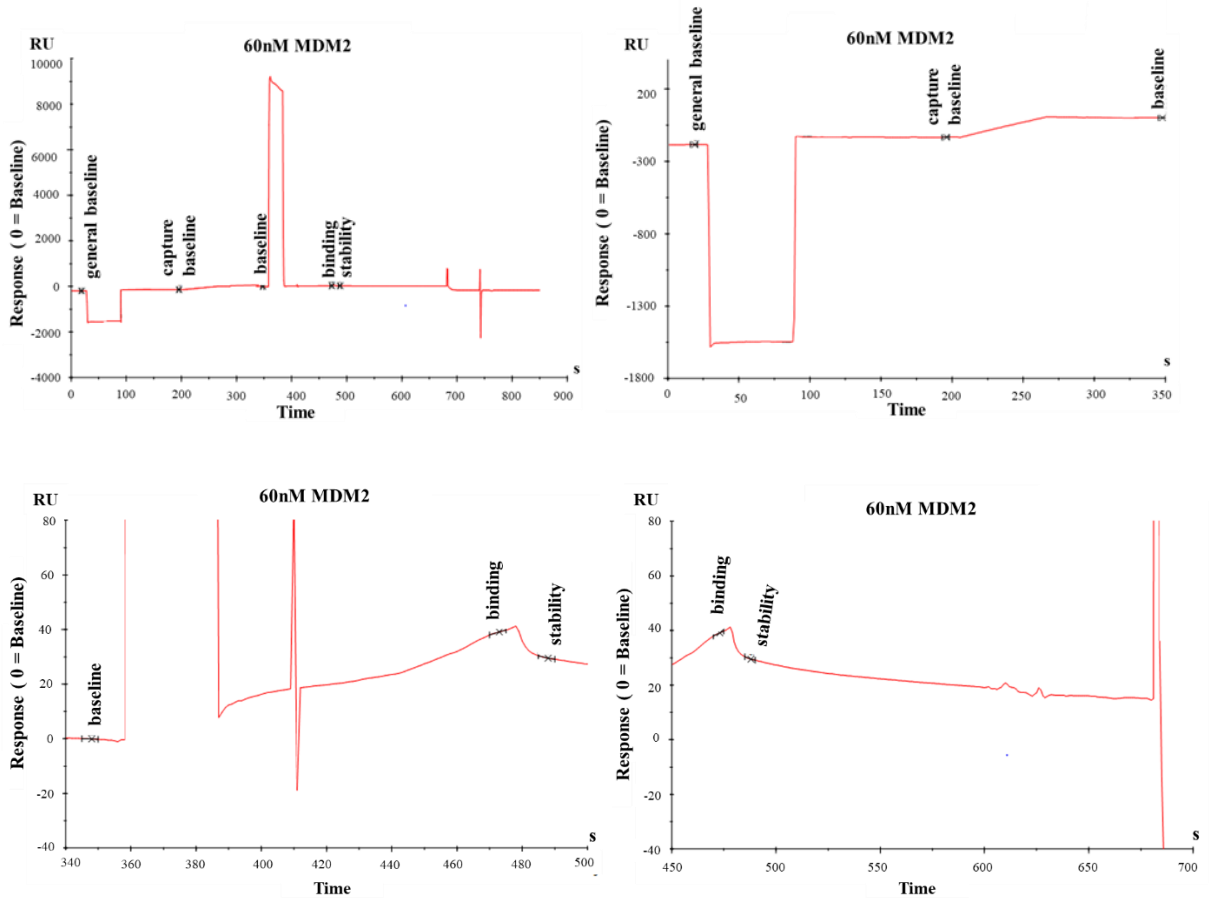


**Figure 4.24. Binding assay of MDM2 protein.** After activating and immobilizing His-tagged TagGFP-p53 protein with a concentration of 1.6 $\mu$ g/ml, we passed 60nM MDM2 protein with a flow rate of 30 $\mu$ l/min for 2 minutes.

## 5. DISCUSSION

In human cancers, the p53 tumor suppressor is generally inactivated through various mechanisms, which results in tumor initiation and progression. Reactivating mutant p53 or restoration of wild-type p53 can result in tumor elimination. The screening of compounds targeting p53 pathway has resulted in the discovery of new drug candidates for anti-cancer strategies<sup>12</sup>. One class of these compounds targets the interaction between p53 and its main antagonist, MDM2 because many human tumors have overexpressed MDM2 that impairs the function of wild-type p53. These compounds have been designed specifically for the p53-binding pocket of MDM2 to release p53 from repression<sup>79</sup>. In this study, we aimed to screen novel compounds targeting the interaction of p53-MDM2 through three different methods for the identification of new promising drug candidates.

Firstly, we generated HCT116 p53<sup>-/-</sup> MDM2<sup>-/-</sup> double knockout cell lines through CRISPR/Cas9 genome editing for analyzing the specificity of the compounds because, in the absence of these two proteins, compounds should not affect the cells. We targeted the second exon of human *MDM2* gene in the HCT116 p53<sup>-/-</sup> cell line. The clustered regularly interspaced short palindromic repeats (CRISPR) is widely used as an efficient method for genome engineering. With the help of a guide RNA for targeting a specific sequence in the genome, the Cas9 enzyme generates a double-stranded break (DSB), which is later repaired by DNA repair mechanisms. This DSB is repaired by either non-homologous end joining (NHEJ) or homology-directed repair (HDR) mechanisms<sup>89</sup>. To knock out the *MDM2* gene, NHEJ resulted in random INDEL mutations in the second exon of *MDM2* gene and later resulted in a shift in its open reading frame.

We generated two different double knockout cell lines, Clone-1F1, and Clone-22C12. Both had big insertions in the targeted region, which resulted in an early stop codon formation. Presumably, these premature stop codons resulted in nonsense-mediated decay of the MDM2 mRNA and caused undetectable MDM2 protein levels in these targeted cells. We compared 4 different cell lines, HCT116 WT, HCT116 p53<sup>-/-</sup>, and two clones derived from the CRISPR treated HCT116 p53<sup>-/-</sup> cells: Clone-1F1 and Clone-22C12. In the cell viability assay, our positive control Nutlin-3a negatively affected the cell viability of wild-type cells; however, the other three cell lines, where the targeted proteins were absent, Nutlin-3a did not affect the cells as expected. Conversely, our one of the selected compounds, 4A1-AN negatively affected the cell viability in all 4 cell types, which showed that the drug candidate was not specific and probably caused DNA damage and

led to cell-death without specifically disrupting the interaction between p53 and MDM2. After this cell viability assay, we demonstrated that screening with these 4 cell lines provides a powerful way of finding the new drug candidates. Moreover, we demonstrated that Clone-1F1 had slower growth rate compared to p53<sup>-/-</sup> cell line. This was expected because MDM2 has some oncogenic functions in promoting tumor growth independent of p53, which may make this double knockout cell line a great tool for studying oncogenic effects of MDM2 *in vitro*<sup>97,98</sup>. The growth rates of Clone-1F1 and Clone-22C12 were significantly different, so the cause of this difference could also be searched.

While screening the compounds, we observed large insertions in the targeted human cell genome, which originated from two different sources: *Escherichia coli* genomic DNA or the pSpCas9(BB)-2A-Puro plasmid backbone. It has been reported that after generating a DSB through the CRISPR/Cas9 genome editing system, the NHEJ mechanism can promote knock-in of large sequences, even more efficient than the HDR system<sup>99</sup>. Therefore, these big insertions were expected results if there were a large amount of bacterial DNA or degraded plasmids in the transfected MDM2-pSpCas9(BB)-2A-Puro mix. Studies to identify the relationship between the purity of the plasmid DNA preparation and insertion sequence identity are underway in the laboratory.

In western blotting, we unexpectedly observed the MDM2 band as a doublet with a size of approximately 90kDa. This could be a result of a difference in one allele affecting post-translational modification, such as sumoylation of MDM2. Moreover, although we found the presence of early stop codons in 5 single cell clones, 3 of them expressed the truncated or the full-size MDM2. We suspected that these colonies did not originate from a single cell and that there could be other alleles present in the mixture, which we could not identify by sequencing. Therefore, more samples from these single cell clones should be analyzed by extensive sequencing.

Secondly, we constructed a fluorescent two-hybrid (F2H) assay, where the interaction domains of p53 and MDM2 were tagged with green and red fluorescent proteins respectively and localized to the Lac operator sites found in BHK cells with the help of the GBP-LacI protein. This assay provides a useful tool for observing the action of compounds in real time using live-cell fluorescent microscopy. If a compound disrupts the p53-MDM2 interaction, red foci disappear while green foci remain in the nucleus in these BHK cells. We observed the effect of our positive control, Nutlin-3a in this assay by counting the green and red foci found in the nucleus. After the addition of Nutlin-3a,

we observed a stable green focus count, whereas the red focus count decreased. Although we could not find any positive results while screening our compound library, the design of the assay is suitable for high-content screening of a large number of compounds and for finding new drug candidates.

While analyzing the effects of these compounds, we counted the numbers of green and red foci using vesicle-like particles analysis. This strategy generated some false positive counts because the strategy included every small feature with a specific range of size and intensity. We predict that the use of a nuclear dye could increase the specificity of this assay by defining the nucleus and restricting the analysis of foci to only those that appear in the nuclei by confocal z-stack microscopy.

Finally, we designed a surface plasmon resonance experiment for the high-throughput screening of the chemical compounds *in vitro*. In this design, we produced the interaction domain of these two proteins in bacteria with a His-tag. After their affinity purification and further purification steps, we immobilized the His-tagged TagGFP-p53 protein to the nickel activated NTA chip and then aimed to pass the MDM2 protein without any tag in the presence or absence of compounds to observe the effects of the compounds *in vitro*. To this end, we immobilized His-tagged TagGFP-p53 at various concentrations to the nickel activated NTA chip. We observed at low concentrations, protein was more stable although there was some dissociation. In the binding assay, we obtained a less than expected binding response after passing MDM2 protein over the His-tagged TagGFP-p53 immobilized chip. Moreover, we found that the bound MDM2 protein dissociated too quickly. This rapid dissociation could be due to the nonspecific binding of MDM2 protein onto the NTA chip, which we already observed when we tested the affinity of this MDM2 protein to the chip in the absence of immobilized His-tagged TagGFP-p53. Moreover, there were some instant high or low signals after the introduction of MDM2 to the system, which could be a result of air bubbles in the flow chamber or aggregates of MDM2 protein.

This SPR assay system can be used for high-throughput screening, and sequential screening of all tested compounds by BIACORE is underway. We are trying to optimize the chip structure and immobilization methods before starting the screening of all the compounds. Importantly, we changed the NTA chip experimental design to the CM5 chip experimental design, where the ligand protein can be covalently linked to the chip without the presence of any tag. This could eliminate the unstable immobilization of His-tagged

TagGFP-p53 protein to the NTA chip and the non-specific interaction of MDM2 protein with this chip.

In summary, although systems require some optimization, we constructed three different assays for the screening of new candidates of p53-MDM2 interaction inhibitors *in vitro*. Next, we aim to perform both high-content and high-throughput screening of different libraries using these three assays for the identification of new candidates. Also, we aim to apply these assays for studying different binding partners.

## 6. REFERENCES

1. Croce CM. Oncogenes and Cancer. *N Engl J Med.* 2008;358(5):502-511. doi:10.1056/NEJMra072367
2. Zhang Z, Li M, Rayburn ER, Hill DL, Zhang R, Wang H. Oncogenes as Novel Targets for Cancer Therapy (Part I). *Am J Pharmacogenomics.* 2005;5(3):173-190. doi:10.2165/00129785-200505030-00004
3. Hahn WC, Weinberg RA. Modelling the molecular circuitry of cancer. *Nat Rev Cancer.* 2002;2(5):331-341. doi:10.1038/nrc795
4. Hassanpour SH, Dehghani M. Review of cancer from perspective of molecular. *J Cancer Res Pract.* 2017;4(4):127-129. doi:10.1016/j.jcrpr.2017.07.001
5. Hanahan D, Weinberg RA. Hallmarks of Cancer: The Next Generation. *Cell.* 2011;144(5):646-674. doi:10.1016/j.cell.2011.02.013
6. Nag S, Qin J, Srivenugopal KS, Wang M, Zhang R. The MDM2-p53 pathway revisited. *J Biomed Res.* 2013;27(4):254-271. doi:10.7555/JBR.27.20130030
7. Zhang Z, Li M, Rayburn ER, Hill DL, Zhang R, Wang H. Oncogenes as novel targets for cancer therapy (part II): Intermediate signaling molecules. *Am J Pharmacogenomics.* 2005;5(4):247-257. <http://www.ncbi.nlm.nih.gov/pubmed/16078861>.
8. Levine AJ, Hu W, Feng Z. Tumor Suppressor Genes. In: *The Molecular Basis of Cancer.* Elsevier; 2008:31-38. doi:10.1016/B978-141603703-3.10003-2
9. Luo J, Solimini NL, Elledge SJ. Principles of Cancer Therapy: Oncogene and Non-oncogene Addiction. *Cell.* 2009;136(5):823-837. doi:10.1016/j.cell.2009.02.024
10. Meng RD, El-Deiry WS. Tumor suppressor gene therapy for cancer: from the bench to the clinic. *Drug Resist Updat.* 1998;1(3):205-210. doi:10.1016/S1368-7646(98)80041-1
11. Liu Y, Hu X, Han C, et al. Targeting tumor suppressor genes for cancer therapy. *BioEssays.* 2015;37(12):1277-1286. doi:10.1002/bies.201500093
12. Joerger AC, Fersht AR. The p53 Pathway: Origins, Inactivation in Cancer, and

- Emerging Therapeutic Approaches. *Annu Rev Biochem.* 2016;85(1):375-404. doi:10.1146/annurev-biochem-060815-014710
13. Michael D, Oren M. The p53–Mdm2 module and the ubiquitin system. *Semin Cancer Biol.* 2003;13(1):49-58. doi:10.1016/S1044-579X(02)00099-8
  14. Karni-Schmidt O, Lokshin M, Prives C. The Roles of MDM2 and MDMX in Cancer. *Annu Rev Pathol Mech Dis.* 2016;11(1):617-644. doi:10.1146/annurev-pathol-012414-040349
  15. Chène P. Inhibiting the p53–MDM2 interaction: an important target for cancer therapy. *Nat Rev Cancer.* 2003;3(2):102-109. doi:10.1038/nrc991
  16. Zhang R, Wang H. MDM2 Oncogene as a Novel Target for Human Cancer Therapy. *Curr Pharm Des.* 2000;6(4):393-416. doi:10.2174/1381612003400911
  17. Bourdon JC, Laurenzi V De, Melino G, Lane D. p53: 25 years of research and more questions to answer. *Cell Death Differ.* 2003;10(4):397-399. doi:10.1038/sj.cdd.4401243
  18. Joerger AC, Fersht AR. Structural Biology of the Tumor Suppressor p53. *Annu Rev Biochem.* 2008;77(1):557-582. doi:10.1146/annurev.biochem.77.060806.091238
  19. Naccarati A, Polakova V, Pardini B, et al. Mutations and polymorphisms in TP53 gene--an overview on the role in colorectal cancer. *Mutagenesis.* 2012;27(2):211-218. doi:10.1093/mutage/ger067
  20. Bell S, Klein C, Müller L, Hansen S, Buchner J. p53 Contains Large Unstructured Regions in its Native State. *J Mol Biol.* 2002;322(5):917-927. doi:10.1016/S0022-2836(02)00848-3
  21. Jeffrey P, Gorina S, Pavletich N. Crystal structure of the tetramerization domain of the p53 tumor suppressor at 1.7 angstroms. *Science (80- ).* 1995;267(5203):1498-1502. doi:10.1126/science.7878469
  22. Gaglia G, Guan Y, Shah J V, Lahav G. Activation and control of p53 tetramerization in individual living cells. *Proc Natl Acad Sci.* 2013;110(38):15497-15501. doi:10.1073/pnas.1311126110

23. Kitayner M, Rozenberg H, Kessler N, et al. Structural Basis of DNA Recognition by p53 Tetramers. *Mol Cell*. 2006;22(6):741-753. doi:10.1016/j.molcel.2006.05.015
24. Weinberg RL, Veprintsev DB, Fersht AR. Cooperative Binding of Tetrameric p53 to DNA. *J Mol Biol*. 2004;341(5):1145-1159. doi:10.1016/j.jmb.2004.06.071
25. Vousden KH, Prives C. Blinded by the Light: The Growing Complexity of p53. *Cell*. 2009;137(3):413-431. doi:10.1016/j.cell.2009.04.037
26. Chen J. The Cell-Cycle Arrest and Apoptotic Functions of p53 in Tumor Initiation and Progression. *Cold Spring Harb Perspect Med*. 2016;6(3):a026104. doi:10.1101/cshperspect.a026104
27. Dimri GP, Nakanishi M, Desprez PY, Smith JR, Campisi J. Inhibition of E2F activity by the cyclin-dependent protein kinase inhibitor p21 in cells expressing or lacking a functional retinoblastoma protein. *Mol Cell Biol*. 1996;16(6):2987-2997. <http://www.ncbi.nlm.nih.gov/pubmed/8649410>.
28. Zheng H, Chen L, Pledger WJ, Fang J, Chen J. p53 promotes repair of heterochromatin DNA by regulating JMJD2b and SUV39H1 expression. *Oncogene*. 2014;33(6):734-744. doi:10.1038/onc.2013.6
29. Qian Y, Chen X. Senescence Regulation by the p53 Protein Family. In: Galluzzi L, Vitale I, Kepp O, Kroemer G, eds. Vol 965. *Methods in Molecular Biology*. Totowa, NJ: Humana Press; 2013:37-61. doi:10.1007/978-1-62703-239-1\_3
30. Brown JP. Bypass of Senescence After Disruption of p21CIP1/WAF1 Gene in Normal Diploid Human Fibroblasts. *Science (80- )*. 1997;277(5327):831-834. doi:10.1126/science.277.5327.831
31. Beausejour CM. Reversal of human cellular senescence: roles of the p53 and p16 pathways. *EMBO J*. 2003;22(16):4212-4222. doi:10.1093/emboj/cdg417
32. Fridman JS, Lowe SW. Control of apoptosis by p53. *Oncogene*. 2003;22(56):9030-9040. doi:10.1038/sj.onc.1207116
33. Sot B, Freund SM V, Fersht AR. Comparative Biophysical Characterization of p53 with the Pro-apoptotic BAK and the Anti-apoptotic BCL-x L. *J Biol Chem*. 2007;282(40):29193-29200. doi:10.1074/jbc.M705544200

34. Kruse J, Gu W. Modes of p53 Regulation. *Cell*. 2009;137(4):609-622. doi:10.1016/j.cell.2009.04.050
35. Toledo F, Wahl GM. Regulating the p53 pathway: in vitro hypotheses, in vivo veritas. *Nat Rev Cancer*. 2006;6(12):909-923. doi:10.1038/nrc2012
36. Wu Z, Earle J, Saito S 'i., Anderson CW, Appella E, Xu Y. Mutation of Mouse p53 Ser23 and the Response to DNA Damage. *Mol Cell Biol*. 2002;22(8):2441-2449. doi:10.1128/MCB.22.8.2441-2449.2002
37. Chao C, Herr D, Chun J, Xu Y. Ser18 and 23 phosphorylation is required for p53-dependent apoptosis and tumor suppression. *EMBO J*. 2006;25(11):2615-2622. doi:10.1038/sj.emboj.7601167
38. Brooks CL, Gu W. Ubiquitination, phosphorylation and acetylation: the molecular basis for p53 regulation. *Curr Opin Cell Biol*. 2003;15(2):164-171. doi:10.1016/S0955-0674(03)00003-6
39. Dai C, Gu W. p53 post-translational modification: deregulated in tumorigenesis. *Trends Mol Med*. 2010;16(11):528-536. doi:10.1016/j.molmed.2010.09.002
40. Tang Y, Zhao W, Chen Y, Zhao Y, Gu W. Acetylation Is Indispensable for p53 Activation. *Cell*. 2008;133(4):612-626. doi:10.1016/j.cell.2008.03.025
41. Kaeser MD, Iggo RD. Chromatin immunoprecipitation analysis fails to support the latency model for regulation of p53 DNA binding activity in vivo. *Proc Natl Acad Sci*. 2002;99(1):95-100. doi:10.1073/pnas.012283399
42. Manfredi JJ. The Mdm2-p53 relationship evolves: Mdm2 swings both ways as an oncogene and a tumor suppressor. *Genes Dev*. 2010;24(15):1580-1589. doi:10.1101/gad.1941710
43. Iwakuma T, Lozano G. MDM2, an introduction. *Mol Cancer Res*. 2003;1(14):993-1000. <http://www.ncbi.nlm.nih.gov/pubmed/14707282>.
44. Bartel F, Taubert H, Harris LC. Alternative and aberrant splicing of MDM2 mRNA in human cancer. *Cancer Cell*. 2002;2(1):9-15. doi:10.1016/S1535-6108(02)00091-0
45. Lee JC, Peter ME. Regulation of apoptosis by ubiquitination. *Immunol Rev*.

- 2003;193(1):39-47. doi:10.1034/j.1600-065X.2003.00043.x
46. Moll UM, Petrenko O. The MDM2-p53 interaction. *Mol Cancer Res.* 2003;1(14):1001-1008. <http://www.ncbi.nlm.nih.gov/pubmed/14707283>.
  47. Yu ZK, Geyer RK, Maki CG. MDM2-dependent ubiquitination of nuclear and cytoplasmic P53. *Oncogene.* 2000;19(51):5892-5897. <http://www.ncbi.nlm.nih.gov/pubmed/11127820>.
  48. Weber JD, Kuo M-L, Bothner B, et al. Cooperative Signals Governing ARF-Mdm2 Interaction and Nucleolar Localization of the Complex. *Mol Cell Biol.* 2000;20(7):2517-2528. doi:10.1128/MCB.20.7.2517-2528.2000
  49. Sherr CJ, Weber JD. The ARF/p53 pathway. *Curr Opin Genet Dev.* 2000;10(1):94-99. doi:10.1016/S0959-437X(99)00038-6
  50. Honda R. Association of p19ARF with Mdm2 inhibits ubiquitin ligase activity of Mdm2 for tumor suppressor p53. *EMBO J.* 1999;18(1):22-27. doi:10.1093/emboj/18.1.22
  51. Stad R, Little NA, Xirodimas DP, et al. Mdmx stabilizes p53 and Mdm2 via two distinct mechanisms. *EMBO Rep.* 2001;2(11):1029-1034. doi:10.1093/embo-reports/kve227
  52. Wang X, Jiang X. Mdm2 and MdmX partner to regulate p53. *FEBS Lett.* 2012;586(10):1390-1396. doi:10.1016/j.febslet.2012.02.049
  53. Marine J, Jochemsen AG. Mdmx and Mdm2: Brothers in Arms? *Cell Cycle.* 2004;3(7):900-904. doi:10.4161/cc.3.7.998
  54. Uldrijan S, Pannekoek W, Vousden KH. An essential function of the extreme C-terminus of MDM2 can be provided by MDMX. *EMBO J.* 2007;26(1):102-112. doi:10.1038/sj.emboj.7601469
  55. Meek DW, Knippschild U. Posttranslational modification of MDM2. *Mol Cancer Res.* 2003;1(14):1017-1026. <http://www.ncbi.nlm.nih.gov/pubmed/14707285>.
  56. Wang X, Taplick J, Geva N, Oren M. Inhibition of p53 degradation by Mdm2 acetylation. *FEBS Lett.* 2004;561(1-3):195-201. doi:10.1016/S0014-5793(04)00168-1

57. Tovar C, Rosinski J, Filipovic Z, et al. Small-molecule MDM2 antagonists reveal aberrant p53 signaling in cancer: Implications for therapy. *Proc Natl Acad Sci.* 2006;103(6):1888-1893. doi:10.1073/pnas.0507493103
58. Leroy B, Anderson M, Soussi T. TP53 Mutations in Human Cancer: Database Reassessment and Prospects for the Next Decade. *Hum Mutat.* 2014;35(6):672-688. doi:10.1002/humu.22552
59. Mello SS, Attardi LD. Not all p53 gain-of-function mutants are created equal. *Cell Death Differ.* 2013;20(7):855-857. doi:10.1038/cdd.2013.53
60. Muller PAJ, Vousden KH. Mutant p53 in Cancer: New Functions and Therapeutic Opportunities. *Cancer Cell.* 2014;25(3):304-317. doi:10.1016/j.ccr.2014.01.021
61. Joerger AC, Ang HC, Fersht AR. Structural basis for understanding oncogenic p53 mutations and designing rescue drugs. *Proc Natl Acad Sci.* 2006;103(41):15056-15061. doi:10.1073/pnas.0607286103
62. Kamaraj B, Bogaerts A. Structure and function of p53-DNA complexes with inactivation and rescue mutations: A molecular dynamics simulation study. *PLoS One.* 2015;10(8):1-16. doi:10.1371/journal.pone.0134638
63. Liu X, Wilcken R, Joerger AC, et al. Small molecule induced reactivation of mutant p53 in cancer cells. *Nucleic Acids Res.* 2013;41(12):6034-6044. doi:10.1093/nar/gkt305
64. Loh SN. The missing Zinc: p53 misfolding and cancer. *Metallomics.* 2010;2(7):442-449. doi:10.1039/c003915b
65. DiGiammarino EL, Lee AS, Cadwell C, et al. A novel mechanism of tumorigenesis involving pH-dependent destabilization of a mutant p53 tetramer. *Nat Struct Biol.* 2002;9(1):12-16. doi:10.1038/nsb730
66. Wassman CD, Baronio R, Demir Ö, et al. Computational identification of a transiently open L1/S3 pocket for reactivation of mutant p53. *Nat Commun.* 2013;4(1):1407. doi:10.1038/ncomms2361
67. Boeckler FM, Joerger AC, Jaggi G, Rutherford TJ, Veprintsev DB, Fersht AR. Targeted rescue of a destabilized mutant of p53 by an in silico screened drug. *Proc Natl Acad Sci.* 2008;105(30):10360-10365. doi:10.1073/pnas.0805326105

68. Blanden AR, Yu X, Wolfe AJ, et al. Synthetic Metallochaperone ZMC1 Rescues Mutant p53 Conformation by Transporting Zinc into Cells as an Ionophore. *Mol Pharmacol*. 2015;87(5):825-831. doi:10.1124/mol.114.097550
69. Zhang M, Heldin A, Palomar-Siles M, Öhlin S, Bykov VJN, Wiman KG. Synergistic Rescue of Nonsense Mutant Tumor Suppressor p53 by Combination Treatment with Aminoglycosides and Mdm2 Inhibitors. *Front Oncol*. 2018;7(January):1-12. doi:10.3389/fonc.2017.00323
70. Keeling KM, Xue X, Gunn G, Bedwell DM. Therapeutics Based on Stop Codon Readthrough. *Annu Rev Genomics Hum Genet*. 2014;15(1):371-394. doi:10.1146/annurev-genom-091212-153527
71. Morris LGT, Chan TA. Therapeutic targeting of tumor suppressor genes. *Cancer*. 2015;121(9):1357-1368. doi:10.1002/cncr.29140
72. Olivier M, Petitjean A, Marcel V, et al. Recent advances in p53 research: an interdisciplinary perspective. *Cancer Gene Ther*. 2009;16(1):1-12. doi:10.1038/cgt.2008.69
73. Senzer N, Nemunaitis J, Nemunaitis M, et al. p53 therapy in a patient with Li-Fraumeni syndrome. *Mol Cancer Ther*. 2007;6(5):1478-1482. doi:10.1158/1535-7163.MCT-07-0125
74. O'Shea CC, Johnson L, Bagus B, et al. Late viral RNA export, rather than p53 inactivation, determines ONYX-015 tumor selectivity. *Cancer Cell*. 2004;6(6):611-623. doi:10.1016/j.ccr.2004.11.012
75. Brown CJ, Lain S, Verma CS, Fersht AR, Lane DP. Awakening guardian angels: drugging the p53 pathway. *Nat Rev Cancer*. 2009;9(12):862-873. doi:10.1038/nrc2763
76. Kirn DH, Thorne SH. Targeted and armed oncolytic poxviruses: a novel multi-mechanistic therapeutic class for cancer. *Nat Rev Cancer*. 2009;9(1):64-71. doi:10.1038/nrc2545
77. Okal A, Cornillie S, Matissek SJ, Matissek KJ, Cheatham TE, Lim CS. Re-Engineered p53 Chimera with Enhanced Homo-Oligomerization That Maintains Tumor Suppressor Activity. *Mol Pharm*. 2014;11(7):2442-2452.

doi:10.1021/mp500202p

78. Wade M, Li Y, Wahl GM. MDM2, MDMX and p53 in oncogenesis and cancer therapy. *Nat Rev Cancer*. 2013;13(2):83-96. doi:10.1038/nrc3430
79. Zhao Y, Aguilar A, Bernard D, Wang S. Small-Molecule Inhibitors of the MDM2–p53 Protein–Protein Interaction (MDM2 Inhibitors) in Clinical Trials for Cancer Treatment. *J Med Chem*. 2015;58(3):1038-1052. doi:10.1021/jm501092z
80. Vassilev LT. In Vivo Activation of the p53 Pathway by Small-Molecule Antagonists of MDM2. *Science* (80- ). 2004;303(5659):844-848. doi:10.1126/science.1092472
81. Graat HCA, Carette JE, Schagen FHE, et al. Enhanced tumor cell kill by combined treatment with a small-molecule antagonist of mouse double minute 2 and adenoviruses encoding p53. *Mol Cancer Ther*. 2007;6(5):1552-1561. doi:10.1158/1535-7163.MCT-06-0631
82. Rew Y, Sun D, Yan X, et al. Discovery of AM-7209, a Potent and Selective 4-Amidobenzoic Acid Inhibitor of the MDM2–p53 Interaction. *J Med Chem*. 2014;57(24):10499-10511. doi:10.1021/jm501550p
83. Sun D, Li Z, Rew Y, et al. Discovery of AMG 232, a Potent, Selective, and Orally Bioavailable MDM2–p53 Inhibitor in Clinical Development. *J Med Chem*. 2014;57(4):1454-1472. doi:10.1021/jm401753e
84. Graves B, Thompson T, Xia M, et al. Activation of the p53 pathway by small-molecule-induced MDM2 and MDMX dimerization. *Proc Natl Acad Sci*. 2012;109(29):11788-11793. doi:10.1073/pnas.1203789109
85. Lain S, Hollick JJ, Campbell J, et al. Discovery, In Vivo Activity, and Mechanism of Action of a Small-Molecule p53 Activator. *Cancer Cell*. 2008;13(5):454-463. doi:10.1016/j.ccr.2008.03.004
86. Li L, Wang L, Li L, et al. Activation of p53 by SIRT1 Inhibition Enhances Elimination of CML Leukemia Stem Cells in Combination with Imatinib. *Cancer Cell*. 2012;21(2):266-281. doi:10.1016/j.ccr.2011.12.020
87. Sander JD, Joung JK. CRISPR-Cas systems for editing, regulating and targeting genomes. *Nat Biotechnol*. 2014;32(4):347-355. doi:10.1038/nbt.2842

88. Wang H, La Russa M, Qi LS. CRISPR/Cas9 in Genome Editing and Beyond. *Annu Rev Biochem.* 2016;85(1):227-264. doi:10.1146/annurev-biochem-060815-014607
89. Ran FA, Hsu PD, Wright J, Agarwala V, Scott DA, Zhang F. Genome engineering using the CRISPR-Cas9 system. *Nat Protoc.* 2013;8(11):2281-2308. doi:10.1038/nprot.2013.143
90. Chylinski K, Makarova KS, Charpentier E, Koonin E V. Classification and evolution of type II CRISPR-Cas systems. *Nucleic Acids Res.* 2014;42(10):6091-6105. doi:10.1093/nar/gku241
91. Sorek R, Lawrence CM, Wiedenheft B. CRISPR-Mediated Adaptive Immune Systems in Bacteria and Archaea. *Annu Rev Biochem.* 2013;82(1):237-266. doi:10.1146/annurev-biochem-072911-172315
92. Jinek M, Chylinski K, Fonfara I, Hauer M, Doudna JA, Charpentier E. A Programmable Dual-RNA-Guided DNA Endonuclease in Adaptive Bacterial Immunity. *Science (80- ).* 2012;337(6096):816-821. doi:10.1126/science.1225829
93. Hirano S, Nishimasu H, Ishitani R, Nureki O. Structural Basis for the Altered PAM Specificities of Engineered CRISPR-Cas9. *Mol Cell.* 2016;61(6):886-894. doi:10.1016/j.molcel.2016.02.018
94. Tsukamoto T, Hashiguchi N, Janicki SM, Tumber T, Belmont AS, Spector DL. Visualization of gene activity in living cells. *Nat Cell Biol.* 2000;2(12):871-878. doi:10.1038/35046510
95. Knutsen T, Padilla-Nash HM, Wangsa D, et al. Definitive molecular cytogenetic characterization of 15 colorectal cancer cell lines. *Genes, Chromosom Cancer.* 2009;49(3):NA-NA. doi:10.1002/gcc.20730
96. Bunz F, Fauth C, Speicher MR, et al. Targeted inactivation of p53 in human cells does not result in aneuploidy. *Cancer Res.* 2002;62(4):1129-1133. <http://www.ncbi.nlm.nih.gov/pubmed/11861393>.
97. Feeley KP, Adams CM, Mitra R, Eischen CM. Mdm2 Is Required for Survival and Growth of p53-Deficient Cancer Cells. *Cancer Res.* 2017;77(14):3823-3833. doi:10.1158/0008-5472.CAN-17-0809

98. Riscal R, Schrepfer E, Arena G. Chromatin-Bound MDM2 Regulates Serine Metabolism and Redox Homeostasis Independently of p53. *Mol Cell*. 2016;62(6):890-902. doi:10.1016/j.molcel.2016.04.033
99. He X, Tan C, Wang F, et al. Knock-in of large reporter genes in human cells via CRISPR/Cas9-induced homology-dependent and independent DNA repair. *Nucleic Acids Res*. 2016;44(9):e85-e85. doi:10.1093/nar/gkw064

## 7. APPENDICES

### 7.1. APPENDIX A- Chemicals

<b>Chemicals and Media Components</b>	<b>Supplier Company</b>
2-Mercaptoethanol	Sigma, Germany
Acetic acid (glacial)	Merck Millipore, USA
Acrylamide/Bis-acrylamide (30%)	Sigma, Germany
Agarose	Sigma, Germany
Ammonium Persulfate	Sigma, Germany
Ampicilin Sodium Salt	Sigma, Germany
Boric Acid	Molekula, France
Chloramphenicol	Deva, Turkey
Coumaric Acid	Sigma, Germany
Coomassie Blue Brilliant Blue R	Sigma, Germany
Distilled Water	Merck Millipore, USA
DMEM	Thermo Fischer Scientific, USA
DMSO	Sigma, Germany
DNA Gel Loading Dye, 6X	NEB, USA
DTT	Fermentas, USA
EDTA	Sigma, Germany
Ethanol	Sigma, Germany
Ethidium Bromide	Sigma, Germany
Fetal Bovine Serum	Thermo Fischer Scientific, USA
Glutathione Sepharose 4 Fast Flow	GE Healthcare Life Sciences, USA
Glycerol	Sigma, Germany
Glycine	Sigma, Germany
HBSS	Thermo Fischer Scientific, USA
HEPES	Sigma, Germany
HisPure Cobalt Superflow Agarose	Thermo Fischer Scientific, USA
Hydrochloric Acid	Sigma, Germany

Hydrogen peroxide	Sigma, Germany
Imidazole	Sigma, Germany
IPTG	Fermentas, USA
Isopropanol	Sigma, Germany
Kanamycin Sulfate	Thermo Fischer Scientific, USA
LB Agar	Sigma, Germany
LB Broth	Invitrogen, USA
L-Glutathione reduced	Sigma, Germany
Luminol	Sigma, Germany
Methanol	Sigma, Germany
PBS	Thermo Fischer Scientific, USA
Penicillin/Streptomycin	Thermo Fischer Scientific, USA
PIPES	Sigma, Germany
Potassium Acetate	Merck Millipore, USA
Protease Tablets (EDTA-free)	Roche, Germany
RNase A	Roche, Germany
SDS	Sigma, Germany
Skim Milk Powder	Sigma, Germany
Sodium Azide	Amresco, USA
Sodium Chloride	Amresco, USA
Sodium Hydroxide	Sigma, Germany
TEMED	AppliChem, Germany
TCEP	Sigma, Germany
Terrific Broth	Sigma, Germany
Tris Base	Sigma, Germany
Tris Hydrochloride	Amresco, USA
Trypan Blue Solution	Thermo Fischer Scientific, USA
Tween20	Sigma, Germany

## 7.2. APPENDIX B – Equipment

<b>Equipment</b>	<b>Supplier Company</b>
Autoclave	HiClave HV-110, Hirayama, Japan
Balance	Isolab, Germany
Biomolecular Imager	ImageQuant LAS 4000 mini, GE Healthcare Life Sciences, USA
Centrifuge	5418R Eppendorf, Germany 5702 Eppendorf, Germany 5415R Eppendorf, Germany Allegra X-15R, Beckman Coulter, USA Sorvall Lynx 6000, Thermo Scientific, USA
Chromatography system	AKTA pure, GE Healthcare Life Sciences, USA
CO <sub>2</sub> Incubator	Binder, Germany
Column	HiLoad 16/60 Superdex p75, GE Healthcare Life Sciences, USA
Countless II Automated Cell Counter	Thermo Fischer Scientific, USA
Deepfreeze	-80°C, Forma 88000 Series, Thermo Fischer Scientific, USA -20°C, Bosch, Germany
Dialysis cassette	Slide-A-Lyzer Dialysis Cassette G2, Thermo Scientific, USA
Electrophoresis Apparatus	VWR, USA BIORAD, USA
Filters (0.22µm and 0.45µm)	Merk Millipore, USA
Freezing Container	Mr. Frosty, Thermo Fischer Scientific, USA
Gel Documentation	Gel Doc EZ, Biorad, USA
Heater	Thermomixer Comfort Eppendorf, Germany
Hemocytometer	Neubauer Improved, Isolab, Germany
Ice Machine	AF20, Scotsman Inc., USA
Incubator Shaker	Innova 44, New Brunswick Scientific USA
Laminar Flow	HeraSafe HS15, Heraeus, Germany HeraSafe HS12, Heraeus, Germany

Liquid Nitrogen Tank	Taylor-Wharton, 300RS, USA
Magnetic Stirrer	SB162, Stuart, UK
Microliter Pipettes	Thermo Fischer Scientific, USA
Microscope	Primovert, Zeiss, Germany CK40, Olympus, Japan
	In Cell Analyzer 2500HS, GE Healthcare Life Sciences, USA
Microwave Oven	Bosch, Germany
pH Meter	SevenCompact, Mettler Toledo, USA
Refrigerator	Bosch, Germany Arcelik, Turkey Panasonic, Japan Thermo Fischer Scientific, USA
Reusable Filter Holder with Receiver	Nalgene, USA
RTCA system	ACEA Biosciences, USA
Sonicator	Qsonica Q500, USA
Spectrophotometer	NanoDrop 2000, Thermo Fischer Scientific, USA Ultrospec 2100 pro, Amersham Biosciences, UK
Surface Plasmon Resonance System	BIACORE T200, GE Healthcare Life Sciences, USA
Thermal Cycler	C1000 Touch, Biorad, USA PTC-200, MJ Reseach Inc., Canada
Vortex	VWR, USA
Water Bath	Innova 3100, New Brunswick Scientific, USA

### 7.3. APPENDIX C- Molecular Biology Kits

<b>Commercial Kit</b>	<b>Supplier Company</b>
Cell Proliferation Kit I (MTT)	Roche, Switzerland
GenElute Agarose Spin Columns	Sigma-Aldrich, USA
InsTAclone PCR Cloning	Thermo Fischer Scientific, USA
NucleoSpin Gel and PCR Clean-up	Macherey-Nagel, USA
PureLink Genomic DNA Mini Kit	Invitrogen, USA
Purelink HiPure Plasmid Midiprep Kit	Invitrogen, USA
PureLink Quick Gel Extraction Kit	Invitrogen, USA
Zero Blunt TOPO PCR Cloning Kit for Sequencing	Thermo Fischer Scientific, USA
ZymoPure Plasmid Maxiprep Kit	Zymo Research, USA

### 7.4. APPENDIX D- Antibodies

<b>Antibody</b>	<b>Supplier Company</b>	<b>Catalog Number</b>
MDM2 monoclonal antibody, IF2	Thermo Fischer Scientific, USA	33-7100
Monoclonal ANTI-FLAG M2 antibody produced in mouse	Sigma, Germany	F3165-1MG
$\beta$ -Actin Rabbit Antibody	Cell Signaling Technology	4967L

## 7.5. APPENDIX E – DNA and Protein Molecular Weight Marker

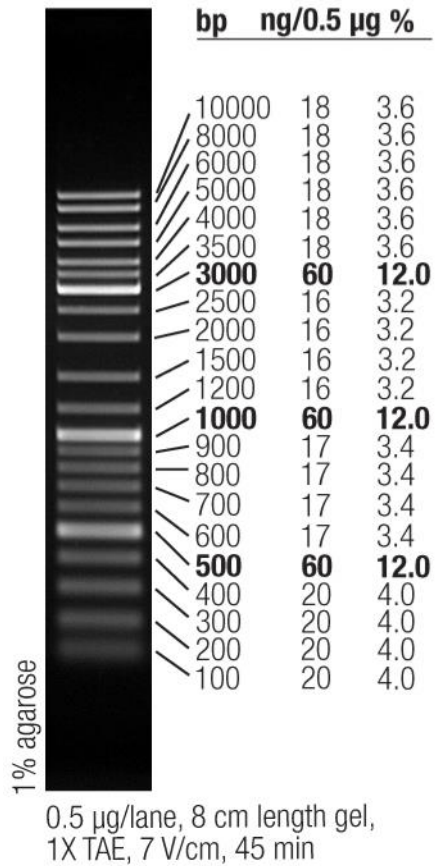


**Figure 7.1. GeneRuler DNA Ladder Mix (SM0331), Thermo Fischer Scientific, USA**

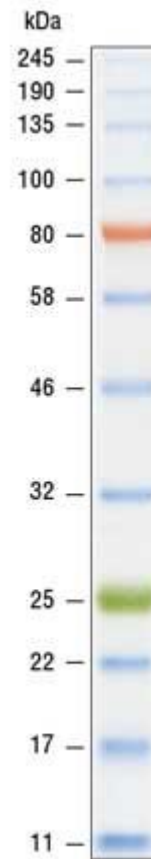


**Figure 7.2. Color Prestained Protein Standard, Broad Range (11-245kDa) (P7712S), New England Biolabs.**

## 7.6. APPENDIX F- Plasmid Maps

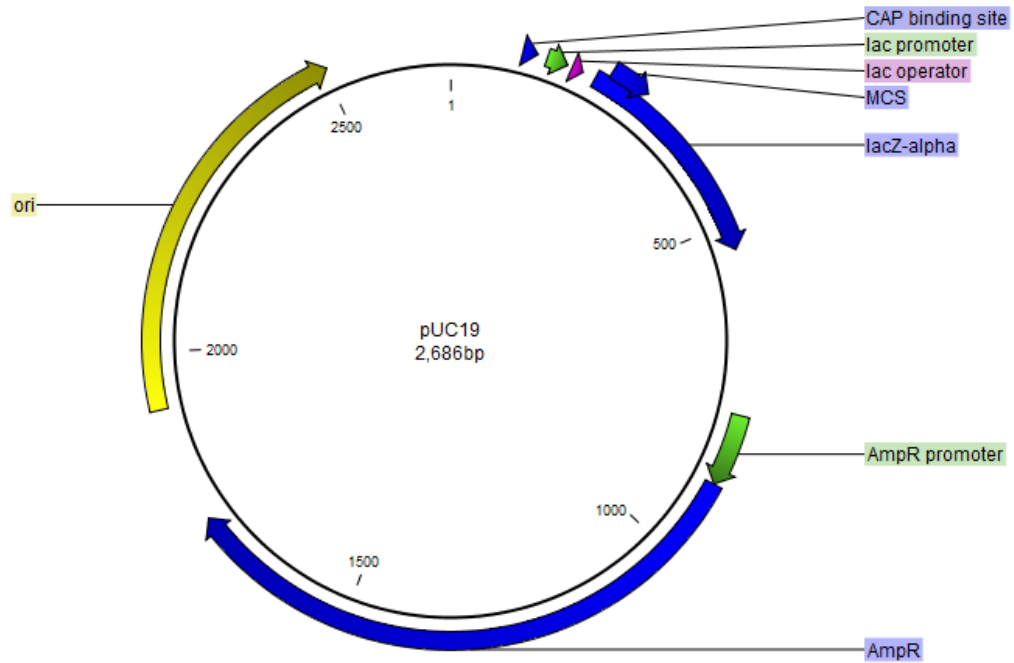


Figure 7.3. The plasmid map of pUC19

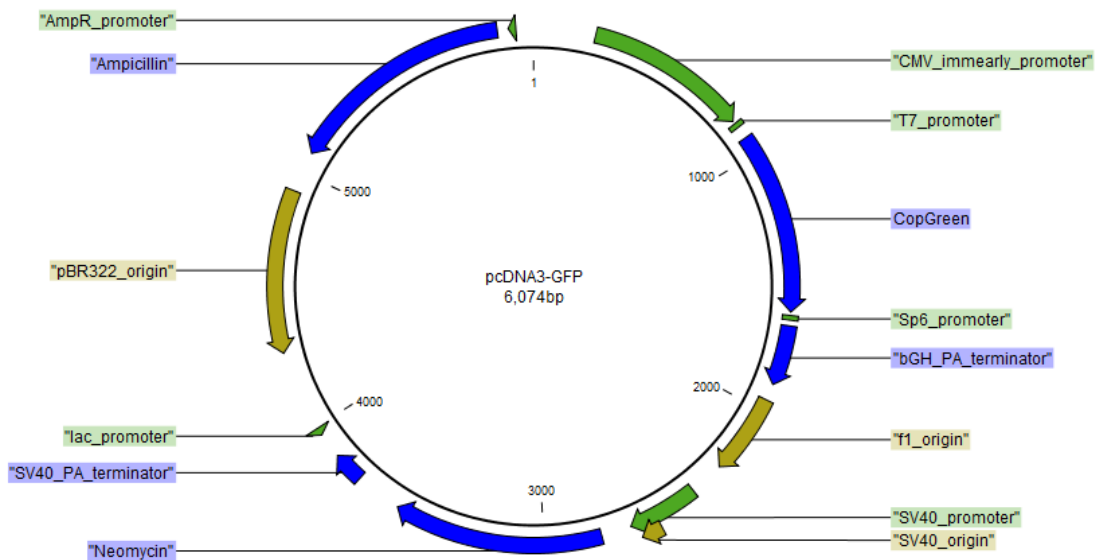
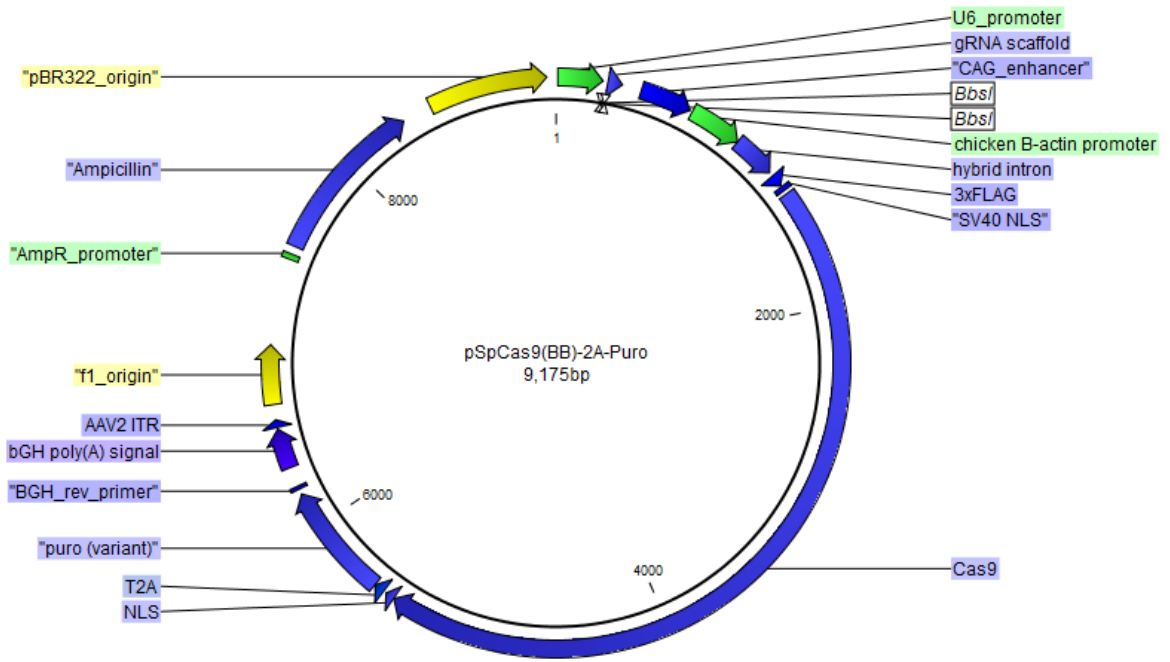
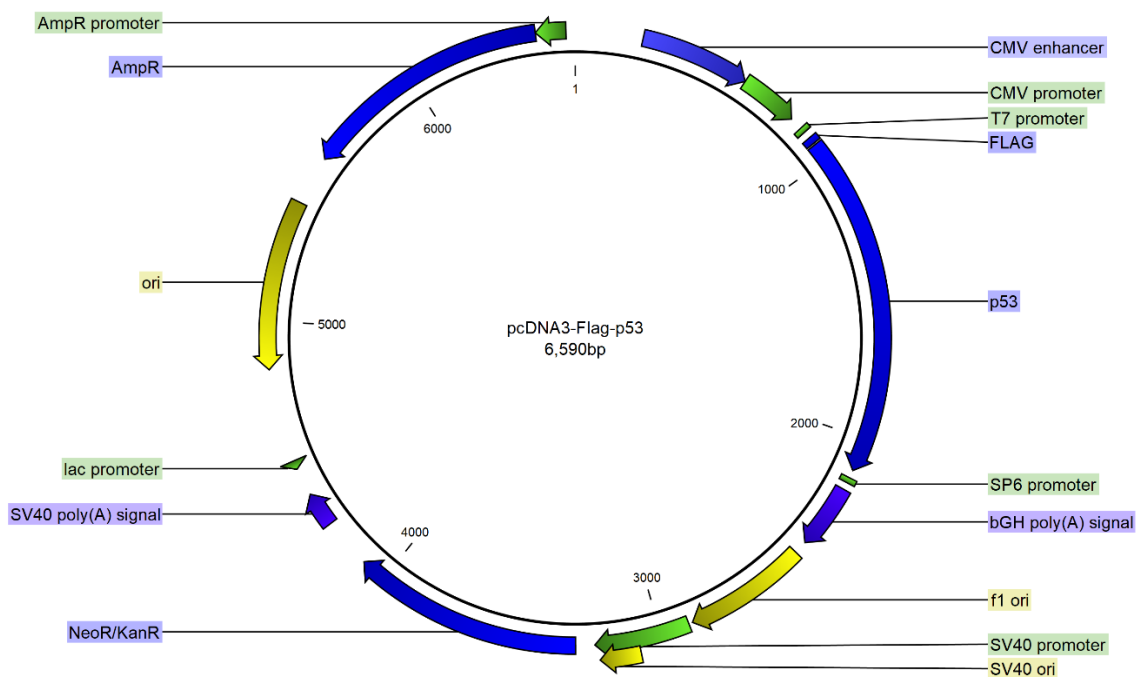


Figure 7.4. The plasmid map of pcDNA3-GFP



**Figure 7.5. The plasmid map of pSpCas9(BB)-2A-Puro**



**Figure 7.6. The Plasmid map of pcDNA3-Flag-p53**

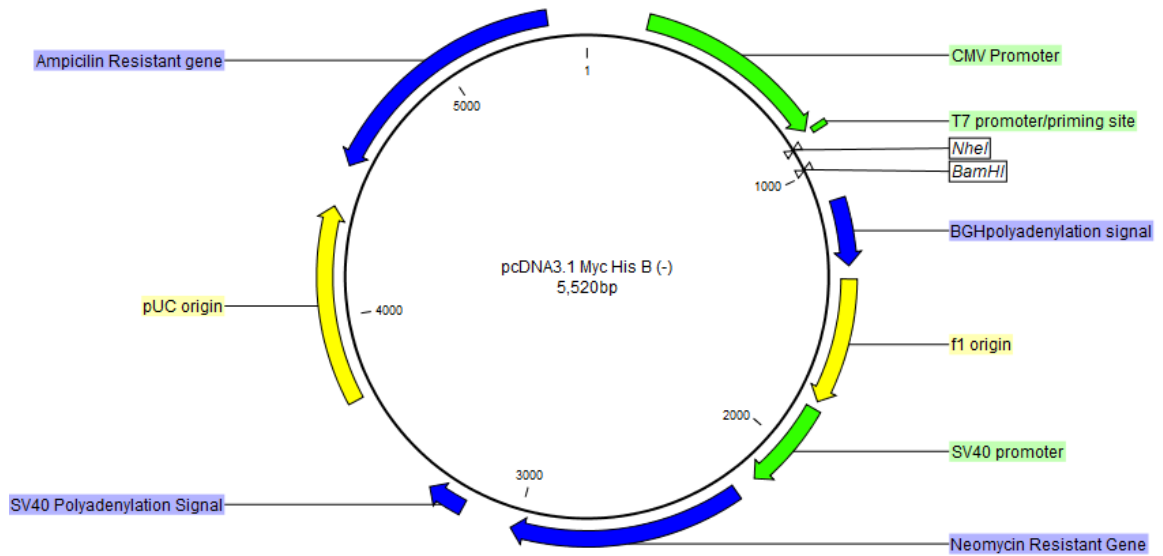


**Figure 7.7. The plasmid map of pcDNA3.1/Myc His (-) B**

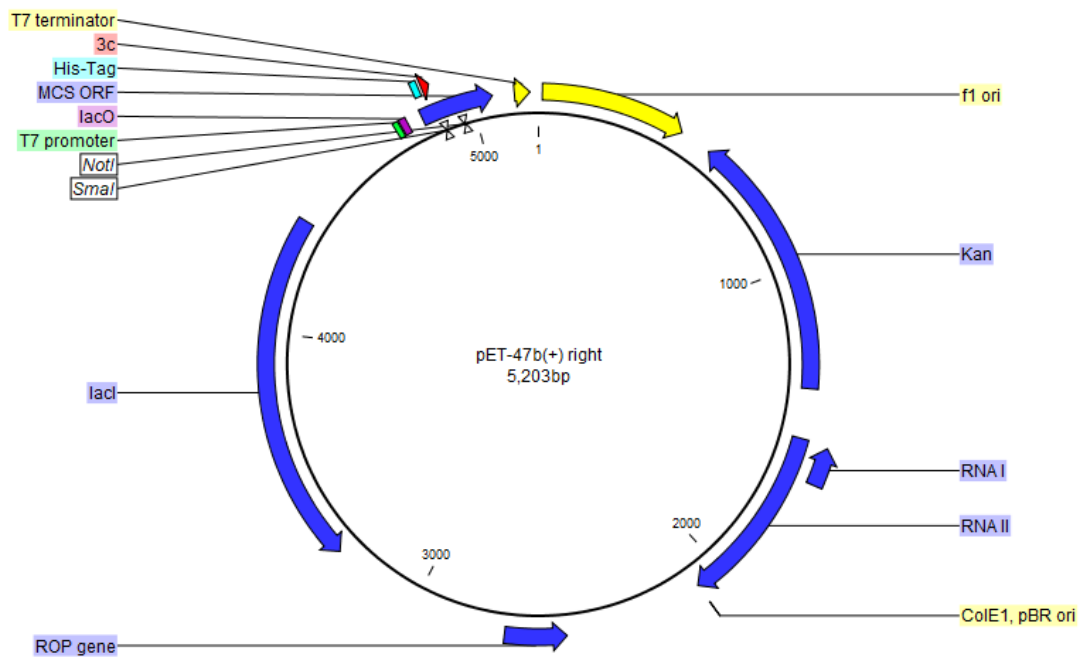


**Figure 7.8. The plasmid map of pET-47b(+)**